Coupled Bending Torsional Vibration of Rotating Shafts Using Finite Element

by

Mohammed Ahmed Mohiuddin

A Thesis Presented to the

FACULTY OF THE COLLEGE OF GRADUATE STUDIES

KING FAHD UNIVERSITY OF PETROLEUM & MINERALS

DHAHRAN, SAUDI ARABIA

In Partial Fulfillment of the
Requirements for the Degree of

MASTER OF SCIENCE

In

MECHANICAL ENGINEERING

October, 1992

Order Number 1354088

Coupled bending torsional vibration of rotating shafts using finite element

Mohiuddin, Mohammed Ahmed, M.S.

King Fahd University of Petroleum and Minerals (Saudi Arabia), 1992

COUPLED BENDING TORSIONAL VIBRATION OF ROTATING SHAFTS USING FINITE ELEMENT

BY

MOHAMMED AHMED MOHIUDDIN

A Thesis Presented to the

FACULTY OF THE COLLEGE OF GRADUATE STUDIES

KING FAHD UNIVERSITY OF PETROLEUM & MINERALS

DHAHRAN, SAUDI ARABIA

In Partial Fulfillment of the
Requirements for the Degree of

MASTER OF SCIENCE

In

MECHANICAL ENGINEERING

OCTOBER, 1992

KING FAHD UNIVERSITY OF PETROLEUM & MINERALS

DHAHRAN, SAUDI ARABIA

This thesis, written by

MOHAMMED AHMED MOHIUDDIN

under the direction of his Thesis Advisor, and approved by his Thesis Committee, has been presented to and accepted by the Dean, College of Graduate Studies, in partial fulfillment of the requirements for the degree of

MASTER OF SCIENCE IN MECHANICAL ENGINEERING

Thesis Committee

Chairman (Dr. Y:A. KHULIEF)

Member (Dr. R.R.D GUNTUR)

Member (Dr. K.A.F. MOUSTAFA)

Member (Dr. A. Z. AL-GARNI)

Department Chairman

Dean College of Graduate Studies

Date : 23-11-92

COLLEGE OF GRAD

ACKNOWLEDGEMENT

First and foremost, praise and thanks be to Almighty Allah, the most Gracious, the most Merciful, and Peace be Upon His Prophet.

Acknowledgement is due to King Fahd University of Petroleum and Minerals for extending all facilities and providing financial support.

I would like to offer my indebtness and sincere appreciation to my academic advisor and thesis committee chairman, Dr. Yehia A. Khulief, who has been a constant source of help and encouragement during this work. I also greatly appreciate the invaluable co-operation and support extended by my thesis committee members: Dr. R. R. Guntur, Dr. K. A. F. Moustafa and Dr. A. Z. Al-Garni.

Sincere thanks are due to department chairman Dr. Muhammad O. Budair for immeasurable cooperation.

I wish to express my gratitude to my parents and relatives, who motivated and guided me through out my carreer.

Finally, I thank all my colleagues who helped me in typing the manuscript.

TABLE OF CONTENTS

LIST OF TABLES

Table *Page*

LIST OF FIGURES

Figure *Page*

NOMENCLATURE

$[A]$	:	transformation matrix
$[C]$	:	damping matrix
E	:	elasticity modulus
$\{e\}$	:	deformation vector
f	:	frequency parameter
G	:	shear modulus
$[G]$	:	gyroscopic matrix
I_D	:	diametral mass moment of inertia
I_p	:	polar mass moment of inertia
$[K]$	:	composite mass matrix
$[K_e]$	:	elastic stiffness matrix
$[K_s]$	:	shear stiffness matrix
$[k_\varphi]$	:	torsional stiffness matrix
L	:	Lagrangian function
$[M]$	:	composite mass matrix
$[M_r]$	:	rotary inertia mass matrix
$[M_t]$	:	translational mass matrix
$[M_\varphi]$	:	torsional mass matrix
N_v	:	translation shape function
N_β, N_γ	:	rotational shape functions
N_φ	:	torsional shape function
$\{p\}$	:	transformed deformation vector

Q	:	vector of generalized forces
q	:	generalized coordinate
R	:	rotating refence frame
R_o	:	fixed reference frame
T	:	kinetic energy of the beam element
U	:	total strain energy of the beam element
U_1	:	strain energy due to bending
U_2	:	strain energy due to shear deformation
V	:	volume of the beam element
v, w	:	translational deformation
v_b, w_b	:	deformation due to bending
v_s, w_s	:	deformation due to shear
I	:	second moment of cross-sectional inertia
$[I]$	:	Identity matrix
X^i, Y^i, Z^i	:	cartesian coordinate system fixed to the undeformed beam element
x, y, z	:	cartesian coordinate system fixed to the deformed beam element

Greek Symbols

Δ	:	logarithmic decrement
κ	:	shear correction factor
κ	:	curvature
λ	:	whirl ratio

μ	:	mass density of the beam element
ν	:	Poisson's ratio
$\bar{\omega}$	:	instantaneous angular velocity
ω	:	whirl speed
Ω	:	constant spin speed
Φ	:	shear correction parameter
ξ	:	non-dimensional position coordinate

Superscript

d	:	disk
s	:	system
e	:	element
b	:	bearing

THESIS ABSTRACT

NAME OF STUDENT	*: MOHAMMED AHMED MOHIUDDIN*
TITLE OF STUDY	*: Coupled Bending and Torsional Vibration of Rotating Shafts Using Finite Element*
MAJOR FIELD	*: Mechanical Engineering*
DATE OF DEGREE	*: October, 1992*

The coupled bending and torsional vibration of a rotating tapered shaft based on Timoshenko beam theory is presented by means of the finite element technique. The shaft which is assumed to have circular cross-section and linear taper is discretized into a number of finite elements with ten degrees of freedom each. The equation of motion of the rotating tapered shaft finite element is derived using Lagrange equation. Explicit expressions for the finite element mass, stiffness and gyroscopic matrices are derived by using consistent mass formulation. The shaft finite element is integrated into a procedure to calculate the natural frequecies of rotor-bearing systems. The generalized eigenvalue problem is defined and numerical solutions are generated for a wide range of whirl ratios, spin speeds and taper ratios. Comparisons are made with exact solutions and with numerical results available in the literature. The results display high accuracy when compared to other numerical results.

MASTER OF SCIENCE DEGREE

KING FAHD UNIVERSITY OF PETROLEUM AND MINERALS

Dhahran , Saudi Arabia

October 1992

خلاصة الرسالة

اسم الطالب الكامل : محمد أحمد محي الدين
عنوان الدراسة : الإهتزاز الإنحنائي والدوراني لمحاور التوصيل بواسطة طريقة العناصر المتناهية في الصغر .
التخصص : هندسة ميكانيكية .
تاريخ الشهادة : أكتوبر ١٩٩٢م .

الإهتزاز الإنحنائي والدوراني لمحور توصيل مائل بالإعتماد على نظرية تيموشينكو للعتبة بواسطة طريقة العناصر المتناهية في الصغر يدرس في هذه الرسالة محور التوصيل الذي يتم دراسته هنا ذا مقطع جانبي دائري وإنحناء متساوي يتم تقسيمه إلى عناصر متناهية الصغر لكل منها عشر اتجاهات في حرية الحركة . معادلة الحركة لمحور التوصيل يتم اشتقاقها بواسطة معادلة لاجرانج . المصفوفات الحاوية للتعابير الرمزية الممثلة للكتلة ومقاومة الإنحناء والدوران يتم إشتقاقها هنا بواسطة طريقة توزيع الكتلة المتكافىء . عناصر المحور المتناهية في الصغر يتم دمجها في نظام لحساب الإهتزازات الطبيعية لأنظمةالحمل الدورانية . بعد تعريف الإهتزازات الطبيعية يتم إيجاد حلول رقمية لعدد كبير في نسب الإهتزازات وسرعات الدوران ودرجات الإنحناء . ثم يتم مقارنة الحلول الموجودة في دراسات سابقة لهذه المشكلة مع الحلول الرقمية التي تم إيجادها في هذه الدراسة . نتائج هذه الدراسة تظهر أكثر دقة في نتائج الدراسات السابقة .

درجة الماجستير في العلوم
جامعة الملك فهد للبترول والمعادن
الظهران ـ المملكة العربية السعودية
أكتوبر ١٩٩٢م

Chapter I

INTRODUCTION

The progress of human civilization is closely associated with motion. In ancient times rotational motion was employed to achieve translation with the wheel and axle, or to store energy as in the sling. Much later, drive belts, gears and related mechanisms gave way to drive shafts, in transferring power from one point to another because of their advantages in efficiency, wear and adjustment. Since strength requirements are related to the torque carried by a shaft and the relationship between torque and rotational speed is inverse, for a given level of transmitted power, there has been a continuing trend towards higher and higher shaft speeds.

The flyball governor, which is among the early devices used to provide feedback control, depends upon rotational dynamics, high speed gyros may be considered their modern counterparts. Gas turbines have rotational speeds that were unheard of only a short time ago. Indeed the uses of rotating machinery are extremely diverse: in power stations, marine propulsion systems, aircraft engines, machine tools, automobiles, medical equipment, household accessories and many other applications.

On account of the ever increasing demand for power and high speed transportation, the rotors of these machines are made flexible, which makes the study of vibratory motion an essential part of design. The shafting of these machine installations is subjected to torsional and bending vibrations. In order to study the complex behavior of the system over a wide range of operating conditions, improved computational techniques are developed. It is estimated that about 1200 papers related to rotor dynamics have appeared by 1974 and another 1000 papers in the next decade. In recent times there is a clear indication that this learning process is accelerating [1].

In the past, the natural frequencies of bending and torsional motion have been so far separated from each other that they made dynamic coupling unlikely. Moreover the rationale behind ignoring coupling is that it is usually determined by mass unbalance, which is a small quantity. With the advent of supercritical-speed shafts, which often have relatively small diameter, the uncoupled torsional frequencies can fall into the same range as the bending frequencies which are below the operating speed. Therefore neglecting bending and torsional coupling may give inaccurate prediction of the critical speeds.

1.1 Literature Survey

The most extensive portion of the literature on the dynamics of rotating shafts is concerned with determining the critical speeds, modal shapes and unbalance response. The earliest papers were concerned with predicting first critical speeds and with balancing shafts for subcritical operations because most rotating machines were designed to operate below the first critical speed [2].

Modern rotating machines operate at very high speeds, far in excess of first critical. The more recent literature therefore treats rotating shafts as flexible with greater range of problems and phenomena. Topics such as the proximity of operating speed in relation to higher critical speeds, the extent of unstable regions and stresses during transition through lower critical speeds are all of practical interest to the designers of modern rotating machines [2].

During the past few decades various models for the determination of critical speeds, modal shapes and unbalance response of rotor-bearing systems have been developed and widely used. These models must allow flexibility in geometry, boundary conditions and loading in order to be applicable to a wide range of rotating machines. A rotor system consists of several elements such as bearings, disks, etc. Each element has a definite influence on the overall dynamic behaviour of the rotor system. Hence accurate modeling and proper articulation of the elements are essential to achieve reliable results. Some of the modeling methods are:

1. Jeffcot rotor model which is essentially a single mass mounted on a shaft supported on bearings.
2. Lumped parameter model, and
3. The finite element model with distributed system properties.

Similarly there are different solution procedures available to solve the resulting equations obtained by different modeling schemes. Some of the solution procedures are:

1. Direct method
2. Transfer matrix method
3. Modal analysis, and
4. Finite element method.

1.2 Direct Method

The direct method solution procedure is used to evaluate dynamic response of simple systems. Eshleman and Eubanks [3] derived the equation of motion of a simple shaft including the effects of applied axial torque, rotary inertia, transverse shear and gyroscopic moments by using second law of motion. They have given approximate formulae for the forward and backward whirl of the rotor. They have concluded that for values of slenderness ratio from zero to 0.0025, the constant axial torque term is important and it tends to lower the effective rotor stiffness and therefore the critical speeds. The importance of this effect decreases for higher critical speeds. The gyroscopic, transverse shear and rotary inertia effects become significant for slenderness ratios greater than 0.0025 and at higher critical speeds. Bernasconi [4] studied the behaviour of rotating shafts with unbalance. He reported that the longitudinal component of angular momentum caused by whirling induces torsional vibrations with a frequency double that of the rotational speed.

1.3 The Transfer Matrix Method.

In the transfer matrix method the generalized forces and displacements at one end of a shaft system are related to those at the other end by means of successive multiplication of matrices, which accounts for the effects of the stiffness and inertia properties of the various sections of the system. This technique yields as many critical speeds as, and to the degree of accuracy determined by, the number of stations into which the shaft is divided. This technique has been used to compute both the natural frequencies as a function of operating speed and the forced response due to unbalance loads, [2].

Prohl [5] presented a method to calculate critical speeds of flexible rotors. In this method the actual rotor must be transformed to an idealized equivalent system consisting of a series of disks connected by sections of elastic but massless shaft. The accuracy of the method depends entirely on how closely the idealized system and the idealized boundary conditions represent the actual rotor and its bearings. Lund [6] described a method for calculating the damped critical speeds of a flexible rotor in a fluid-film journal bearings. The rotor considered in this reference, consists of a uniform shaft supported at the ends on identical bearings. The contribution from shear deformation, rotary inertia and gyroscopic moments are neglected in the formulation, but it includes hysteretic internal damping in the shaft as well as the aerodynamic forces. Gu [7] proposed a transfer matrix - direct integration method which employs the transfer matrix method to derive the equation of motion of a " characteristic disk " and utilizes the direct integratrion method to determine the critical speeds and mode shapes of a rotor - bearing system. The rotor - bearing system considered consists of a uniform shaft. Yim et al [8] studied the effect of tangential load torque on the dynamics of rotors. They calculated the critical speeds using Galerkin's approach and a modified transfer matrix method. They have considered uniform shaft and excluded the effects of rotary inertia, shear deformation and gyroscopic moments in the formulation. Diken and Tadjbaksh [9] investigated the effect of coupling with torsion on the unbalance response of flexible rotors, supported by flexible isotropic and damped bearings. Internal damping, gyroscopic moments, rotary inertia and shear effects are taken into account. The governing differential equation of motion is solved numerically by transfer matrix method.

1.4 Modal Analysis

The idea of modal analysis is to uncouple the equation of motion by means of a linear coordinate transformation. The transformation matrix is called the modal matrix. The successful application of the method requires the solution of an eigenvalue problem associated with the given system.

Adams [10] presented an analysis which accounts for the nonlinear forces produced by fluid-film journal bearings under large amplitude vibration of rotor-bearing systems. The method presented in this paper can simulate steady state and transient vibrations of the system. Lee and Jei [11] calculated the backward and forward whirl speeds and mode shapes of a rotating uniform shaft for various spin speeds and boundary conditions using modal analysis. They derived the equation of motion of the rotor bearing system considering the shaft as nonuniform in cross-section but solved it only for the uniform case. Their formulation did not include the shear effect.

1.5 The Finite Element Method

The finite element method is a numerical procedure for solving a continuum mechanics problem with an accuracy acceptable to engineers. It is a relatively recent approach in which the continuum is discretized into finite elements. The deformations of the finite elements are described by interpolation functions. The rotating shaft is modeled using beam elements and the deformations are described by polynomials with piecewise constant coefficients. These coefficients are expressed as functions of the deflections at the nodal points [12].

1.5.1 Uniform Shaft

Ruhl and Booker [13] presented a procedure for calculating the critical speeds and unbalance response of a turborotor - bearing system. They derived the governing differential equations of motion of the shaft, bearings and disks separately. They considered a uniform shaft and did not include the effects of rotary inertia, shear and gyroscopic moments of the shaft. They have concluded that the finite element method is superior to transfer matrix method for problems of complex system topology. Nelson and McVaugh [14] studied rotor bearing systems, considering rotary inertia and gyroscopic moment effects. The equation of motion of the system is derived for a uniform shaft, both in rotating reference frame and fixed reference frame. They have presented the natural frequencies of a typical rotor bearing system consisting of a stepped shaft, a disk and bearings. The authors pointed out that the equation of motion in rotating reference frame is useful for isotropic systems since the two planes of motion can be treated separately, while the fixed frame equations provide the generality of handling problems with non symmetric stiffness and damping. Zorzi and Nelson [15] investigated the effect of constant axial torque on the dynamics of rotor bearing systems using the finite element method. The equation of motion is derived for a uniform shaft while the shear effect is neglected. The inclusion of axial torque gives rise to an incremental torsional stiffness matrix. They have corroborated the findings of Eshleman and Eubanks [3] that the critical speeds tend to decrease as the axial torque increases. Childs and Graviss [16] introduced an ordering scheme for the deflection variables in finite element based rotor dynamics models. This scheme permits solution of the equations through symmetric matrix procedures. This procedure is used to calculate the whirl speeds which coincide with multiples or fractions of the rotor natural frequencies.

However, this procedure cannot calculate rotor natural frequencies for a specified running speed. Rajan et al.[17] presented eigenvalue sensitivity coefficients for the damped natural frequencies for a linear rotor-bearing system modeled by the finite element method. However a uniform shaft is considered and shear effects are neglected in the formulation. Sakata et al.[18] analyzed the vibration of a light weight rotor system comprising a flexible disk with flexible blades and a flexible uniform shaft with rigid bearings in the case of steady turn of an aircraft. They have compared the computed values with experimental results. Sauer and Wolf [19] formulated the equations of motion for linear continuous structures containing gyroscopic effects. They derived a consistent gyroscopic matrix for a beam element assuming the polar moment of inertia as varying linearly over the length of the element. They have also given an analytical eigenfrequency formula to test the gyroscopic matrix.

Nelson [20] used Timoshenko beam theory to establish the shape functions for transverse vibration analysis of rotating uniform shafts. The model includes the effects of translational and rotary inertia, gyroscopic moments, bending and shear deformations, and axial loads. The shaft is assumed to be supported on rigid bearings. Flexible bearings and disks are not incorporated in the model. Ozguven and Ozkan [21] presented a dynamic model of rotor bearing systems with rigid disks, a flexible uniform shaft, and flexible bearings. The model presented include the effects of rotary inertia, gyroscopic moments, axial load, transverse shear deformation, internal viscous and hysteritic damping. They have given the natural frequencies of a uniform shaft supported on flexible bearings. Chen and Ku [22] used a three nodal C^0 Timoshenko beam finite element to analyze the natural whirl speeds of a rotating shaft with different end conditions, including the effects of translational and rotary inertia, gyroscopic moments, bending and shear deformations. The stiffness, mass and gyroscopic matrices are evaluated using numerical integration. The stiffness terms due to shear deformations are evaluated by using reduced integration. This avoids shear locking that occur when the beam is thin. Suarez et al.[23] developed equation of motion of a rotor subjected to base excitation by applying variational principles. To evaluate the importance of gyroscopic and parametric terms, they studied the seismic response characteristics of a rotating machine subjected to simulated base excitations. They observed that even for strong rotational inputs the parametric terms in the equation of motion may be neglected without affecting the response.

1.5.2 Tapered Shaft

The formulations reviewed in the previous section are based on a constant cross-section within the element. In practice rotors have tapered portions and a means of modeling such portions is desirable. Rouch and Kao [24] developed a tapered beam finite element for rotor dynamic analysis. They considered shear as a nodal variable and condensed it prior to assembly of system matrices. The element mass, stiffness and gyroscopic matrices are evaluated by means of Gauss-Legendre numerical integration technique. No results are presented for tapered rotating shafts. In addition to representing shear deformations by extra nodal coordinates, this formulation suffers the numerical burden of numerically evaluating the element matrices. Greenhill et al.[25] developed a conical beam finite element for rotor dynamic analysis, including the effects of rotary inertia, gyroscopic moments, damping and shear deformation. They included the shear deformation as a nodal variable and condensed it prior to assembly into the global system matrices. They did not present natural frequencies of tapered shafts. Their method, however, relies on the condensation technique which aims at eliminating the additional shear deformation nodal variables. Genta and Gugliotta [26] developed an axisymmetrical conical beam finite element with two complex degrees of freedom at each node based on Timoshenko beam theory. The numerical results are compared to the natural frequencies of tapered conical nonrotating cantilevers presented in reference [27], but the natural frequencies of tapered rotating shafts are not given. The formulation of reference [26], however, becomes cumbersome if the whole system is not axisymmetric. It is also apparent that the accuracy has been compromised for the sake of efficiency. Gmur and Rodrigues [28] presented linearly tapered C^0 - compatible finite elements which have a variable number of nodal points for modeling the rotor-bearing systems. They included the effects of translational and rotary inertia, gyroscopic moments, damping, and shear deformation. The element matrices are found by means of numerical quadrature. These elements show a convergence pattern similar to the one obtained with the conventional C^1 - compatible shaft elements. They presented the first backward and forward bending frequencies of a tapered, hollow rotating shaft. However, the element matrices were numerically generated.

It has been noted that the formulations in which shear deformation is taken as nodal variables are suited to applications involving simple structures constrained only at the ends, and without geometric nonlinearities, [26]. Such methods when applied to complex rotor system, envoke the matrix condensation technique at the element level, thus dropping the degrees of freedom related to shear deformations. Accordingly, the discontinuities of shear deformations are neglected.

1.6 Other Techniques

Researchers, have developed several other elastodynamic models to analyze the dynamic behavior of rotor bearing systems. Genta [29] derived the equation of motion for the study of the flexural dynamic behaviour of unsymmetrical rotors, based on the finite element method and the use of complex coordinates. The model takes into account the nonrotating parts of the machine including both viscous and hysteritic damping. Nikolajsen and Holmes [30] described a numerical method for free and forced vibration analysis of a rotor-bearing system. In this method, the flexibility influence coefficients are used to set up equation of motion of the system. Haddara [31] presented an approximate method to calculate the natural frequencies of transverse vibrations of a propeller shaft system by modeling the propeller as a rotor. Shiau and Hwang [32] presented an approach in which they used the assumed mode expansion method to derive the equation of motion of the system and the properties of Rayleigh quotient to analyze the critical speeds of undamped rotor-bearing systems. They have not included the effect of shear in the formulation, which is valid for shafts with uniform cross-sections only. Shiau and Hwang [12] modified the approach presented in reference [32] and designated it as Generalized Polynomial Expansion Method (GPEM). They investigated the critical speeds and mode shapes of linear, damped rotor-bearing system using GPEM. Hwang and Shiau [33] utilized the GPEM to model a large order flexible-rotor system with nonlinear supports.

Apparently, there is a need to formulate a general elastodynamic model using finite element. A fairly general model must account for the dynamic coupling between bending and torsional deformations. In addition, the finite element formulation takes into account the shear deformations, rotary inertia, gyroscopic effects, damping, as well as variable shaft geometry and bearing locations.

The literature survey for eigenproblem solution is presented in section 3.5.1.

1.7 Proposed Research

The following are the objectives of this study:

1. To formulate the elastodynamic model of a general rotor-bearing system using the finite element method. The developed model accounts for the coupling between bending and torsional vibration, as well as the effect of rotary inertia, shear deformation and the gyroscopic moment.
2. To develop a conical beam finite element to accurately model the geometry of the shaft. The finite element has two nodes at its ends. Each node has five degrees of freedom; two transverse displacements, two bending rotations and a torsional rotation. The effect of shear is included in the shape functions by means of a shear parameter. This avoids taking shear as nodal variable, thus reducing the bandwidth of the system matrices. The explicit form of mass, stiffness and gyroscopic matrices of the conical beam finite element are derived and tabulated.
3. To incorporate the conical beam finite element in the model developed for the free vibrational analysis of rotor-bearing systems. A rotor-bearing system consists of disks and bearings in addition to the shaft. The disks are modeled as rigid, and linear bearing models are used. The bearings can be damped and orthotropic. The equation of motion of the disk and bearings, and their respective inertia, stiffness and damping matrices are derived. The rotor-bearing system equation of motion is obtained by assembling the component equations of motion. The associated generalized eigenvalue problem

is then formulated. A finite element program is developed to generate the consistent element matrices where the effects of rotary inertia, gyroscopic moments, shear deformations and damping in bearings are accounted for at the element level.

4. To perform numerical studies on the natural frequencies of a tapered rotating shaft. The natural frequencies are obtained by solving the eigenvalue problem in either the fixed frame coordinates or the rotating frame coordinates. The eigenvalue problem in the fixed and the rotating frames cannot be solved by a single numerical scheme, therefore two different numerical schemes are employed.

Chapter II

THE ELASTODYNAMIC MODEL OF A ROTOR

2.1 Introduction

The basic elements of a rotor are the shaft, the disk and the bearing. The dynamic analysis of rotors, in general, includes the following important features:

1. Shear deflection and rotary inertia effects.
2. Gyroscopic effects which couple the motion in two directions.
3. Variable shaft geometry, e.g. tapered, stepped, solid as well as hollow shaft sections.
4. Type of bearings, e.g. rigid, isotropic, orthrotropic, etc.
5. Internal damping and aerodynamic effects.

In this chapter, the general assumptions are stated. The kinetic and potential energy equations are obtained, and finally, the general governing differential equation of motion for the rotor are derived by means of the Lagrangian approach.

The system to be analyzed is shown in Figure 2.1. The rotor of length L is rotating at a speed of $\dot{\theta}(t)$. Two reference frames are employed to describe the system motion. One is the fixed reference R_o ($X\ Y\ Z$) and the other is a rotating reference R ($x\ y\ z$). The X- and x- axis are colinear and coincident with the undeformed rotor centerline. The two reference frames are defined by a difference in angle of θ about X-axis.

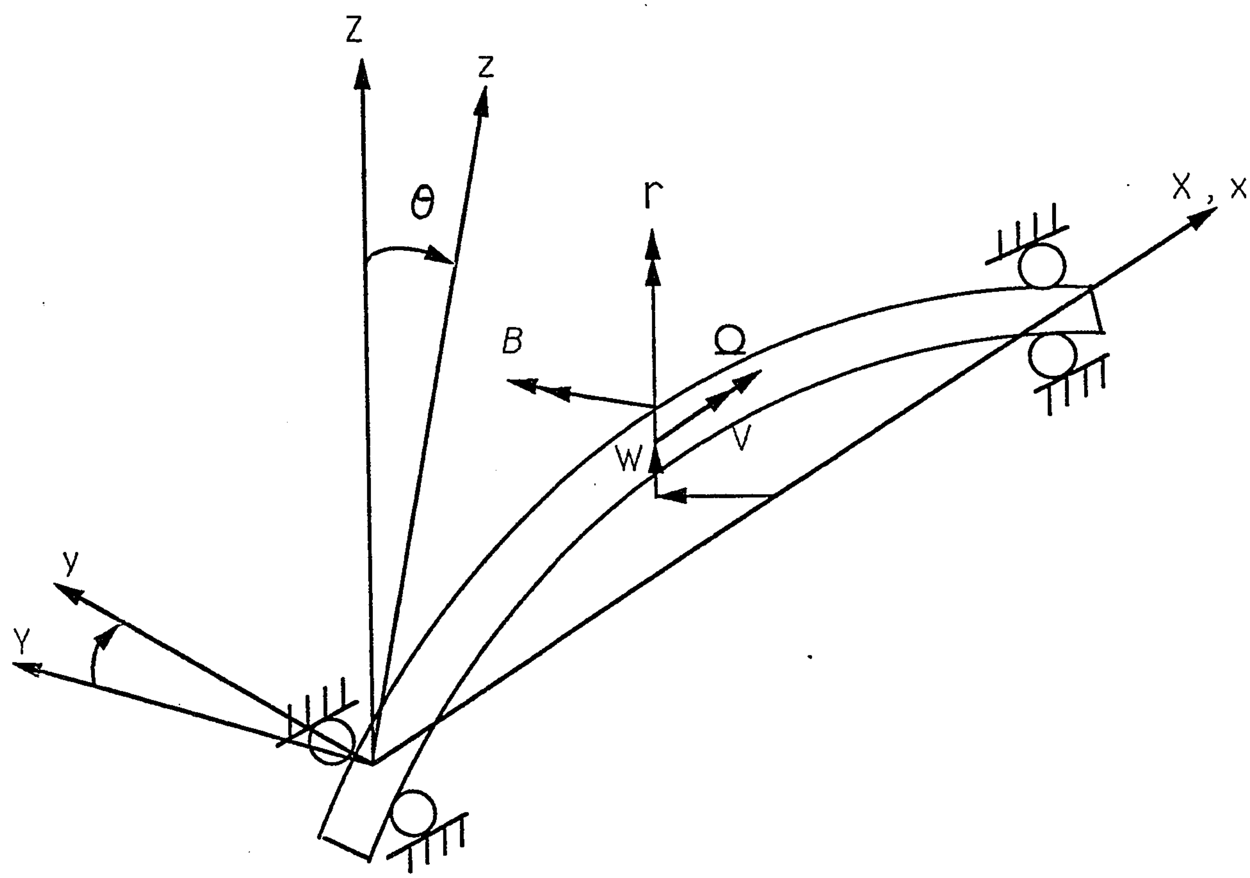

Figure 2.1: Displacement Variables and Coordinate Systems of a Rotating Shaft

2.1.1 General Assumptions

1. The material of the rotor is elastic, homogeneous and isotropic.
2. The plane cross-sections initially perpendicular to the neutral axis of the rotor remain plane, but no longer perpendicular to the neutral axis during bending.
3. The deflection of the rotor is produced by the displacement of points of the center line.
4. The axial motion of the rotor is small and can be neglected.
5. The shaft is flexible, while disks are treated as rigid.
6. Internal damping and aerodynamic forces are neglected.

2.2 The Shaft

The finite element method is used to model the shaft. Referring to Figure 2.2 let $X^i\ Y^i\ Z^i$ be a cartesian coordinate system with its origin affixed to the undeformed beam element. The $x\,y\,z$ is a cartesian coordinate system after the deformation of the beam element. The $x\,y\,z$ coordinate system is related to the $X^i\ Y^i\ Z^i$ coordinate system through a set of angles φ ,β and γ. To achieve the orientation of any cross-section of the beam element, one first rotates it by an angle $(\theta + \varphi)$ around the X^i – axis, then by an angle β around the new y axis, denoted by y_2 and lastly by an angle γ around the final z axis. The instantaneous angular velocity vector $\bar{\omega}$ of the $x\ y\ z$ frame may be expressed as

$$\bar{\omega} = (\dot{\theta} + \dot{\varphi})\,\hat{i} + \dot{\beta}\,\hat{j}_2 + \dot{\gamma}\,\hat{k} \qquad (\hat{k}_3 = \hat{k}) \tag{2.1}$$

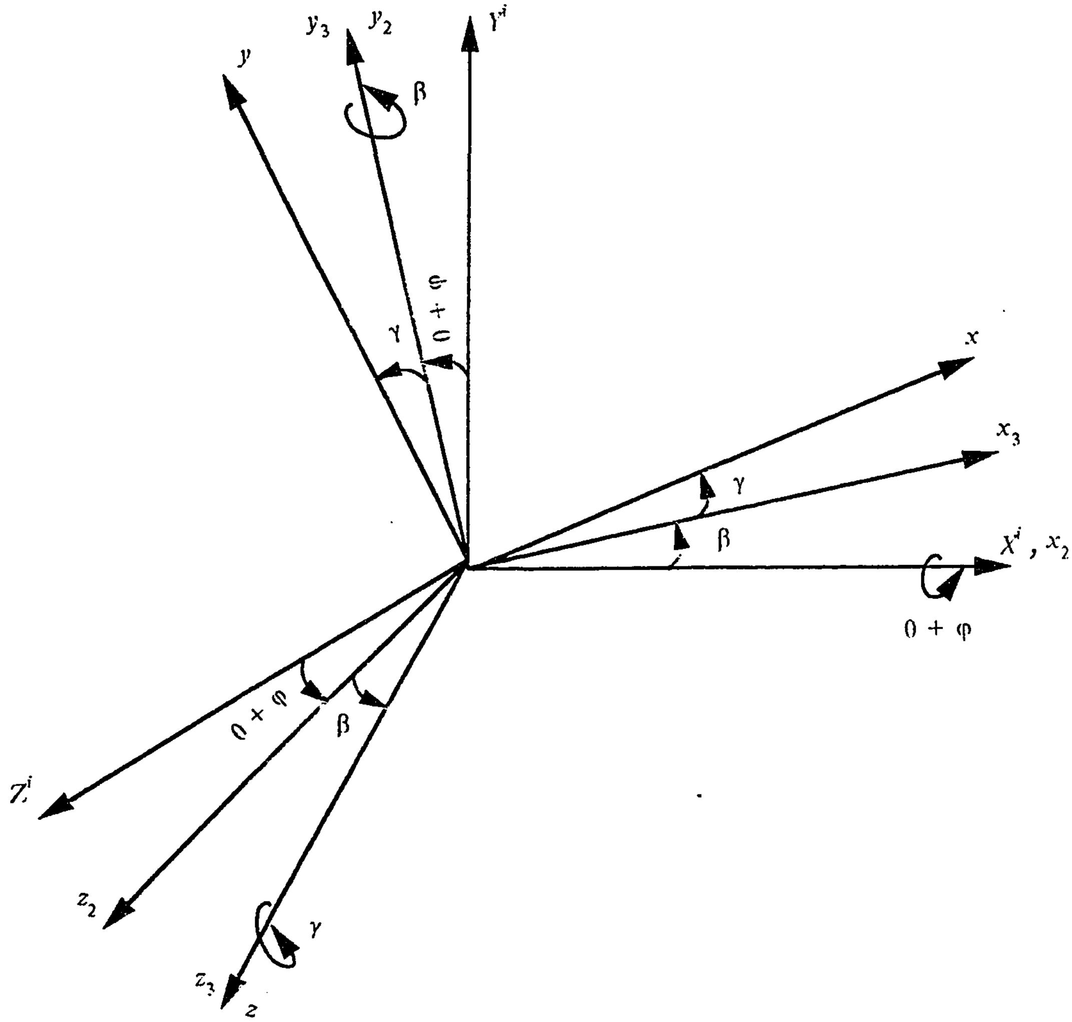

Figure 2.2: Cross-section Rotation Angles

where $\hat{I}, \hat{j}_2$ and $\hat{k}$ are unit vectors along the axes X, y_2 and z. Transforming eqn (2.1) to $X\,Y\,Z$ coordinate system, we can write

$$\bar{\omega} = (\dot{\theta} + \dot{\varphi})\hat{I} + \dot{\beta}\,[\cos(\theta + \varphi)\hat{J} + \sin(\theta + \varphi)\hat{K}] + \dot{\gamma}\,[-\sin\beta\,\hat{I} - \sin(\theta + \varphi)\cos\beta\,\hat{J} + \cos\beta\,\cos(\theta + \varphi)\hat{K}] \tag{2.2}$$

Assuming γ and β to be small, that is

$$\cos\beta = \cos\gamma = 1$$

and

$$\sin\beta = \beta, \quad \sin\gamma = \gamma$$

The angular velocity vector becomes

$$\begin{aligned}
\bar{\omega} &= (\dot{\theta} + \dot{\varphi})\hat{I} + \dot{\beta}\,[\cos(\theta + \varphi)\hat{J} + \sin(\theta + \varphi)\hat{K}] \\
&\quad + \dot{\gamma}\,[-\beta\,\hat{I} - \sin(\theta + \varphi)\hat{J} + \cos(\theta + \varphi)\hat{K}] \\
&= (\dot{\theta} + \dot{\varphi} - \dot{\gamma}\beta)\hat{I} + [\dot{\beta}\cos(\theta + \varphi) - \dot{\gamma}\sin(\theta + \varphi)]\hat{J} \\
&\quad + [\dot{\beta}\sin(\theta + \varphi) + \dot{\gamma}\cos(\theta + \varphi)]\hat{K}
\end{aligned}$$

or

$$\bar{\omega} = \begin{Bmatrix} \omega_x \\ \omega_y \\ \omega_z \end{Bmatrix} = \begin{Bmatrix} \dot{\theta} + \dot{\varphi} - \dot{\gamma}\beta \\ \dot{\beta}\cos(\theta + \varphi) - \dot{\gamma}\sin(\theta + \varphi) \\ \dot{\beta}\sin(\theta + \varphi) + \dot{\gamma}\cos(\theta + \varphi) \end{Bmatrix} \tag{2.3}$$

2.2.1 Kinetic Energy

Referring to Figure 2.3 let p^i be any point in the undeformed beam element. With respect to $X^i\,Y^i\,Z^i$ coordinate system, point p^i is defined by the vector $\bar{r}_o$. In the deformed beam element point p represents point p^i. The location of p with respect to $X^i\,Y^i\,Z^i$ coordinate system is given by the vector $\bar{r}$. The point p is located globally by the vector $\bar{r}_p$.

$$\bar{r}_p = \bar{R} + \bar{r}$$

Where $\bar{R}$ defines the location of the origin of the $X^i\ Y^i\ Z^i$ coordinate system with respect to global coordinate system $X\ Y\ Z$.

The vector $\bar{r}$ can be represented as

$$\bar{r} = \bar{r}_o + \bar{u}$$

Therefore the position vector $\bar{r}_p$ of point p can be written as

$$\bar{r}_p = \bar{R} + \bar{r}_o + \bar{u} \tag{2.4}$$

where $\bar{u}$ represents the deformation vector of point p^i. Differentiating $\bar{r}_p$ with respect to time yields the velocity of point p.

$$\begin{aligned} \frac{d\bar{r}_p}{dt} &= \dot{\bar{r}}_p + \bar{\omega} \times \bar{r}_p \\ &= \dot{\bar{r}}_p + [\tilde{\omega}]\{r_p\} \end{aligned} \tag{2.5}$$

where the matrix $[\tilde{\omega}]$ is given by

$$[\tilde{\omega}] = \begin{bmatrix} 0 & -\omega_z & \omega_y \\ \omega_z & 0 & -\omega_x \\ -\omega_y & \omega_x & 0 \end{bmatrix}$$

Using the finite element analysis the vector $\bar{u}$ can be written as

$$\bar{u} = \{u\} = [N_v]\{e\} \tag{2.6}$$

where $\{e\}$ is the vector containing the nodal coordinates and $[N_v]$ is the translation shape function, which is fully defined in the next chapter.

There is no change in the magnitude of $\bar{R}$ and $\bar{r}_o$ when the beam element deforms. Therefore the rate of change of magnitude of the position vector $\bar{r}_p$ is given by

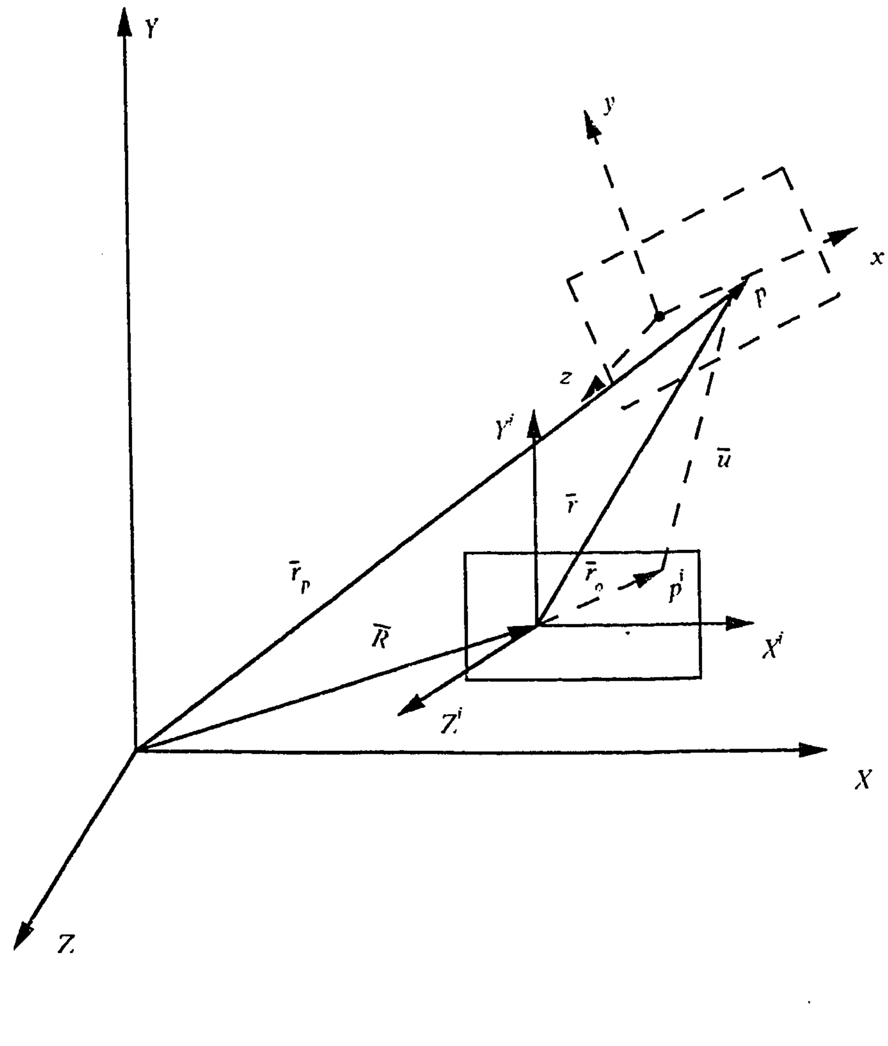

Figure 2.3: Generalized Coordinates of the ith Element

$$\{\dot{r}_p\} = \{\dot{u}\} = [N_v]\{\dot{e}\} \tag{2.7}$$

substituting eqn (2.7) in eqn (2.5), we get

$$\frac{d\bar{r}_p}{dt} = [N_v]\{\dot{e}\} + [\tilde{\omega}]\{r_p\}$$

$$= [N_v \;\; \tilde{\omega}]\begin{Bmatrix}\dot{e}\\ r_p\end{Bmatrix} \tag{2.8}$$

The kinetic energy of the element is obtained by integrating the kinetic energy of the infinitesimal volume at point p over the volume V

$$T = \frac{1}{2}\int_V \mu \left\{\frac{dr_p}{dt}\right\}^T \left\{\frac{dr_p}{dt}\right\} dV$$

$$= \frac{1}{2}\int_V \mu \left[\dot{e}^T \;\; r_p^T\right] \begin{Bmatrix}N_v^T\\ \tilde{\omega}^T\end{Bmatrix} \left[N_v \;\; \tilde{\omega}\right] \begin{Bmatrix}\dot{e}\\ r_p\end{Bmatrix} dV$$

$$= \frac{1}{2}\int_V \mu \Big[\{\dot{e}\}^T [N_v]^T [N_v]\{\dot{e}\} + \{\dot{e}\}^T [N_v]^T [\tilde{\omega}]\{r_p\} + \{r_p\}^T [\tilde{\omega}]^T [N_v]\{\dot{e}\}$$

$$+ [r_p]^T [\tilde{\omega}]^T [\tilde{\omega}]\{r_p\} \Big] dV \tag{2.9}$$

where μ is the mass density of the beam element.

The first term in eqn (2.9) gives the kinetic energy due to translation, the second and third terms are identically zero if moments of inertia are calculated with respect to centre of mass of the element. The last term gives kinetic energy due to rotation that includes gyroscopic moments. To evaluate the last. term one can utilize the following expression:

$$[\tilde{\omega}]^T[\tilde{\omega}] = \begin{bmatrix} \omega_z^2 + \omega_y^2 & -\omega_x\omega_y & -\omega_z\omega_x \\ -\omega_x\omega_y & \omega_z^2 + \omega_x^2 & -\omega_y\omega_z \\ -\omega_x\omega_z & -\omega_y\omega_z & \omega_y^2 + \omega_x^2 \end{bmatrix} \tag{2.10}$$

Therefore

$$\int_V \mu \{r_p\}^T [\tilde{\omega}]^T [\tilde{\omega}] \{r_p\}\, dV = \int_0^l \mu \left(I_x \omega_x^2 + I_y \omega_y^2 + I_z \omega_z^2 \right) dx \qquad (2.11)$$

Substituting eqn (2.3) in eqn (2.11), we get

$$\int_V \mu \{r_p\}^T [\tilde{\omega}]^T [\tilde{\omega}] \{r_p\}\, dV = \int_0^l \mu \Big[I_x (\dot{\theta} + \dot{\varphi} - \dot{\gamma}\beta)^2 + I_y \{ \dot{\beta} \cos(\theta + \varphi)$$

$$- \dot{\gamma} \sin(\theta + \varphi) \}^2 + I_z \{ \dot{\beta} \sin(\theta + \varphi) + \dot{\gamma} \cos(\theta + \varphi) \}^2 \Big] dx \qquad (2.12)$$

Equation (2.12) can be written in the form

$$\frac{1}{2} \int_V \mu \{r_p\}^T [\tilde{\omega}]^T [\tilde{\omega}] \{r_p\}\, dV = \frac{1}{2} \int_0^l I_p (\dot{\theta}^2 + \dot{\varphi}^2)\, dx + \int_0^l I_p \dot{\theta} \dot{\varphi}\, dx$$

$$- \int_0^l I_p (\dot{\theta} + \dot{\varphi}) \dot{\gamma} \beta\, dx + \frac{1}{2} \int_0^l I_D (\dot{\beta}^2 + \dot{\gamma}^2)\, dx$$

or simply as

$$= \frac{1}{2} \int_0^l I_p \dot{\theta}^2\, dx + \frac{1}{2} \int_0^l I_p \dot{\varphi}^T \dot{\varphi}\, dx + \int_0^l I_p \dot{\theta} \dot{\varphi}\, dx$$

$$- \int_0^l I_p (\dot{\theta} + \dot{\varphi}) \dot{\gamma}^T \beta\, dx + \frac{1}{2} \int_0^l I_D \begin{Bmatrix} \dot{\beta} \\ \dot{\gamma} \end{Bmatrix}^T \cdot \begin{Bmatrix} \dot{\beta} \\ \dot{\gamma} \end{Bmatrix} dx \qquad (2.13)$$

where

$$\mu I_y = \mu I_z = I_D \quad \text{and} \quad \mu I_x = I_p$$

One can express the following variables as:

$$\begin{aligned} \varphi &= [N_\varphi] \{e\}, & \dot{\varphi} &= [N_\varphi] \{\dot{e}\} \\ \beta &= [N_\beta] \{e\}, & \dot{\beta} &= [N_\beta] \{\dot{e}\} \\ \gamma &= [N_\gamma] \{e\}, & \dot{\gamma} &= [N_\gamma] \{\dot{e}\} \end{aligned} \qquad (2.14)$$

where

$[N_\varphi]$ = torsional shape function

$[N_\beta], [N_\gamma]$ = rotational shape function

Therefore, eqn (2.13) becomes

$$\frac{1}{2}\int_V \mu \{r_p\}^T [\tilde{\omega}]^T [\tilde{\omega}] \{r_p\} \, dV = \frac{1}{2}\int_0^l I_p \dot{\theta}^2 \, dx + \frac{1}{2}\int_0^l \{\dot{e}\}^T [N_\varphi]^T I_p [N_\varphi] \{\dot{e}\} \, dx + \int_0^l I_p \dot{\theta} \dot{\varphi} \, dx$$

$$- \int_0^l \{\dot{e}\}^T [N_\gamma]^T I_p \dot{\theta} [N_\beta] \{e\} \, dx - \int_0^l \{\dot{e}\}^T [N_\gamma]^T I_p [N_\beta] \{e\} [N_\varphi] \{\dot{e}\} \, dx$$

$$+ \frac{1}{2}\int_0^l \{\dot{e}\}^T \begin{bmatrix} N_\beta \\ N_\gamma \end{bmatrix}^T I_D \begin{bmatrix} N_\beta \\ N_\gamma \end{bmatrix} \{\dot{e}\} \, dx \qquad (2.15)$$

The term $\int_0^l I_p \dot{\theta} \dot{\varphi} \, dx$ gives the inertia coupling between rigid body coordinates and elastic coordinates. For constant $\dot{\theta}$ this term has no contribution to the equation of motion of the rotor. Neglecting this term and introducing the following expressions:

$$\int_0^l I_p \, dx = C_1$$

$$\int_0^l I_p [N_\varphi]^T [N_\varphi] \, dx = [M_\varphi]$$

$$\int_0^l I_p [N_\gamma]^T [N_\beta] \, dx = [G_1]$$

$$\int_0^l I_p [N_\gamma]^T [N_\beta] \{e\} [N_\varphi] \, dx = [M_e]$$

and

$$\int_0^l I_D \begin{bmatrix} N_\beta \\ N_\gamma \end{bmatrix}^T \begin{bmatrix} N_\beta \\ N_\gamma \end{bmatrix} dx = [M_r]$$

Equation (2.15) reduces to

$$\frac{1}{2}\int_V \mu \{r_p\}^T [\tilde{\omega}]^T [\tilde{\omega}] \{r_p\}\, dV = \frac{1}{2} C_1 \dot{\theta}^2 + \frac{1}{2}\{\dot{e}\}^T [M_\varphi] \{\dot{e}\} - \dot{\theta}\{\dot{e}\}^T [G_1] \{e\}$$

$$- \{\dot{e}\}^T [M_c] \{\dot{e}\} + \frac{1}{2}\{\dot{e}\}^T [M_r] \{\dot{e}\} \tag{2.16}$$

Hence, the kinetic energy of the beam element given by eqn (2.9) can be written as

$$T = \frac{1}{2}\{\dot{e}\}^T [M_t] \{\dot{e}\} + \frac{1}{2} C_1 \dot{\theta}^2 + \frac{1}{2}\{\dot{e}\}^T [M_\varphi] \{\dot{e}\} - \dot{\theta}\{\dot{e}\}^T [G_1] \{e\}$$

$$- \{\dot{e}\}^T [M_c] \{\dot{e}\} + \frac{1}{2}\{\dot{e}\}^T [M_r] \{\dot{e}\}$$

$$= \frac{1}{2}\{\dot{e}\}^T [M] \{\dot{e}\} + \frac{1}{2} C_1 \dot{\theta}^2 - \dot{\theta}\{\dot{e}\}^T [G_1] \{e\} \tag{2.17}$$

where

$$[M] = [M_t] + [M_r] + [M_\varphi] - 2[M_c] \tag{2.18}$$

is the composite mass matrix and $\dot{\theta}$ denotes the rigid body rotation.

2.2.2 Strain Energy

Since the axial deformation is neglected, a typical cross-section of the shaft located at a distance x from the left end, in a deformed state, is described by the translations $v(x, t)$ and $w(x, t)$ in the $Y-$ and $Z-$ directions and small rotations $\varphi(x, t)$, $\beta(x, t)$ and $\gamma(x, t)$ about X, j_2 and k axes.

The two translations (v, w) consist of a contribution (v_b, w_b) due to bending and a contribution (v_s, w_s) due to shear deformations. These may be written as

$$v(x, t) = v_b(x, t) + v_s(x, t)$$

$$w(x, t) = w_b(x, t) + w_s(x, t) \tag{2.19}$$

The rotations (β, γ) are related to bending deformations (v_b, w_b) by the following expressions:

$$\beta(x,t) = -\frac{\partial w_b(x,t)}{\partial x}$$

$$\gamma(x,t) = \frac{\partial v_b(x,t)}{\partial x} \tag{2.20}$$

The strain energy expression is

$$U_1 = \frac{1}{2}\int_V \varepsilon^t \sigma \, dV \tag{2.21}$$

where ε is the strain due to bending, which can be expressed as

$$\varepsilon = -y\frac{\partial^2 v_b^*}{\partial x^2} - z\frac{\partial^2 w_b^*}{\partial x^2} \tag{2.22}$$

Recalling the stress-strain relationship $\sigma = E\,\varepsilon$, one can write the strain energy in the form

$$U_1 = \frac{E}{2}\int_V \varepsilon^t \varepsilon \, dV \quad = \quad \frac{E}{2}\int_V \varepsilon^2 \, dV \tag{2.23}$$

Using eqn (2.22) into eqn (2.23), one gets

$$U_1 = \frac{E}{2}\int_0^l \int_A \left(-y\frac{\partial^2 v_b^*}{\partial x^2} - z\frac{\partial^2 w_b^*}{\partial x^2} \right)^2 dA\,dx$$

$$= \frac{E}{2}\iint_{0A}^{l} \left[y^2\left(\frac{\partial^2 v_b^*}{\partial x^2}\right)^2 + z^2\left(\frac{\partial^2 w_b^*}{\partial x^2}\right)^2 + 2yz\,\frac{\partial^2 v_b^*}{\partial x^2}\,\frac{\partial^2 w_b^*}{\partial x^2} \right] dA\,dx \tag{2.24}$$

Because of symmetry the integral corresponding to the third term in eqn (2.24) is zero.

We have

$$I_z = \int_A y^2 \, dA \quad \text{and} \quad I_y = \int_A z^2 \, dA \tag{2.25}$$

Therefore the strain energy due to bending is

$$U_1 = \frac{E}{2} \int_0^l \left[I_z \left(\frac{\partial^2 v_b^*}{\partial x^2} \right)^2 + I_y \left(\frac{\partial^2 w_b^*}{\partial x^2} \right)^2 \right] dx \tag{2.26}$$

The shear strain in X-Z plane is

$$\nu_{xz} = \frac{\partial u}{\partial z} + \frac{\partial w_s}{\partial x} = \frac{\partial w^*}{\partial x} - \frac{\partial w_b^*}{\partial x} \tag{2.27}$$

Similarly, shear strain in X-Y plane is

$$\nu_{xy} = \frac{\partial v^*}{\partial x} - \frac{\partial v_b^*}{\partial x} \tag{2.28}$$

Strain energy due to shear deformation is given by

$$U_2 = \int_V (\tau_{xy} \, \nu_{xy} + \tau_{xz} \, \nu_{xz}) \, dV \tag{2.29}$$

The shear stress τ_{xy} corresponding to a given shear force vary over the cross-section. It follows that the corresponding shear strain will also vary over the cross-section. This variation can be accounted for by introducing the shear correction factor κ, which depends upon the shape of the cross-section, such that

$$\tau_{xy} = \kappa G \nu_{xy} \quad \text{and} \quad \tau_{xz} = \kappa G \nu_{xz} \tag{2.30}$$

For an isotropic material the shear modulus G is given by

$$G = \frac{E}{2(1 + \nu)} \tag{2.31}$$

where ν is Poission's ratio. The shear correction factor κ is given by, [34]

$$\kappa = \frac{6(1+\nu)}{7+6\nu} \qquad \text{for solid circular cross-section} \tag{2.32}$$

and

$$\kappa = \frac{6(1+\nu)(1+m^2)^2}{(7+6\nu)(1+m^2)^2 + (20+12\nu)m^2} \qquad \text{for hollow circular cross-section} \tag{2.33}$$

where m is the ratio of inner radius to the outer radius.

Therefore, eqn (2.29) can be expressed in the form

$$U_2 = \frac{1}{2}\int_V \kappa G(\gamma_{xy}^{\ 2} + \gamma_{xz}^{\ 2})$$

$$= \frac{1}{2}\int_0^l \kappa\, G\, A(x)\left[\left(\frac{\partial v^*}{\partial x} - \frac{\partial v_b^*}{\partial x}\right)^2 + \left(\frac{\partial w^*}{\partial x} - \frac{\partial w_b^*}{\partial x}\right)^2\right] dx \tag{2.34}$$

Expressing the strain energies as a function of v and w , components of displacement in R_0, using

$$v^* = v\cos\theta - w\sin\theta$$

$$w^* = v\sin\theta + w\cos\theta \tag{2.35}$$

Therefore,

$$U_1 = \frac{E}{2}\int_0^l \left[I_z\left(\cos\theta\,\frac{\partial^2 v_b}{\partial x^2} - \sin\theta\,\frac{\partial^2 w_b}{\partial x^2}\right)^2 \right.$$

$$\left. + I_y\left(\cos\theta\,\frac{\partial^2 w_b}{\partial x^2} + \sin\theta\,\frac{\partial^2 v_b}{\partial x^2}\right)^2\right] dx \tag{2.36}$$

Since the shaft is symmetric ($I_y = I_z = I$), the strain energy due to bending becomes,

$$U_1 = \frac{E}{2}\int_0^l I(x)\left[\left(\frac{\partial^2 v_b}{\partial x^2}\right)^2 + \left(\frac{\partial^2 w_b}{\partial x^2}\right)^2 \right] dx$$

$$= \frac{E}{2}\int_0^l I(x)\left[\left(\frac{\partial \gamma}{\partial x}\right)^2 + \left(\frac{\partial \beta}{\partial x}\right)^2 \right] dx \tag{2.37}$$

Similarly the strain energy due to shear becomes

$$U_2 = \frac{1}{2}\int_0^l \kappa\, G\, A(x)\left[\left(\frac{\partial v_s}{\partial x}\right)^2 + \left(\frac{\partial w_s}{\partial x}\right)^2 \right] dx \tag{2.38}$$

Also, the strain energy due to torsion is given by

$$U_3 = \frac{1}{2}\int_0^l G\, J\left(\frac{\partial \varphi}{\partial x}\right)^2 dx \tag{2.39}$$

Therefore, the total strain energy of the shaft is

$$U = \frac{1}{2}\int_0^l E\, I(x)\left[\left(\frac{\partial \gamma}{\partial x}\right)^2 + \left(\frac{\partial \beta}{\partial x}\right)^2 \right] dx$$

$$+ \frac{1}{2}\int_0^l \kappa\, G\, A(x)\left[\left(\frac{\partial v_s}{\partial x}\right)^2 + \left(\frac{\partial w_s}{\partial x}\right)^2 \right] dx + \frac{1}{2}\int_0^l G\, J\left(\frac{\partial \varphi}{\partial x}\right)^2 dx \tag{2.40}$$

After substituting eqns (2.19) and (2.20), into eqn (2.40), it can be written as

$$U = \frac{1}{2}\int_0^l E\, I\left\{ \left(\frac{\partial \beta}{\partial x}\right)^2 + \left(\frac{\partial \gamma}{\partial x}\right)^2 \right\} dx + \frac{1}{2}\int_0^l \kappa\, G\, A\left\{ \left(\frac{\partial v}{\partial x} - \gamma\right)^2 + \left(\frac{\partial w}{\partial x} + \beta\right)^2 \right\} dx$$

$$+ \frac{1}{2}\int_0^l G\, J\left(\frac{\partial \varphi}{\partial x}\right)^2 dx \tag{2.41}$$

Equation (2.41) can be written in matrix form as

$$[U] = \frac{1}{2}\{e\}^T [K]\{e\} \tag{2.42}$$

where $[K]$ is the composite stiffness matrix given by

$$[K] = [K_e] + [K_s] + [K_\varphi] \tag{2.43}$$

where

$[K_e]$ = elastic stiffness matrix

$[K_s]$ = shear stiffness matrix

$[K_\varphi]$ = torsional stiffness matrix

2.3 Equation of Motion of the Element

The equation of motion of the element can be derived using Lagrange equation, which can be mathematically written as

$$\frac{d}{dt}\left(\frac{\partial L}{\partial \dot{q}}\right) - \frac{\partial L}{\partial q} = Q \tag{2.44}$$

where

$L = T - U =$ Lagrangian function

q = generalized coordinates

Q = vector of generalized forces

Substituting L in the above equation, the equation of motion are obtained as

$$C_1\ddot{\theta} = Q \tag{2.45}$$

where C_1 is as defined in eqn (2.16) and

$$[M]\{\ddot{e}\} - \dot{\theta}\left([G_1]^T - [G_1]\right)\{\dot{e}\} + [K]\{e\} = Q \tag{2.46}$$

Denoting

$$[G_1] - [G_1]^T = [G]$$

Then, eqn (2.46) becomes

$$[M]\{\ddot{e}\} + \dot{\theta}[G]\{\dot{e}\} + [K]\{e\} = Q \tag{2.47}$$

where

$[M]$ = composite mass matrix

$[G]$ = gyroscopic matrix

$[K]$ = composite stiffness matrix

Chapter III

FINITE ELEMENT FORMULATION

The rotor configuration can be defined by a properly generated mesh of finite beam elements. The disk and bearing properties are added at respective nodes. In this formulation beam elements are linearly tapered. A linearly tapered beam element of circular cross-section has its radius varying linearly with length, so that area and moment of inertia are second and fourth order functions of axial position, respectively. Combination of unequal beam elements are permitted by the model developed in this study. The element consists of two nodes and each node has five degrees of freedom; two transverse displacements (v, w), two bending rotations (β, γ) and a torsional rotation (φ).

3.1 Tapered Beam Element

A typical axial cross-section of a linearly tapered finite element is shown in Figure 3.1. It is assumed that the cross-sectional properties in a given element are a continuous function of axial position, and the element cross-section has two planes of symmetry X-Z and X-Y.

Each end of the element is associated with an inner and outer radius, denoted by r and R, with the subscripts k and j referring to the left end ($x = 0$) and right end ($x = l$) of the element, respectively. Defining a non-dimensional position coordinate ξ equal to the ratio x/l, the inner and outer radii may be expressed as

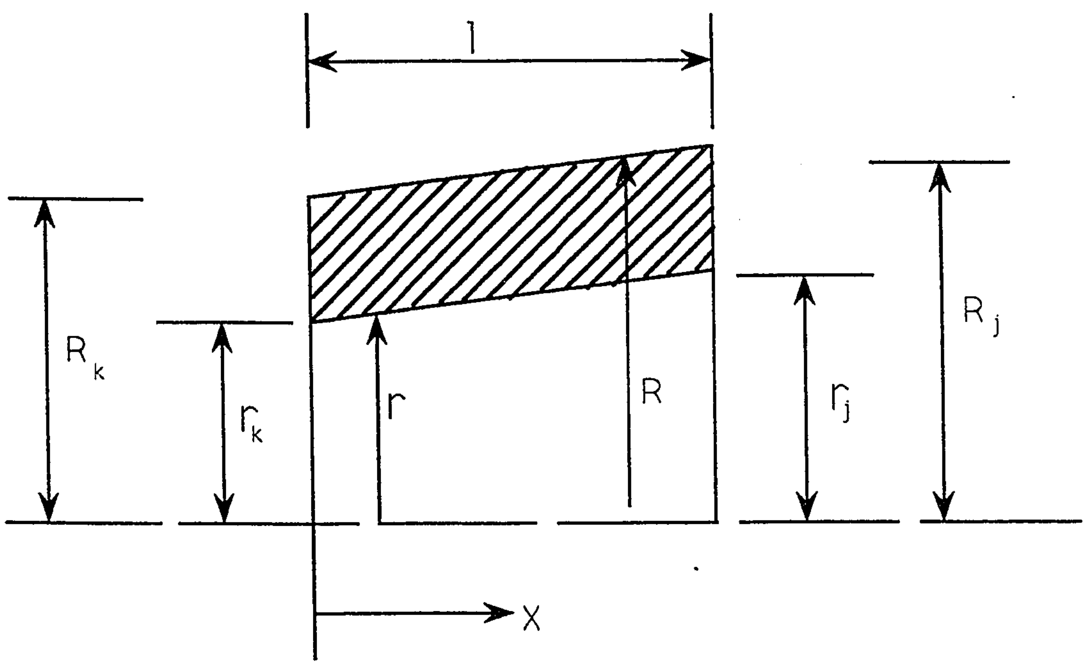

Figure 3.1: Conical Element Axial Cross-section Geometry

$$r = r_k(1 - \xi) + r_j \xi$$

$$R = R_k(1 - \xi) + R_j \xi \tag{3.1}$$

Representing the ratios of inner and outer radii on each end as ρ and α , which are equal to r_j / r_k and R_j / R_k respectively, allows eqn (3.1) to be rewritten as

$$r = r_k(1 + (\rho - 1)\xi)$$

$$R = R_k(1 + (\alpha - 1)\xi) \tag{3.2}$$

Using eqn (3.2) in the cross-sectional area expression results in the following second order polynomial expression:

$$A = \pi(R^2 - r^2) = A_k[1 + \alpha_1 \xi + \alpha_2 \xi^2] \tag{3.3}$$

where the following coefficients are introduced:

$$A_k = \pi(R_k^2 - r_k^2)$$

$$\alpha_1 = 2[R_k^2(\alpha - 1) - r_k^2(\rho - 1)] / (R_k^2 - r_k^2)$$

$$\alpha_2 = [R_k^2(\alpha - 1)^2 - r_k^2(\rho - 1)^2] / (R_k^2 - r_k^2)$$

Similarly for cross-sectional inertia, the use of eqn (3.2) results in a fourth order polynomial expression

$$I = \pi(R^4 - r^4) / 4 = I_k[1 + \delta_1 \xi + \delta_2 \xi^2 + \delta_3 \xi^3 + \delta_4 \xi^4] \tag{3.4}$$

where the coefficients are given by

$$I_k = \pi(R_k^4 - r_k^4) / 4$$

$$\delta_1 = 4[R_k^4(\alpha - 1) - r_k^4(\rho - 1)] / (R_k^4 - r_k^4)$$

$$\delta_2 = 6[R_k^4(\alpha - 1)^2 - r_k^4(\rho - 1)^2] / (R_k^4 - r_k^4)$$

$$\delta_3 = 4[R_k^4(\alpha - 1)^3 - r_k^4(\rho - 1)^3] / (R_k^4 - r_k^4)$$

$$\delta_4 = [R_k^4(\alpha - 1)^4 - r_k^4(\rho - 1)^4] / (R_k^4 - r_k^4)$$

The translational deformation of an arbitrary point internal to the element can be represented as, [25]

$$\begin{Bmatrix} v(x,t) \\ w(x,t) \end{Bmatrix} = \begin{bmatrix} N_{v_1} & 0 & 0 & N_{v_2} & 0 & N_{v_3} & 0 & 0 & N_{v_4} & 0 \\ 0 & N_{v_1} & -N_{v_2} & 0 & 0 & 0 & N_{v_3} & -N_{v_4} & 0 & 0 \end{bmatrix} \{e(t)\}$$

$$= [N_v(x)]\{e(t)\} = \begin{bmatrix} N_{vv}(x) \\ N_{vw}(x) \end{bmatrix} \{e(t)\} \qquad (3.5)$$

The rotation of a typical cross-section of the element is represented by, [25]

$$\begin{Bmatrix} \beta(x,t) \\ \gamma(x,t) \end{Bmatrix} = \begin{bmatrix} 0 & -N_{\beta_1} & N_{\beta_2} & 0 & 0 & 0 & -N_{\beta_3} & N_{\beta_4} & 0 & 0 \\ N_{\beta_1} & 0 & 0 & N_{\beta_2} & 0 & N_{\beta_3} & 0 & 0 & N_{\beta_4} & 0 \end{bmatrix} \{e(t)\}$$

$$= [N_\beta(x)]\{e(t)\} = \begin{bmatrix} N_{\beta\beta}(x) \\ N_{\beta\gamma}(x) \end{bmatrix} \{e(t)\} \qquad (3.6)$$

The torsional displacement of a typical cross-section of the element is approximated by

$$\{\varphi(x,t)\} = [0\ 0\ 0\ 0\ N_{\varphi_1}\ 0\ 0\ 0\ 0\ N_{\varphi_2}]\{e(t)\} = [N_\varphi(x)]\{e(t)\} \qquad (3.7)$$

The individual shape functions N_{v_i} where i = 1,2,3,4; represent static displacement modes associated with unit displacement of one of the end point coordinates with all other coordinates constrained to zero. N_{β_i} where i = 1,2,3,4; represent static rotation shape functions associated with unit displacements of one of the endpoint coordinates with all other coordinates constrained to zero. N_{φ_i} where i = 1,2; represent static torsion shape functions associated with unit displacement of one of the endpoint coordinate with all other coordinates constrained to zero.

The individual shape functions are given by references [35] and [36] as

$$
\begin{aligned}
N_{v_1} &= \frac{1}{1+\Phi}[1-3\xi^2+2\xi^3+\Phi(1-\xi)] \\
N_{v_2} &= \frac{l}{1+\Phi}[\xi-2\xi^2+\xi^3+\frac{\Phi}{2}(\xi-\xi^2)] \\
N_{v_3} &= \frac{1}{1+\Phi}[3\xi^2-2\xi^3+\Phi(\xi)] \\
N_{v_4} &= \frac{l}{1+\Phi}[-\xi^2+\xi^3+\frac{\Phi}{2}(-\xi+\xi^2)] \\
N_{\beta_1} &= \frac{6}{l(1+\Phi)}[\xi^2-\xi] \\
N_{\beta_2} &= \frac{1}{1+\Phi}[1-4\xi+3\xi^2+\Phi(1-\xi)] \\
N_{\beta_3} &= \frac{6}{l(1+\Phi)}[-\xi^2+\xi] \\
N_{\beta_4} &= \frac{1}{1+\Phi}[3\xi^2-2\xi+\Phi\xi] \\
N_{\varphi_1} &= 1-\xi \\
N_{\varphi_2} &= \xi
\end{aligned}
\tag{3.8}
$$

where

$$\xi = \frac{x}{l} \tag{3.9}$$

and

$$\Phi = \frac{12\,E\,I}{\kappa\,A\,G\,l^2} \tag{3.10}$$

The parameter Φ is known as the shear deformation parameter (the ratio between bending stiffness and shear stiffness), E is the modulus of elasticity, I is the second moment of the cross-sectional area, A is the cross-sectional area of the beam element, G is the shear modulus, l is the element length, and κ is the shear correction factor depending on the shape of the cross-section. The shear correction factor κ is given by eqns (2.32) and (2.33).

3.2 The Shaft

3.2.1 Stiffness Matrices

The strain energy expression of a rotating tapered beam element of length l, in the matrix form is given by

$$[U] = \frac{1}{2}\{e\}^T [K]\{e\} \tag{3.11}$$

The matrix $[K]$ is the composite stiffness matrix given by

$$[K] = [K_e] + [K_s] + [K_\varphi] \tag{3.12}$$

where

$$[K_e] = \int_0^l [B_e]^T EI\ [B_e]\ dx = \text{elastic stiffness matrix} \tag{3.13}$$

$$[K_s] = \int_0^l [B_s]^T \kappa GA\ [B_s]\ dx = \text{shear stiffness matrix} \tag{3.14}$$

$$[K_\varphi] = \int_0^l [B_\varphi]^T GJ\ [B_\varphi]\ dx = \text{torsional stiffness matrix} \tag{3.15}$$

The curvature κ and the shear strain v_{xy} within the element are expressed as

$$\kappa = \frac{\partial \gamma}{\partial x} = [B_e]\{e\} \tag{3.16}$$

$$v_{xy} = \frac{\partial v}{\partial x} - \gamma = [B_s]\{e\} \tag{3.17}$$

where

$$[B_\varphi] = \frac{\partial}{\partial x}[N_\varphi] \tag{3.18}$$

$$[B_e] = \frac{\partial}{\partial x}[N_\beta] \tag{3.19}$$

$$[B_s] = \frac{\partial}{\partial x}[N_v] - [N_\beta] \tag{3.20}$$

Carrying out the integration of eqn (3.13), the elastic stiffness matrix $[K_e]$ is obtained with nonzero entries as presented in Table 3.1. The explicit expression for the element shear stiffness matrix $[K_s]$ is obtained by carrying out the integration of eqn (3.14). The shear stiffness matrix $[K_s]$ is obtained with nonzero entries as presented in Table 3.2. Similarly, the torsional stiffness matrix $[K_\varphi]$ is established by evaluating the integral of eqn (3.15). The nonzero entries of torsional stiffness matrix $[K_\varphi]$ are presented in Table 3.3.

3.2.2 Inertia Properties

The kinetic energy of a rotating tapered beam element of length l in matrix form is given by

$$T = \frac{1}{2}\{\dot{e}\}^T[M]\{\dot{e}\} + \frac{1}{2}C_1\dot{\theta}^2 - \dot{\theta}\{\dot{e}\}^T[G_1]\{\dot{e}\} \tag{3.21}$$

The matrix $[M]$ is the composite mass matrix given by

$$[M] = [M_t] + [M_r] + [M_\varphi] - 2[M_c] \tag{3.22}$$

This is known as the consistent mass matrix because it is formulated from the same shape functions $[N_v]$, $[N_\beta]$ and $[N_\varphi]$ that are used to formulate the stiffness matrix. The matrix $[M_c]$ gives the coupling between torsional and transverse vibration and is time dependent. It is neglected for eigenvalue analysis as eigenvalue is system inherent property and is independent of time. The components of the mass matrix are

$$[M_t] = \int_0^l [N_v]^T \mu A [N_v] dx = \text{translational mass matrix} \tag{3.23}$$

$$[M_r] = \int_0^l [N_\beta]^T I_D [N_\beta] dx = \text{rotary inertia mass matrix} \tag{3.24}$$

$$[M_\varphi] = \int_0^l [N_\varphi]^T I_p [N_\varphi] dx = \text{torsional mass matrix} \tag{3.25}$$

The explicit expressions for the element translational mass matrix $[M_t]$, the rotary inertia mass matrix $[M_r]$ and the element torsional mass matrix $[M_\varphi]$ are obtained by carrying out the integration of eqns (3.23), (3.24) and (3.25), respectively. The nonzero entries of $[M_t]$, $[M_r]$ and $[M_\varphi]$ are presented in Tables 3.4, 3.5 and 3.6 respectively.

The gyroscopic matrix $[G]$ is given by

$$[G] = [G_1] - [G_1]^T \tag{3.26}$$

where for constant rotating speed $[G_1]$ can be calculated by

$$[G_1] = \int_0^l [N_{\beta\gamma}]^T I_p [N_{\beta\beta}] \, dx \tag{3.27}$$

The explicit expressions for the elemental gyroscopic mass matrix $[G]$ are obtained by integrating eqn (3.27), and then substituting it into eqn.(3.26). The nonzero entries of $[G]$ are presented in Table 3.7.

Table 3.1 Elastic stiffness matrix of rotating tapered beam element

$$[K_e] = \frac{EI_K}{(1+\Phi)^2}[K_{ab}^{(e)}] \; ; \; a, b = 1, 2, \ldots\ldots, 10$$

The nonzero entries of the upper triangular part of $[K_{ab}^{(e)}]$ are given by

$$K_{11}^{(e)} = -K_{16}^{(e)} = K_{22}^{(e)} = -K_{27}^{(e)} = K_{66}^{(e)} = K_{77}^{(e)}$$

$$= \frac{3}{l^3}\left(\frac{44}{35}\delta_4 + \frac{7}{5}\delta_3 + \frac{8}{5}\delta_2 + 2\delta_1 + 4\right)$$

$$K_{14}^{(e)} = -K_{23}^{(e)} = K_{37}^{(e)} = -K_{46}^{(e)}$$

$$= \frac{1}{l^2}\left[\left(\frac{38}{35} - \frac{4}{5}\Phi\right)\delta_4 + \left(\frac{6}{5} - \frac{9}{10}\Phi\right)\delta_3 + \left(\frac{7}{5} - \Phi\right)\delta_2 + (2 - \Phi)\delta_1 + 6\right]$$

$$K_{19}^{(e)} = -K_{28}^{(e)} = -K_{69}^{(e)} = K_{78}^{(e)}$$

$$= \frac{1}{l^2}\left[\left(\frac{94}{35} + \frac{4}{5}\Phi\right)\delta_4 + \left(3 + \frac{9}{10}\Phi\right)\delta_3 + \left(\frac{17}{5} + \Phi\right)\delta_2 + (4 + \Phi)\delta_1 + 6\right]$$

$$K_{33}^{(e)} = K_{44}^{(e)} = \frac{1}{l}\left[\left(\frac{12}{35} - \frac{2}{5}\Phi + \frac{1}{5}\Phi^2\right)\delta_4 + \left(\frac{2}{5} - \frac{2}{5}\Phi + \frac{1}{4}\Phi^2\right)\delta_3\right.$$

$$\left. + \left(\frac{8}{15} - \frac{1}{3}\Phi + \frac{1}{3}\Phi^2\right)\delta_2 + \left(1 + \frac{1}{2}\Phi^2\right)\delta_1 + (4 + 2\Phi + \Phi^2)\right]$$

$$K_{38}^{(e)} = K_{49}^{(e)} = \frac{1}{l}\left[\left(\frac{26}{35} - \frac{2}{5}\Phi - \frac{1}{5}\Phi^2\right)\delta_4 + \left(\frac{4}{5} - \frac{1}{2}\Phi - \frac{1}{4}\Phi^2\right)\delta_3\right.$$

$$\left. + \left(\frac{13}{15} - \frac{2}{3}\Phi - \frac{1}{3}\Phi^2\right)\delta_2 + \left(1 - \Phi - \frac{1}{2}\Phi^2\right)\delta_1 + (2 - 2\Phi - \Phi^2)\right]$$

$$K_{88}^{(e)} = K_{99}^{(e)} = \frac{1}{l}\left[\left(\frac{68}{35} + \frac{6}{5}\Phi + \frac{1}{5}\Phi^2\right)\delta_4 + \left(\frac{11}{5} + \frac{7}{5}\Phi + \frac{1}{4}\Phi^2\right)\delta_3\right.$$

$$\left. + \left(\frac{38}{15} + \frac{5}{3}\Phi + \frac{1}{3}\Phi^2\right)\delta_2 + \left(3 + 2\Phi + \frac{1}{2}\Phi^2\right)\delta_1 + (4 + 2\Phi + \Phi^2)\right]$$

Table 3.2 Shear stiffness matrix of rotating tapered beam element

$$[K_s] = \frac{G A_K \kappa \Phi^2}{(1+\Phi)^2}[K_{ab}^{(s)}]\ ;\ a, b = 1, 2, \ldots, 10$$

The nonzero entries of the upper triangular part of $[K_{ab}^{(s)}]$ are given by

$$K_{11}^{(s)} = -K_{16}^{(s)} = K_{22}^{(s)} = K_{66}^{(s)} = K_{77}^{(s)} = -K_{27}^{(s)}$$

$$= \frac{1}{l}\left(\frac{1}{2}\alpha_1 + \frac{1}{3}\alpha_2 + 1\right)$$

$$K_{14}^{(s)} = K_{19}^{(s)} = -K_{23}^{(s)} = -K_{28}^{(s)} = K_{37}^{(s)} = -K_{69}^{(s)} = K_{78}^{(s)}$$

$$= \left(\frac{1}{4}\alpha_1 + \frac{1}{6}\alpha_2 + \frac{1}{2}\right)$$

$$K_{33}^{(s)} = K_{38}^{(s)} = K_{44}^{(s)} = -K_{46}^{(s)} = K_{49}^{(s)} = K_{88}^{(s)} = K_{99}^{(s)}$$

$$= l\left(\frac{1}{8}\alpha_1 + \frac{1}{12}\alpha_2 + \frac{1}{4}\right)$$

Table 3.3 Torsional stiffness matrix of rotating tapered beam element

$$[K_\sigma] = G J_K [[K_{ab}^{(\sigma)}]\ ;\ a, b = 1, 2, \ldots\ldots 10$$

The nonzero elements of the upper triangular part of $[K_{ab}^{(\sigma)}]$ are given by

$$K_{55}^{(\sigma)} = -K_{5,10}^{(\sigma)} = K_{10,10}^{(\sigma)} = \frac{1}{l}\left(\frac{1}{5}\delta_4 + \frac{1}{4}\delta_3 + \frac{1}{3}\delta_2 + \frac{1}{2}\delta_1 + 1\right)$$

Table 3.4 Translational mass matrix of rotating tapered beam element

$$M_t = \frac{\mu A_k}{(1+\Phi)^2} [M_{ab}^{(t)}] ; a, b = 1, 2 ..... 10.$$

The nonzero elements of the upper triangular part of [$M_{ab}^{(t)}$] are given by

$$M_{11}^{(t)} = M_{22}^{(t)} = l [(\frac{3}{35} + \frac{1}{6}\Phi + \frac{1}{12}\Phi^2) \alpha_1$$

$$+ (\frac{19}{630} + \frac{13}{210}\Phi + \frac{1}{30}\Phi^2) \alpha_2 + (\frac{19}{35} + \frac{7}{10}\Phi + \frac{1}{3}\Phi^2)]$$

$$M_{14}^{(t)} = - M_{22}^{(t)} = l^2 [(\frac{1}{60} + \frac{9}{280}\Phi + \frac{1}{60}\Phi^2) \alpha_1$$

$$+ (\frac{17}{2520} + \frac{1}{70}\Phi + \frac{1}{120}\Phi^2) \alpha_2 + (\frac{11}{210} + \frac{11}{120}\Phi + \frac{1}{24}\Phi^2)]$$

$$M_{16}^{(t)} = M_{27}^{(t)} = l [(\frac{9}{140} + \frac{3}{20}\Phi + \frac{1}{12}\Phi^2) \alpha_1$$

$$+ (\frac{23}{630} + \frac{37}{420}\Phi + \frac{1}{20}\Phi^2) \alpha_2 + (\frac{9}{70} + \frac{3}{10}\Phi + \frac{1}{6}\Phi^2)]$$

$$- M_{19}^{(t)} = M_{28}^{(t)} = l^2 [(\frac{1}{70} + \frac{9}{280}\Phi + \frac{1}{60}\Phi^2) \alpha_1$$

$$+ (\frac{19}{2520} + \frac{1}{60}\Phi + \frac{1}{120}\Phi^2) \alpha_2 + (\frac{13}{420} + \frac{3}{40}\Phi + \frac{1}{24}\Phi^2)]$$

$$M_{33}^{(t)} = M_{44}^{(t)} = l^3 [(\frac{1}{280} + \frac{1}{140}\Phi + \frac{1}{240}\Phi^2) \alpha_1$$

$$+ (\frac{1}{630} + \frac{1}{280}\Phi + \frac{1}{420}\Phi^2) \alpha_2 + (\frac{1}{105} + \frac{1}{60}\Phi + \frac{1}{120}\Phi^2)]$$

$$- M_{37}^{(t)} = M_{46}^{(t)} = l^2 [(\frac{1}{60} + \frac{3}{70}\Phi + \frac{1}{40}\Phi^2) \alpha_1$$

$$+ (\frac{5}{504} + \frac{23}{840}\Phi + \frac{1}{60}\Phi^2) \alpha_2 + (\frac{13}{420} + \frac{3}{40}\Phi + \frac{1}{24}\Phi^2)]$$

$$M_{38}^{(t)} = M_{49}^{(t)} = - l^3 [(\frac{1}{280} + \frac{1}{120}\Phi + \frac{1}{240}\Phi^2) \alpha_1$$

$$+ (\frac{1}{504} + \frac{1}{210}\Phi + \frac{1}{420}\Phi^2) \alpha_2 + (\frac{1}{140} + \frac{1}{60}\Phi + \frac{1}{120}\Phi^2)]$$

Table 3.4 (continued)

$$M_{66}^{(l)} = M_{77}^{(l)} = l[(\frac{2}{7} + \frac{8}{15}\Phi + \frac{1}{4}\Phi^2)\alpha_1 + (\frac{29}{126} + \frac{3}{7}\Phi + \frac{1}{5}\Phi^2)\alpha_2 + (\frac{13}{35} + \frac{7}{10}\Phi + \frac{1}{3}\Phi^2)]$$

$$-M_{69}^{(l)} = M_{78}^{(l)} = l^2[(\frac{1}{28} + \frac{5}{84}\Phi + \frac{1}{40}\Phi^2)\alpha_1 + (\frac{13}{504} + \frac{1}{24}\Phi + \frac{1}{60}\Phi^2)\alpha_2 + (\frac{11}{210} + \frac{11}{120}\Phi + \frac{1}{24}\Phi^2)]$$

$$M_{88}^{(l)} = M_{99}^{(l)} = l^3[(\frac{1}{168} + \frac{1}{105}\Phi + \frac{1}{240}\Phi^2)\alpha_1 + (\frac{1}{252} + \frac{1}{168}\Phi + \frac{1}{420}\Phi^2)\alpha_2 + (\frac{1}{105} + \frac{1}{60}\Phi + \frac{1}{120}\Phi^2)]$$

Table 3.5 Rotational mass matrix of rotating tapered beam element

$$[M_r] = \frac{I_D}{(1+\Phi)^2}[M^{(r)}_{ab}]\ ;\ a\,,b = 1\,,2,\ \ldots\ldots\,,10$$

The nonzero entries of the upper triangular part of $[M^{(r)}_{ab}]$ are given by

$$M^{(r)}_{11} = -M^{(r)}_{16} = M^{(r)}_{22} = -M^{(r)}_{17} = M^{(r)}_{66} = M^{(r)}_{77}$$

$$= \frac{1}{l}\left(\frac{1}{7}\delta_4 + \frac{3}{14}\delta_3 + \frac{12}{35}\delta_2 + \frac{3}{5}\delta_1 + \frac{6}{5}\right)$$

$$M^{(r)}_{14} = -M^{(r)}_{23} = M^{(r)}_{37} = -M^{(r)}_{46} = \left(\frac{1}{28} - \frac{1}{28}\Phi\right)\delta_4 + \left(\frac{1}{20} - \frac{2}{35}\Phi\right)\delta_3$$

$$+ \left(\frac{1}{14} - \frac{1}{10}\Phi\right)\delta_2 + \left(\frac{1}{10} - \frac{1}{5}\Phi\right)\delta_1 + \left(\frac{1}{10} - \frac{1}{2}\Phi\right)$$

$$-M^{(r)}_{19} = M^{(r)}_{28} = M^{(r)}_{69} = -M^{(r)}_{78} = \left(\frac{1}{28} + \frac{3}{28}\Phi\right)\delta_4 + \left(\frac{1}{28} + \frac{1}{7}\Phi\right)\delta_3$$

$$+ \left(\frac{1}{35} + \frac{1}{5}\Phi\right)\delta_2 + \left(\frac{3}{10}\Phi\right)\delta_1 + \left(-\frac{1}{10} + \frac{1}{2}\Phi\right)$$

$$M^{(r)}_{33} = M^{(r)}_{44} = l\Big[\left(\frac{1}{105} - \frac{1}{60}\Phi + \frac{1}{105}\Phi^2\right)\delta_4 + \left(\frac{11}{840} - \frac{1}{42}\Phi + \frac{1}{60}\Phi^2\right)\delta_3$$

$$+ \left(\frac{2}{105} - \frac{1}{30}\Phi + \frac{1}{30}\Phi^2\right)\delta_2 + \left(\frac{1}{30} - \frac{1}{30}\Phi + \frac{1}{12}\Phi^2\right)\delta_1$$

$$+ \left(\frac{2}{15} + \frac{1}{6}\Phi + \frac{1}{3}\Phi^2\right)\Big]$$

$$M^{(r)}_{38} = M^{(r)}_{49} = l\Big[\left(-\frac{1}{84} - \frac{1}{42}\Phi + \frac{1}{42}\Phi^2\right)\delta_4 + \left(-\frac{11}{840} - \frac{1}{30}\Phi + \frac{1}{30}\Phi^2\right)\delta_3$$

$$+ \left(-\frac{2}{70} - \frac{1}{20}\Phi + \frac{1}{20}\Phi^2\right)\delta_2 + \left(-\frac{1}{60} - \frac{1}{12}\Phi + \frac{1}{12}\Phi^2\right)\delta_1$$

$$+ \left(-\frac{1}{30} - \frac{1}{6}\Phi + \frac{1}{6}\Phi^2\right)\Big]$$

$$M^{(r)}_{88} = M^{(r)}_{99} = l\Big[\left(\frac{1}{14} + \frac{5}{28}\Phi + \frac{1}{7}\Phi^2\right)\delta_4 + \left(\frac{13}{168} + \frac{4}{21}\Phi + \frac{1}{6}\Phi^2\right)\delta_3$$

$$+ \left(\frac{3}{35} + \frac{1}{5}\Phi + \frac{1}{5}\Phi^2\right)\delta_2 + \left(\frac{1}{10} + \frac{1}{5}\Phi + \frac{1}{4}\Phi^2\right)\delta_1$$

$$+ \left(\frac{2}{15} + \frac{1}{6}\Phi + \frac{1}{3}\Phi^2\right)\Big]$$

Table 3.6 Torsional mass matrix of rotating tapered beam element

$$[M_\varphi] = I_p\,[M^{(\varphi)}_{ab}]\;;\; a\,,b = 1\,,2\,,\ldots\ldots\,,10$$

The nonzero entries of the upper triangular part of $[M^{(\varphi)}_{ab}]$ are given by

$$M^{(\varphi)}_{55} = \frac{1}{105}\,\delta_4 + \frac{1}{60}\,\delta_3 + \frac{1}{30}\,\delta_2 + \frac{1}{12}\,\delta_1 + \frac{1}{3}$$

$$M^{(\varphi)}_{5,10} = \frac{1}{42}\,\delta_4 + \frac{1}{30}\,\delta_3 + \frac{1}{20}\,\delta_2 + \frac{1}{12}\,\delta_1 + \frac{1}{6}$$

$$M^{(\varphi)}_{10,10} = \frac{1}{7}\,\delta_4 + \frac{1}{6}\,\delta_3 + \frac{1}{5}\,\delta_2 + \frac{1}{4}\,\delta_1 + \frac{1}{3}$$

Table 3.7 Gyroscopic mass matrix of rotating tapered beam element (asymmetric)

$$[G] = \frac{I_p}{(1+\Phi)^2}[G_{ab}]\ ;\ a\,,\,b = 1\,,\,2\,,\ldots\ldots,\,10$$

The nonzero entries of the upper triangular part of $[G_{ab}]$ are given by

$$G_{12} = -G_{17} = G_{26} = G_{67} = \frac{1}{l}(\frac{1}{7}\delta_4 + \frac{3}{14}\delta_3 + \frac{12}{35}\delta_2 + \frac{3}{5}\delta_1 + \frac{6}{5})$$

$$G_{13} = G_{24} = G_{36} = G_{47} = (\frac{1}{28} - \frac{1}{28}\Phi)\delta_4 + (\frac{1}{20} - \frac{2}{35}\Phi)\delta_3$$

$$+ (\frac{1}{14} - \frac{1}{10}\Phi)\delta_2 + (\frac{1}{10} - \frac{1}{5}\Phi)\delta_1 + (\frac{1}{10} - \frac{1}{2}\Phi)$$

$$G_{18} = G_{29} = -G_{68} = -G_{79} = (\frac{1}{28} + \frac{3}{28}\Phi)\delta_4 + (\frac{1}{28} + \frac{1}{7}\Phi)\delta_3$$

$$+ (\frac{1}{35} + \frac{1}{5}\Phi)\delta_2 + (\frac{3}{10}\Phi)\delta_1 + (-\frac{1}{10} + \frac{1}{2}\Phi)$$

$$G_{34} = l[(\frac{1}{105} - \frac{1}{60}\Phi + \frac{1}{105}\Phi^2)\delta_4 + (\frac{11}{840} - \frac{1}{42}\Phi + \frac{1}{60}\Phi^2)\delta_3$$

$$+ (\frac{2}{105} - \frac{1}{30}\Phi + \frac{1}{30}\Phi^2)\delta_2 + (\frac{1}{30} - \frac{1}{30}\Phi + \frac{1}{12}\Phi^2)\delta_1$$

$$+ (\frac{2}{15} + \frac{1}{6}\Phi + \frac{1}{3}\Phi^2)]$$

$$G_{39} = -G_{48} = l[(-\frac{1}{84} - \frac{1}{42}\Phi + \frac{1}{42}\Phi^2)\delta_4 + (-\frac{11}{840} - \frac{1}{30}\Phi + \frac{1}{30}\Phi^2)\delta_3$$

$$+ (-\frac{2}{70} - \frac{1}{20}\Phi + \frac{1}{20}\Phi^2)\delta_2 + (-\frac{1}{60} - \frac{1}{12}\Phi + \frac{1}{12}\Phi^2)\delta_1$$

$$+ (-\frac{1}{30} - \frac{1}{6}\Phi + \frac{1}{6}\Phi^2)]$$

$$G_{89} = l[(\frac{1}{14} + \frac{5}{28}\Phi + \frac{1}{7}\Phi^2)\delta_4 + (\frac{13}{168} + \frac{4}{21}\Phi + \frac{1}{6}\Phi^2)\delta_3$$

$$+ (\frac{3}{35} + \frac{1}{5}\Phi + \frac{1}{5}\Phi^2)\delta_2 + (\frac{1}{10} + \frac{1}{5}\Phi + \frac{1}{4}\Phi^2)\delta_1 + (\frac{2}{15} + \frac{1}{6}\Phi + \frac{1}{3}\Phi^2)]$$

3.3 The Disk

The disk is assumed to be rigid and is solely characterized by its kinetic energy. The expression for kinetic energy of the disk can be derived using the procedure followed for the shaft element. Let v and w designate the coordinates of the centre of mass 'O' of the disk in $X^i\ Y^i\ Z^i$ coordinate system. The disk deforms in the $y - z$ plane.

The expression for the kinetic energy of the disk can be derived as

$$T^d = \frac{1}{2}m^d(\dot{v}^2 + \dot{w}^2) + \frac{1}{2}I_D(\dot{\beta}^2 + \dot{\gamma}^2) + \frac{1}{2}I_p(\dot{\theta}^2 + \dot{\varphi}^2) + I_p\dot{\theta}\dot{\varphi} - I_p(\dot{\theta} + \dot{\varphi})\dot{\gamma}\beta \qquad (3.28)$$

Similar to eqn (2.17), eqn (3.28) can be written in matrix form as

$$T^d = \frac{1}{2}\{\dot{e}^d\}^T[M^d]\{\dot{e}^d\} + \frac{1}{2}I_p\dot{\theta}^2 - \dot{\theta}\{\dot{e}^d\}^T[G_1^d]\{e^d\} \qquad (3.29)$$

where $\{e^d\}$ is the vector containing the nodal coordinates of the disk and

$$[M^d] = [M_t^d] + [M_r^d] + [M_\varphi^d] - 2[M_e^d] \qquad (3.30)$$

The constituent matrices of eqn (3.30) are

$$[M_t^d] = \begin{bmatrix} m^d & 0 & 0 & 0 & 0 \\ 0 & m^d & 0 & 0 & 0 \\ 0 & 0 & 0 & 0 & 0 \\ 0 & 0 & 0 & 0 & 0 \\ 0 & 0 & 0 & 0 & 0 \end{bmatrix}, \quad [M_r^d] = \begin{bmatrix} 0 & 0 & 0 & 0 & 0 \\ 0 & 0 & 0 & 0 & 0 \\ 0 & 0 & I_D^d & 0 & 0 \\ 0 & 0 & 0 & I_D^d & 0 \\ 0 & 0 & 0 & 0 & 0 \end{bmatrix} \qquad (3.31)$$

$$[M_{\phi}^d] = \begin{bmatrix} 0 & 0 & 0 & 0 & 0 \\ 0 & 0 & 0 & 0 & 0 \\ 0 & 0 & 0 & 0 & 0 \\ 0 & 0 & 0 & 0 & 0 \\ 0 & 0 & 0 & 0 & I_p^d \end{bmatrix}, \quad [M_e^d] = \begin{bmatrix} 0 & 0 & 0 & 0 & 0 \\ 0 & 0 & 0 & 0 & 0 \\ 0 & 0 & 0 & 0 & 0 \\ 0 & 0 & \beta & 0 & 0 \\ 0 & 0 & 0 & 0 & 0 \end{bmatrix} \tag{3.32}$$

and

$$[G_1^d] = \begin{bmatrix} 0 & 0 & 0 & 0 & 0 \\ 0 & 0 & 0 & 0 & 0 \\ 0 & 0 & 0 & I_p^d & 0 \\ 0 & 0 & 0 & 0 & 0 \\ 0 & 0 & 0 & 0 & 0 \end{bmatrix} \tag{3.33}$$

Applying Lagrange equation, the equation of motion of the rigid disk is derived as

$$[M^d]\{\ddot{e}^d\} + \dot{\theta}[G^d]\{\dot{e}^d\} = Q^d \tag{3.34}$$

where Q^d is the generalized force for the disk and

$$[G^d] = [G_1^d] - [G_1^d]^T$$

3.4 The Bearings

The stiffness and damping terms are assumed to be known. The virtual work δW of the forces acting on the shaft can be written as

$$\delta W = -K_{yy}v\,\delta v - K_{yz}w\,\delta v - K_{zz}w\,\delta w - K_{zy}v\,\delta w$$
$$- C_{yy}\dot{v}\,\delta v - C_{yz}\dot{w}\,\delta v - C_{zz}\dot{w}\,\delta w - C_{zy}\dot{v}\,\delta w \tag{3.35}$$

or

$$\delta W = F_v \delta v + F_w \delta w \tag{3.36}$$

where F_v and F_w are the components of the generalized force. In matrix form eqns (3.35) and (3.36) can be written as

$$\begin{Bmatrix} F_v \\ F_w \end{Bmatrix} = -\begin{bmatrix} K_{yy} & K_{yz} \\ K_{zy} & K_{zz} \end{bmatrix} \begin{Bmatrix} v \\ w \end{Bmatrix} - \begin{bmatrix} C_{yy} & C_{yz} \\ C_{zy} & C_{zz} \end{bmatrix} \begin{Bmatrix} \dot{v} \\ \dot{w} \end{Bmatrix} \tag{3.37}$$

Equation (3.37) can be written in matrix form as

$$[C^b]\{\dot{e}^b\} + [K^b]\{e^b\} = \{Q^b\} \tag{3.38}$$

where

$$[K^b] = \begin{bmatrix} K_{yy} & K_{yz} \\ K_{zy} & K_{zz} \end{bmatrix} \quad \text{and} \quad [C^b] = \begin{bmatrix} C_{yy} & C_{yz} \\ C_{zy} & C_{zz} \end{bmatrix} \tag{3.39}$$

3.5 Eigenvalue Problem

The free vibrational equation of motion of a rotor bearing system can be written in the assembled general form as

$$[M]\{\ddot{e}\} + [C]\{\dot{e}\} + [K]\{e\} = \{0\} \tag{3.40}$$

with

$$[M] = [M^e] + [M^d]$$

$$[C] = [G^e] + [C^b] + [G^d]$$

$$[K] = [K^e] + [K^b]$$

where

$[M^e]$ = inertial matrix of the shaft

$[M^d]$ = inertial matrix of the disk

$[G^e]$ = gyroscopic matrix of the shaft

$[G^d]$ = gyroscopic matrix of the disk

$[C^b]$ = damping matrix of the bearing

$[K^e]$ = stiffness matrix of the shaft

$[K^b]$ = stiffness matrix of the bearing

$\{e\}$ = deformation vector

These constituent matrices are highly banded in nature. Matrix $[M]$ is symmetric, whereas $[G^e]$ and $[G^d]$ are skew symmetric. The matrix $[K]$ is symmetric when the bearings are rigid or when they have stiffness coefficients in the principal directions. The matrix $[C]$ is skew symmetric only when the bearing is undamped ($C_{yy} = C_{zz} = C_{yz} = C_{zy} = 0$). If the bearings are damped, the matrix $[C]$ is a non-symmetric real matrix.

The solution of eqn (3.40) may be obtained by representing it in the following state space form:

$$\begin{bmatrix} [0] & -[M] \\ [M] & [C] \end{bmatrix} \begin{Bmatrix} \{\ddot{e}\} \\ \{\dot{e}\} \end{Bmatrix} + \begin{bmatrix} [M] & [0] \\ [0] & [K] \end{bmatrix} \begin{Bmatrix} \{\dot{e}\} \\ \{e\} \end{Bmatrix} = \{0\} \tag{3.41}$$

Or, simply as

$$[E]\{\dot{y}\} + [F]\{y\} = \{0\} \tag{3.42}$$

in which

$$\{y\} = \begin{Bmatrix} \dot{c} \\ c \end{Bmatrix} \tag{3.43}$$

The matrices $[E]$ and $[F]$ are highly banded. If the bearing is undamped then the matrix $[E]$ is skew symmetric. The matrix $[F]$ is symmetric when the bearings are isotropic with ($K_{yz} = K_{zy} = 0$). If the bearings are damped or orthrotropic or both then nothing can be said about the symmetry or skew-symmetry of the matrices $[E]$ and $[F]$. Thus, the type of bearings used in the rotor-bearing system play an important role in selecting a numerical strategy to solve the equation of motion.

3.5.1 Literature Review

In the past two decades, researchers have shown interest in solving eqn (3.42) exploiting the banded nature of the matrices. Gupta [37] presented an algorithm based on Sturm sequence property for free vibration analysis of undamped spinning structural systems. In his formulation, the matrices $[M]$ and $[K]$ are symmetric and positive definite whereas the matrix $[C]$ is skew symmetric. This algorithm takes advantage of the banded nature of matrices, thus saving computer storage and solution time. Gupta [38] presented a numerical algorithm for the eigenproblem solution of discrete damped structures, including spinning. That algorithm is based on a combined Sturm sequence and an inverse iteration technique, which exploits the banded form of the relevant matrices. For damped sturctures, the roots of eqn (3.42) are complex. The procedure presented in reference [38] starts by isolating the corresponding real roots out of the desired complex ones, then applying the Sturm sequence technique to the relevant undamped free vibration formulation, when the bounds of each individual root are obtained. The algebraic values of the middle points of such bounds are then employed to accurately locate the individual desired roots and the associated vectors of the damped system. Meirovitch [39] presented a method of solution of the eigenvalue problem for gyroscopic systems defined by two real nonsingular matrices; one symmetric and the other skew symmetric. This method reduces the eigenvalue problem defined by symmetric and skew symmetric matrices to a standard eigenvalue problem, defined by two real symmetric matrices. The resulting reduced eigenvalue problem resembles, in structure, that of a nonrotating system. Gupta [40] presented a numerical algorithm for the determination of natural frequencies and mode shapes of free vibration of spinning and nonspinning structures. His algorithm takes into account the presence of viscous and structural damping. In that paper, a symmetric matrix decomposition scheme is adopted for matrix triangularization, which is claimed to render the program more efficient. Also a bisection scheme is described that accelerates the solution convergence rate, particularly for the case of repeated roots. Gupta [41] described a procedure for iterative eigenproblem solution of spinning structures. The method uses a combined Sturm sequence and a bisection procedure to isolate the roots of the eigenvalue problem. The eigenvalues and eigenvectors of the damped spinning system are then derived by an inverse iteration procedure, using the middle point of the bound of the isolated root as the starting root iteration value. Gupta and Lawson [42] described an eigenproblem solution method for free vibrational analysis of spinning structural systems. Their method uses the block Lanczo's algorithm which employs only real numbers in all relevant computations and also exploits the sparsity of the associated matrices. In this reference the system mass and stiffness matrices are assumed to be symmetric and positive definite, whereas the gyroscopic matrix is assumed as skew symmetric.

3.5.2 Solution Schemes

To find the natural frequencies of the rotor-bearing system, the equation of motion can be viewed in two ways. In the first method, the natural frequencies are extracted from eqn (3.42), which is the free vibrational equation derived with respect to the fixed frame and rewritten in state variable form. The solution of the eigenvalue problem described by eqn (3.42) can be obtained by using EISPACK eigenvalue solver. It yeilds both forward and backward whirl speeds from the same eigenvector. The eigenvalues are found in complex form as

$$\Psi = \psi + \iota\,\omega \tag{3.44}$$

where the imaginary part ω is the whirl speed. The real part of eqn (3.44) is used to express the logarithmic decrement Δ as

$$\Delta = \frac{-2\pi\,\psi}{\omega} \tag{3.45}$$

Logarithmic decrement is a measure of the rate of decay of free oscillations and is defined as the natural logarithm of the ratio of any two successive amplitudes. It is a convenient way of determining the amount of damping present in a system. There is no restriction on the type of bearings when this method is used to solve the system equation of motion.

In the second method, the system equation of motion is transformed to the rotating frame. In this method, only bending frequencies can be found as the transformation to the rotating frame looses track of the torsional motion. Now, the displacements (v, w,β, γ,) of a typical cross-section relative to fixed frame R_o are transformed to corresponding displacements (v, w, β, γ) relative to R by the orthogonal transformation

$$\{e\} = [A]\{p\} \tag{3.46}$$

with

$$\{e\} = \begin{Bmatrix} v \\ w \\ \beta \\ \gamma \end{Bmatrix}, \quad \{p\} = \begin{Bmatrix} v \\ w \\ \beta \\ \gamma \end{Bmatrix}$$

Now, assuming that the two reference frames are defined by a difference of ωt about X-axis. We have

$$[A] = \begin{bmatrix} \cos\omega t & -\sin\omega t & 0 & 0 \\ \sin\omega t & \cos\omega t & 0 & 0 \\ 0 & 0 & \cos\omega t & -\sin\omega t \\ 0 & 0 & \sin\omega t & \cos\omega t \end{bmatrix} \tag{3.47}$$

For simplicity, from now onwards $\{p\}$ is written as

$$\{p\} = \lfloor v \ w \ \beta \ \gamma \rfloor^T$$

but its understood that $\{p\}$ is the transformed vector of $\{e\}$.

The first two time derivatives of eqn (3.46) are

$$\{\dot{e}\} = \omega[S]\{p\} + [A]\{\dot{p}\} \tag{3.48}$$

$$\{\ddot{e}\} = [A](\{\ddot{p}\} - \omega^2\{p\}) + 2\omega[S]\{\dot{p}\} \tag{3.49}$$

where $[S]$ is given by

$$[S] = \frac{1}{\omega}[\dot{A}] = \begin{bmatrix} -\sin\omega t & -\cos\omega t & 0 & 0 \\ \cos\omega t & -\sin\omega t & 0 & 0 \\ 0 & 0 & -\sin\omega t & -\cos\omega t \\ 0 & 0 & \cos\omega t & -\sin\omega t \end{bmatrix} \tag{3.50}$$

Using eqn (3.46) and eqns (3.48) - (3.50) the equation of motion in the rotating frame R is assembled from the component equations of motion of the disk, the shaft and the bearings.

Neglecting torsional deformation, the kinetic energy of the rigid disk for constant rotational speed ($\dot{\theta} = \Omega$) is given by

$$T^d = \frac{1}{2}\begin{Bmatrix}\dot{v}\\ \dot{w}\end{Bmatrix}^T \begin{bmatrix} m^d & 0 \\ 0 & m^d \end{bmatrix} \begin{Bmatrix}\dot{v}\\ \dot{w}\end{Bmatrix} + \frac{1}{2}\begin{Bmatrix}\dot{\beta}\\ \dot{\gamma}\end{Bmatrix}^T \begin{bmatrix} I_D & 0 \\ 0 & I_D \end{bmatrix} \begin{Bmatrix}\dot{\beta}\\ \dot{\gamma}\end{Bmatrix} - \Omega\, I_p\, \dot{\gamma}\, \beta \tag{3.51}$$

The Lagrangian equation of motion of the rigid disk for free vibration is

$$\left([M_t^d] + [M_r^d] \right) \{\ddot{e}^d\} - \Omega\, [G^d]\, \{\dot{e}^d\} = \{0\} \tag{3.52}$$

By using eqns (3.48), (3.49) and (3.50) and premultiplying by $[A]^T$, eqn (3.52) transforms to

$$\begin{aligned} &([M_t^d] + [M_r^d]) \{\ddot{p}^d\} + \omega (2 ([\hat{M}_t^d] + [\hat{M}_r^d]) - \lambda [G^d]) \{\dot{p}^d\} \\ &\quad - \omega^2 (([M_t^d] + [M_r^d]) + \lambda [\hat{G}^d]) \{p^d\} = \{0\} \end{aligned} \tag{3.53}$$

For the case of thin disks ($I_p = 2\, I_D$) , eqn (3.53) reduces to

$$\begin{aligned} &([M_t^d] + [M_r^d]) \{\ddot{p}^d\} + \omega (2 [\hat{M}_t^d] + (1 - \lambda) [G^d] (\{\dot{p}^d\} \\ &\quad - \omega^2 ([M_t^d] + (1 - 2\lambda) [M_r^d]) \{ p^d \} = \{0\} \end{aligned} \tag{3.54}$$

Equation (3.54) is the equation of motion of a rigid disk in the rotating frame R with whirl ratio $\lambda = \dfrac{\Omega}{\omega}$.

Neglecting torsional deformation, the Lagrangian equation of motion for free vibration of the finite rotor element at constant spin speed is

$$([M_t^e] + [M_r^e])\{\ddot{e}^e\} - \Omega[G^e]\{\dot{e}^e\} + ([K_e^e] + [K_t^e])\{e^e\} = \{0\} \tag{3.55}$$

and is referred to fixed frame coordinates. All the matrices of eqn (3.55) are symmetric except the gyroscopic matrix $[G^e]$ which is skew symmetric. Equation (3.55) is transformed to the rotating frame coordinates by using eqns (3.48), (3.49) and (3.50), extended to include four coordinates at each end of the element and then premultiplying by $[A]^T$. Since $I_p = 2\,I_D$ the following identity can be written:

$$[A]^T[M_r^e][S] = \frac{1}{2}[G^e] \tag{3.56}$$

The transformed equation is

$$([M_t^e] + [M_r^e](\{\ddot{p}^e\} + \omega(2[\hat{M}_t^e] + (1 - \lambda)[G^e])\{\dot{p}^e\}$$

$$+ ([K_b^e] - \omega^2([M_t^e] + (1 - 2\lambda)[M_r^e])\{p^e\} = \{0\} \tag{3.57}$$

with

$$[\hat{M}_t^e] = [A]^T[M_t^e][S] \tag{3.58}$$

Equation (3.57) is the equation of motion of a rotating beam element refered to R.

The governing equation for the bearing in the fixed frame coordinates is

$$[C^b]\{\dot{e}^b\} + [K^b]\{e^b\} = [Q^b] \tag{3.59}$$

Using eqns (3.48), (3.49) and (3.50) in eqn (3.59) and premultiplying by $[A]^T$ gives the transformed form

$$[A]^T[G^b][A]\{\dot{p}^b\} + [A]^T[K^b][A]\{p^b\} = \{P^b\} \tag{3.60}$$

which is expressed in the rotating frame coordinates. For nonisotropic bearings eqn (3.60) contains periodic coefficients. This results in parametrically excited equation of motion. For isotropic bearings, however, eqn (3.60) reduces to the following equation with constant coefficients:

$$c\,[I]\,\{\dot{p}^b\} + k\,[I]\,\{p^b\} = \{P^b\} \tag{3.61}$$

where c and k are the isotropic bearing damping and stiffness coefficients, respectively.

The rotor-bearing system equation of motion is obtained by assembling the component equations of motion given by (3.54), (3.57) and (3.61). Therefore the system equation of motion can be written as

$$[M^s]\,\{\ddot{p}^s\} + \omega\,(\,2\,[\hat{M}^s] - \lambda\,[\hat{G}^s]\,)\,\{\dot{p}^s\}$$
$$+ \,(\,[K^s] - \omega^2\,(\,[M^s] + \lambda\,[\hat{G}^s]\,)\,)\,\{p^s\} = 0 \tag{3.62}$$

The natural circular whirl speeds and mode shapes can be obtained from eqn (3.62). These modes are constant relative to R and the two planes of motion are 90° out of phase. Assuming a constant solution $\{p^s\} = \{p_o\} =$ constant , the associated eigenvalue problem becomes

$$[K^s]\,\{p_o\} = \omega^2\,(\,[M^s] + \lambda\,[G^s]\,)\,\{p_o\} \tag{3.63}$$

The 2n-eigenvalues ω_r; where n is the dimension of the matrices in eqn (3.63), are real and the positive values, together with the associated vectors $\{p_o\}^{(r)}$ represent natural circular whirl speeds and mode shapes relative to R at the specified whirl ratio λ.

When the eigenvalue problem is solved in fixed frame, as is evident from eqn (3.42), the dimensions of the matrices involved is 2n and one of the matrices is not symmetric. The advantage of defining the eigenvalue problem in rotating frame is that the matrices involved in the formulation are symmetric and of half the dimension (i.e. n). Because of this advantage most of the work in the literature is done by formulating the eigenvalue problem in the rotating reference frame. In this thesis both the solution schemes are used to compare the results.

Chapter IV

RESULTS AND DISCUSSIONS

The whirl speeds of the rotor system with undamped isotropic bearings are computed from the eigenvalue problem of eqn (3.63) for different whirl ratios λ. To demonstrate the accuracy of the model developed in this study, the results presented in references [20], [22] and [24] are reproduced. In these references, the first two natural frequencies are given for a uniform simply supported shaft for whirl ratios $\lambda = 0, 1, -1$, and a range of the slenderness ratio $(R/2L)$. The natural frequencies computed using eqn (3.63) are compared to references [20], [22] and [24] in Tables 4.1 - 4.3. The natural frequencies are nondimensionalized by the following equation, [22]:

$$f^4 = \frac{\mu A L^4 \omega^2}{E I} \tag{4.1}$$

To demonstrate the accuracy of the present model for the case of undamped isotropic bearings, a uniform steel rotor system of 10.16 cm diameter and 127 cm long which is supported by identical undamped isotropic bearings of stiffness $K_{yy} = K_{zz} = 1.751 \times 10^7\ N/m$ is studied. The elastic modulus E and density μ of the shaft are $2.068 \times 10^{11}\ N/m^2$ and $7833\ kg/m^3$, respectively. The first five natural frequencies at the spin speed of 418.88 rad/s (4000 rpm) are summarized in Table 4.4. These frequencies are compared to those presented in reference [21].

The whirl speeds of the rotor system with damped, orthotropic bearings are computed from the eigenvalue problem of eqn (3.42) for different spin speeds Ω. In order to illustrate the capability of the present model for computing the natural frequencies of a rotor system with damped nonisotropic bearings, the case presented in reference [12] is studied. The rotor system consists of a uniform shaft of diameter $d = 10.16\ cm$ and length $l = 127\ cm$ and two identical nonisotropic flexible bearings. The stiffness coefficients of the bearings are $K_{yy} = K_{zz} = 1.751 \times 10^7\ N/m$, $K_{yz} = K_{zy} = -2.917 \times 10^6\ N/m$, and the damping coefficients are $C_{yy} = C_{zz} = 1.752 \times 10^3\ N.s/m$, and $C_{yz} = C_{zy} = 0.0 N.s/m$. The density and elastic modulus are $\mu = 7833\ kg/m^3$ and $E = 2.068 \times 10^{11}\ N/m^2$, respectively. The first five natural frequencies of the above system at spin speed $\Omega = 400.0$ rad/s are presented in Table 4.5. These values are compared to those presented in reference [12].

No rotor system is complete without the presence of disks. To demonstrate the application and accuracy of the present finite element model, a typical rotor bearing system as illustrated in Figure 4.1 is analyzed to determine its whirl speeds. A density of 7806.0 kg/m^3 and elastic modulus $2.078 \times 10^{11}\ N/m^2$ are used for the distributed rotor and a concentrated disk with a mass of 1.401 kg , polar moment of inertia 0.002 kg/m^3, and diametral inertia 0.00136 $kg\text{-}m^2$. The disk is located at node 5. The distributed rotor is modeled by eighteen elements. The geometric data of these elements is listed are Table 4.6. Two identical bearings idealized as undamped and linear with stiffness coefficients $K_{yy} = K_{zz} = 4.378 \times 10^7\ N/m$ and $K_{yz} = K_{zy} = 0$ are located at nodes 11 and 15. The first five natural frequencies of this system for different whirl ratios λ are given in Table 4.7. These natural frequencies are compared to those presented in reference [14].

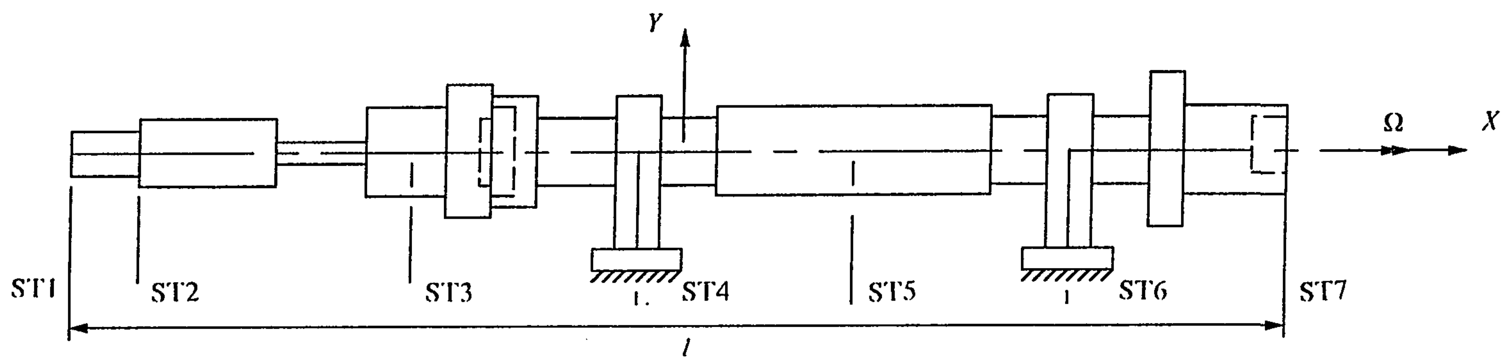

Figure 4.1: The Configuration of Multi-stepped Rotor Bearing System

In all the cases studied so far the rotor shaft was assumed to be of uniform cross-section along the length. In practice, shafts have tapered segments. The pioneering work in modeling a tapered shaft was done by Rouch and Kao [24]. In the last decade, new improved models were presented by investigators, but a set of nondimensionalized natural frequencies for various geometries of a rotating tapered shaft could not be cited in the literature. This investigation attempts to bridge this gap in the literature.

There are very few published results for nonrotating or rotating tapered shafts. Downs [27] presented dimensionless Euler natural frequencies of truncated conical non-rotating cantilever with truncation ratios varying from 0.1 to 0.8. These natural frequencies are calculated from exact analytical solutions. In Table 4.8, the dimensionless Euler natural frequencies of a truncated conical cantilever computed using the present model are compared to reference [27]. In Table 4.9, the nondimensional natural frequencies of a tapared, solid and hollow Timoshenko conical cantilever beam are given.

Genta and Gugliotta [26] presented nondimensional Euler natural frequencies for a tapered conical nonrotating cantilever with taper ratio 0.1 and l_s/d_1 ratio 160. These results are compared to the natural frequencies computed using the present model in Table 4.10. They also presented the nondimensional natural frequencies for a tapered conical cantilever with taper ratio 0.1 and l_s/d_1 ratio 3.2. They have concluded that these natural frequencies cannot be compared to those of reference [27] as the specifications of the beam fall under the definition of a short beam. In short beams, the shear effect is more prominent and the Timoshenko natural frequency values are less, when compared to the corresponding Euler natural frequencies. This effect is more pronounced at higher modes. The natural frequencies presented for this case in reference [26] does not agree with the natural frequencies computed using the present method.

The pattern of natural frequencies computed using the present method is consistent with the above reasoning.

Gmur and Rodrigues [28] presented the first backward and forward natural frequencies of a hollow tapered simply supported shaft rotating at 10000 rpm. The shaft is shown in Figure 4.2. Its length is 1m, the external diameter at the left end is 0.1m and the internal diameter is 0.05m. The taper angle α of the shaft is 15°. The elasticity modulus E , mass density μ and poisson ratio ν are 2.0×10^{11} Pa, 7800 kg/m^3 and 0.3 , respectively. These results are compared to those computed using the present model in Table 4.11.

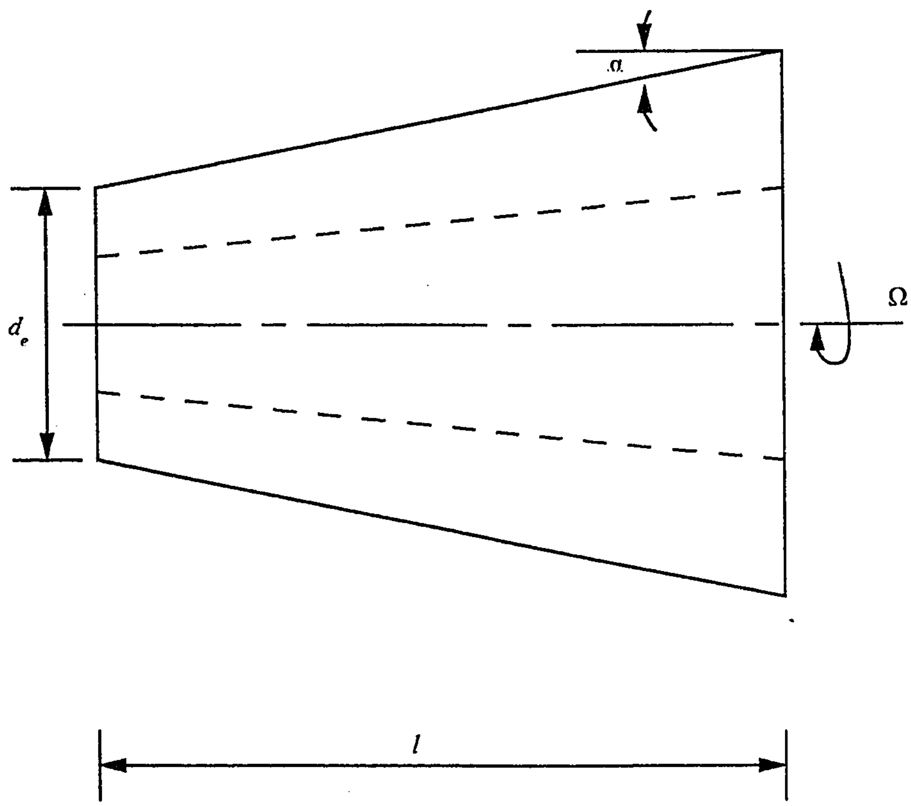

Figure 4.2: Linearly Tapered Hollow Shaft

Table 4.1 Frequency parameter f of uniform solid Timoshenko shaft

R/2L	Whirl ratio λ = 0.0				
	frequency parameter f				
	f_1	f_2	f_3	f_4	f_5
0.02	3.12974 3.1313 * 3.1295 ** 3.1312 ***	6.19593 6.2074 * – 6.2027 ***	9.16661 – – –	12.05146 – – –	14.88678 – – –
0.04	3.09572 3.1017 * 3.0935 ** 3.1012 ***	5.97075 6.0079 * – 5.9950 ***	8.57543 – – –	10.98033 – – –	13.26777 – – –
0.06	3.04415 3.0561 * – 3.0551 ***	5.68439 5.7482 * – 5.7263 ***	7.93970 – – –	9.95984 – – –	11.86271 – – –
0.08	2.97954 2.9989 * – 2.9974 ***	5.38861 5.4752 * – 5.4456 ***	7.36178 – – –	9.11061 – – –	9.75648 – – –
0.1	2.90775 2.9343 * 2.8964 ** 2.9321 ***	5.10913 5.2126 * – 5.1772 ***	6.86403 – – –	7.74822 – – –	8.41373 – – –

* reference [20]

** reference [22]

*** reference [24]

Table 4.2 Frequency parameter f of uniform solid Timoshenko shaft

R/2L	Whirl ratio λ = 1.0				
	frequency parameter f				
	f_1	f_2	f_3	f_4	f_5
0.02	3.13578 3.1374 * 3.1356 ** 3.1373 ***	6.24101 6.2532 * 6.2383 ** 6.2484 ***	9.30431 – – –	12.34338 – – –	15.39495 – – –
0.04	3.11815 3.1246 * 3.1173 ** 3.1240 ***	6.10916 6.1551 * 6.0918 ** 6.1395 ***	8.90897 – – –	11.53819 – – –	14.03273 – – –
0.06	3.08898 3.1027 * 3.0867 ** 3.1016 ***	5.89672 5.9873 * 5.8604 ** 5.9568 ***	8.33150 – – –	10.53819 – – –	12.46280 – – –
0.08	3.04764 3.0715 * 3.0442 ** 3.0696 ***	5.62984 5.7623 * 5.5778 ** 5.7174 ***	7.71530 – – –	9.519247 – – –	11.15052 – – –
0.1	2.99595 3.0311 * 2.9909 ** 3.0282 ***	5.34492 5.5069 * 5.5069 ** 5.4518 ***	7.15446 – – –	8.718045 – – –	10.13314 – – –

* reference [20]

** reference [22]

*** reference [24]

Table 4.3 Frequency parameter f of uniform solid Timoshenko shaft

R/2L	Whirl ratio λ = -1.0				
	frequency parameter f				
	f_1	f_2	f_3	f_4	f_5
0.02	3.12375 3.1253 * 3.1236 ** 3.1252 ***	6.15240 6.1631 * 6.1500 ** 6.1586 ***	9.03810 – – –	11.78918 – – –	14.44719 – – –
0.04	3.07402 3.0796 * 3.0733 ** 3.0792 ***	5.84443 5.8748 * 5.8318 ** 5.8629 ***	8.28099 – – –	10.49075 – – –	12.58057 – – –
0.06	3.00202 3.0125 * 3.0001 ** 3.0116 ***	5.49242 5.5380 * 5.4698 ** 5.5184 ***	7.56841 – – –	9.42029 – – –	10.03115 – – –
0.08	2.91689 2.9328 * 2.9144 ** 2.9313 ***	5.15909 5.2146 * 5.1296 ** 5.1887 ***	6.97342 – – –	7.41347 – – –	8.04834 – – –
0.1	2.82719 2.8475 * 2.8239 ** 2.8455 ***	4.86307 4.9238 * 4.2886 ** 4.8932 ***	5.88740 – – –	6.48568 – – –	6.59549 – – –

* reference [20]

** reference [22]

*** reference [24]

Table 4.4 Natural frequencies of uniform, solid Timoshenko shaft
(undamped flexible bearings at both ends)

Spin speed Ω		Natural frequencies (rad/s)				
		mode 1	mode 2	mode 3	mode 4	mode 5
418.8	B	519.248 519.54 *	1091.351 1091.77 *	2227.263 2229.82 *	4965.105 4986.74 *	9255.99 _
	F	519.799 520.10 *	1094.857 1095.28 *	2242.066 2244.72 *	4997.928 5020.12 *	9307.458 _

B - Backward , F - Forward

* reference [21]

Table 4.5 Natural frequencies of uniform, solid Timoshenko shaft
(damped flexible bearings at both ends)

Spin speed Ω		Natural frequencies (rad/s)				
		mode 1	mode 2	mode 3	mode 4	mode 5
400.0	B	491.056 491.90 *	1006.797 1005.0 *	2165.118 2171.70 *	4946.456 5038.70 *	9251.351 _
	F	543.488 544.79 *	1174.393 1174.20 *	2305.760 2312.70 *	5015.064 5107.40 *	9309.549 _

* reference [12]

Table 4.6 Multi-stepped rotor configuration data

Element node no.	Node location (cm)	Bearing/ disk	Outer radius (cm)	Inner radius (cm)
1	-17.90		0.51	
2	-16.63		1.02	
3	-12.82		0.76	
4	-10.28		2.03	
5	-9.01	Disk No.1	2.03	
6	-7.74		3.30	
7	-7.23		3.30	1.52
8	-6.47		2.54	1.78
9	-5.20		2.54	
10	-4.44		1.27	
11	-1.39	Bearing No.1	1.27	
12	1.15		1.52	
13	4.96		1.52	
14	8.77		1.27	
15	10.80	Bearing No.2	1.27	
16	12.58		3.81	
17	13.60		2.03	
18	16.64		2.03	1.52
19	17.91			

Table 4.7 Natural frequencies of uniform stepped shaft with bearings and disks

Natural frequency (RPM)	Whirl ratio λ								
	2	-2	1	-1	1/2	-1/2	1/4	-1/4	0
1	18753	14386	17432	15260	16830	15746	16545	16003	16269
	18148 *	14758 *	17159 *	15470 *	16700 *	15858 *	16481 *	16060 *	16267 *
2	50743	43926	49303	45907	48528	46833	48123	47277	47706
	51430 *	44695 *	49983 *	46612 *	49204 *	47520 *	48800 *	47957 *	48384 *
3	112966	56041	100243	62631	87750	68128	81567	71779	76221
	111455 *	58424 *	96457 *	64752 *	85552 *	69640 *	80649 *	72737 *	76382 *
4	177938	110823	140145	115547	127892	117911	124257	119663	121643
	–	–	–	–	–	–	–	–	–
5	657243	115290	415536	130197	245591	144005	194972	154390	169570
	–	–	–	–	–	–	–	–	–

*reference [14]

Table 4.8 Frequency parameter f of tapered solid Euler conical cantilever

Taper ratio	f_1	f_2	f_3	f_4	f_5	f_6	f_7	f_8	f_9	f_{10}
0.1	7.205198 7.20486*	18.68046 18.6802*	37.13099 37.1328*	63.56442 63.5049*	98.42188 98.1657*	142.0936 141.233*	195.2531 192.764*	259.0747 252.788*	334.0487 _	414.2527 _
0.5	4.626112 4.62554*	19.54798 19.5476*	48.58773 48.5789*	91.86226 91.8128*	149.5876 149.390*	221.9444 221.328*	309.2076 307.637*	411.7490 408.321*	530.0263 _	664.6032 _
0.8	3.854703 3.84642*	21.05470 21.0569*	56.64504 56.6303*	109.8325 109.763*	180.8487 180.611*	269.9120 269.166*	377.3734 _	503.7376 _	649.6738 _	815.7649 _

Table 4.9 Frequency parameter f of tapered Timoshenko conical cantilever

Taper ratio		f_1	f_2	f_3	f_4	f_5	f_6	f_7	f_8	f_9	f_{10}
0.1	S	7.000152	17.48770	32.77311	52.31137	75.40230	101.5963	130.6746	162.5421	197.1581	229.9317
	H	6.831187	16.64549	30.33712	47.21133	66.99269	89.09135	113.3414	139.4667	163.1440	170.0072
0.5	S	4.486051	17.23155	37.97037	63.47644	92.42803	124.1731	158.4376	193.8193	206.4912	233.3928
	H	4.390560	16.03501	33.86426	54.98230	78.54379	103.9258	130.8342	141.6109	160.3779	175.4667
0.8	S	3.650703	16.29081	36.04674	58.35081	82.59425	106.8987	123.8337	131.5389	150.8472	162.8355
	H	3.729958	17.78090	41.11400	68.65332	99.16873	131.6894	165:6034	179.6753	201.5378	210.4414

*reference [27]. S - Solid . H - Hollow

Table 4.10 Non-dimensional values of the first four natural frequencies for a beam with taper ratio 0.1 and $l_s / d_1 = 160$

Mode	[28]	1 element	2 element	4 element	8 element	16 element
1	7.2048	7.21137 7.2115 *	7.20858 7.2086 *	7.20557 7.2056 *	7.20488 7.2051 *	7.20482 7.2050 *
2	18.6802	21.27958 21.2796 *	19.04066 19.0408 *	18.73003 18.7301 *	18.68435 18.6826 *	18.68063 18.6802 *
3	37.1238	- -	38.81527 38.8155 *	37.71053 37.7106 *	37.17597 37.1698 *	37.13111 37.1245 *
4	63.5049	- -	88.92094 88.9216 *	65.52983 65.5302 *	63.83147 63.8160 *	63.52632 63.5143 *

* reference [26]

Table 4.11 First backward and forward bending frequencies (in Hz) of tapered hollow shaft at 10,000 rpm

Spin speed Ω(rpm)		Natural frequency f
		mode 1
10000	B	401.0386 395.41 *
	F	448.2599 442.62 *

* reference [28]

The comparisons demonstrate clearly that the finite element model developed in this thesis manifests good accuracy. In the following pages nondimensional natural frequencies of a Timoshenko tapered rotating shaft are presented. Nine different rotor systems are considered for generating the nondimensional natural frequencies. These are;

1. Solid tapered shaft supported on rigid bearings at the widest end.
2. Solid tapered shaft supported on isotropic, undamped bearing at the widest end.
3. Hollow tapered shaft supported on rigid bearing at the widest end.
4. Hollow tapered shaft supported on isotropic undamped bearing at the widest end.
5. Solid tapered shaft supported on rigid bearings at both ends.
6. Solid tapered shaft supported on isotropic undamped bearings at both ends.
7. Hollow tapered shaft supported on rigid bearings at both ends.
8. Hollow tapered shaft supported on isotropic undamped bearings at both ends.
9. Hollow tapered shaft supported on orthrotropic damped bearings at both ends.

The natural frequencies are nondimensionalized by eqn (4.1) where A and I are cross-sectional area and inertia at the widest end. The nondimensional natural frequencies for the cases mentioned above are computed for various values of the whirl ratio λ and spin rate Ω. The dimensions of the tapered shaft are $l_s/d_1 = 4.0$ and $l_s = 1\ m$. If the shaft is hollow then the inner diameter is taken as half of the outer diameter. The stiffness properties of isotropic undamped bearings are $K_{yy} = K_{zz} = 1.751 \times 10^7\ N/m$.

The natural frequencies for the nine different rotor systems are tabulated in nondimensional form in Tables 4.12 - 4.60.

Table 4.12 Frequency parameter f of tapered solid Timoshenko shaft
(taper ratio = 0.1; Rigid bearing at widest end)

Whirl ratio	Frequency parameter f									
λ	f_1	f_2	f_3	f_4	f_5	f_6	f_7	f_8	f_9	f_{10}
0.0	12.88223	27.87249	47.72311	71.57553	98.69805	128.6935	161.3992	181.4507	197.3341	236.6434
1.0	13.25025	29.21815	50.94144	77.44668	107.7523	141.2749	171.0288	177.7610	217.2356	253.61311
-1.0	12.54279	26.66725	44.86360	66.27209	90.22044	109.8146	117.2484	145.5287	165.9821	176.8064

Table 4.13 Frequency parameter f of tapered solid Timoshenko shaft
(taper ratio = 0.5; Rigid bearing at widest end)

Whirl ratio	Frequency parameter f									
λ	f_1	f_2	f_3	f_4	f_5	f_6	f_7	f_8	f_9	f_{10}
0.0	12.42914	32.86136	59.28415	89.40498	122.2765	157.5683	172.5641	195.2199	226.8379	234.5455
1.0	13.02156	35.88607	66.35131	101.0370	138.4911	166.7046	178.3968	215.7939	220.5624	253.5822
-1.0	11.90436	30.33816	53.31502	78.99784	102.3234	107.018	136.4092	137.6607	165.2444	170.0265

Table 4.14 Frequency parameter f of tapered solid Timoshenko shaft
(taper ratio = 0.8; Rigid bearing at widest end)

Whirl ratio	Frequency parameter f									
λ	f_1	f_2	f_3	f_4	f_5	f_6	f_7	f_8	f_9	f_{10}
0.0	13.33361	36.42607	65.08869	96.74634	130.4224	163.3318	165.9013	191.7257	203.7049	225.6595
1.0	14.26914	41.02045	74.67875	111.1533	149.4797	161.1723	167.6650	190.5926	225.9147	232.0305
-1.0	12.54144	32.74894	56.97532	83.26090	96.03701	110.0394	118.9538	137.8099	148.2697	169.2608

Table 4.15 Frequency parameter f of tapered solid Timoshenko shaft (taper ratio = 0.1; Rigid bearing at widest end)

spin speed Ω		Frequency parameter f									
		f_1	f_2	f_3	f_4	f_5	f_6	f_7	f_8	f_9	f_{10}
200	B	12.86491	27.84361	47.68280	71.52582	98.64125	128.6314	161.3311	180.8630	197.2647	236.5767
	F	12.89956	27.90137	47.76341	71.62520	98.75481	128.7555	161.4671	182.0407	197.4036	236.7100
400	B	12.84762	27.81476	47.64249	71.47609	98.58440	128.5692	161.2627	180.2777	197.1955	236.5100
	F	12.91692	27.93026	47.83071	71.67486	98.81153	128.8174	161.5348	182.6331	197.4733	236.7765
600	B	12.83084	27.78591	47.60217	71.42633	98.52752	128.5070	161.1941	179.6949	197.1264	236.4432
	F	12.93430	27.95917	47.84400	71.72450	98.86821	128.8793	161.6023	183.2279	197.5432	236.8430
800	B	12.81310	27.75708	47.56185	71.37656	98.47060	128.4448	161.1252	179.1145	197.0575	236.3764
	F	12.95171	27.98809	47.88429	71.77411	98.92485	128.9412	161.6696	183.8249	197.6134	236.9094
1000	B	12.79587	27.72826	47.52153	71.32676	98.41363	128.3824	161.0560	178.5367	196.9886	236.3095
	F	12.96913	28.01702	47.92457	71.82370	98.98144	129.0030	161.7368	184.4241	197.6839	236.9758

Table 4.16 Frequency parameter f of tapered solid Timoshenko shaft
(taper ratio = 0.5; Rigid bearing at widest end)

spin speed Ω		Frequency parameter f									
		f_1	f_2	f_3	f_4	f_5	f_6	f_7	f_8	f_9	f_{10}
200	B	12.40086	32.80823	59.21405	89.32483	122.1903	157.4763	171.9560	195.1259	226.2423	234.4456
	F	12.45746	32.91450	59.35421	89.48505	122.3625	157.6601	173.1747	195.3139	227.4353	234.6455
400	B	12.37263	32.75511	59.14392	89.24461	122.1042	157.3841	171.3506	195.0317	228.0343	234.7456
	F	12.48583	32.96766	59.42424	89.56505	122.4485	157.7516	173.7879	195.4078	228.0342	234.7455
600	B	12.34444	32.70202	59.07376	89.08396	121.9315	157.1989	170.1474	194.8429	224.4659	234.1458
	F	12.51424	33.02084	59.49422	89.64497	122.5342	157.8428	174.4035	195.5016	228.6347	234.8458
800	B	12.31630	32.64894	59.00357	89.08396	121.9315	157.1988	170.1474	194.8430	224.4658	234.1457
	F	12.54271	33.07402	59.56418	89.72483	122.6200	157.9340	175.0218	195.5952	229.2367	234.9465
1000	B	12.28821	32.59588	58.93334	89.00353	121.8449	157.1058	169.5498	194.7484	223.8773	234.0457
	F	12.57121	33.12722	59.63410	89.80461	122.7057	158.0249	175.6426	195.6887	229.8399	235.0475

Table 4.17 Frequency parameter f of tapered solid Timoshenko shaft
(taper ratio = 0.8; Rigid bearings at widest end)

spin speed Ω		Frequency parameter f									
		f_1	f_2	f_3	f_4	f_5	f_6	f_7	f_8	f_9	f_{10}
200	B	13.29294	36.35430	64.99974	96.64758	130.3139	162.8103	165.6686	191.2491	203.4395	225.2784
	F	13.37435	36.49784	65.17755	96.84498	130.5307	163.8215	166.1676	192.1994	203.9746	226.0408
400	B	13.25236	36.28254	64.91072	96.54869	130.2053	162.2667	165.4599	190.7702	203.1779	224.8978
	F	13.41516	36.56961	65.26635	96.94349	130.6388	164.2687	166.4785	192.6700	204.2488	226.4225
600	B	13.21184	36.21078	64.82162	96.44967	130.0965	161.7081	165.2683	190.2892	202.9199	224.5176
	F	13.45604	36.64139	65.35506	97.04186	130.7467	164.6639	166.8433	193.1371	204.5279	226.8043
800	B	13.17141	36.13904	64.73247	96.35053	129.9875	161.1395	165.0887	189.8064	202.6650	224.1379
	F	13.49699	36.71316	65.44369	97.14009	130.8545	165.0041	167.2651	193.6003	204.8123	227.1862
1000	B	13.13104	36.06731	64.64323	96.25127	129.8783	160.5644	164.9174	189.3221	202.4132	223.7589
	F	13.53802	36.78492	65.53223	97.23821	130.9620	165.2940	167.7393	194.0592	205.1024	227.5681

Table 4.18 Frequency parameter f of tapered solid Timoshenko shaft
(taper ratio = 0.1; Flexible bearing at widest end)

Whirl ratio	Frequency parameter f									
λ	f_1	f_2	f_3	f_4	f_5	f_6	f_7	f_8	f_9	f_{10}
0.0	1.784431	14.65258	30.84500	51.68048	76.18391	103.5076	132.9075	163.3234	192.8844	221.1657
1.0	1.841357	15.56371	33.84743	58.31152	87.65068	120.6928	156.7909	195.6976	237.3684	281.7710
-1.0	1.735958	13.90725	28.54865	46.78796	67.77394	90.83021	115.1477	136.7809	151.0395	173.6076

Table 4.19 Frequency parameter f of tapered solid Timoshenko shaft
(taper ratio = 0.5; Flexible bearing at widest end)

Whirl ratio	Frequency parameter f									
λ	f_1	f_2	f_3	f_4	f_5	f_6	f_7	f_8	f_9	f_{10}
0.0	1.529498	15.76439	37.86398	62.25104	95.59143	127.6956	159.7668	187.8856	209.9654	231.1429
1.0	1.565407	17.35474	44.09292	78.00674	115.3845	154.6749	195.6711	238.6545	281.6938	319.882
-1.0	1.497312	14.51624	33.32651	55.84230	80.27053	105.2455	121.5845	135.8085	150.4118	167.1619

Table 4.20 Frequency parameter f of tapered solid Timoshenko shaft
(taper ratio = 0.8; Flexible bearing at widest end)

Whirl ratio	Frequency parameter f									
λ	f_1	f_2	f_3	f_4	f_5	f_6	f_7	f_8	f_9	f_{10}
0.0	1.399647	18.04649	42.63739	72.04415	103.4786	135.7339	163.8094	184.3488	192.2656	223.7667
1.0	1.439017	20.39485	50.99944	87.17901	125.1906	164.5998	205.5099	245.9509	278.3102	305.4802
-1.0	1.364183	16.22606	36.37701	59.88721	84.03943	106.3951	110.0629	132.4104	137.6354	163.8097

Table 4.21 Frequency parameter f of tapered solid Timoshenko shaft
(taper ratio = 0.1; Flexible bearing at widest end)

spin speed Ω		Frequency parameter f									
		f_1	f_2	f_3	f_4	f_5	f_6	f_7	f_8	f_9	f_{10}
200	B	1.766221	14.61722	30.79119	51.60961	76.09824	103.4079	132.7911	163.1811	192.7043	220.9611
	F	1.803308	14.68808	30.89892	51.75142	76.09824	103.6074	133.0240	163.4658	193.0650	221.3706
400	B	1.748662	14.58199	30.73751	51.53884	76.01263	103.3082	132.6747	163.0390	192.5246	220.7565
	F	1.822870	14.72371	30.95294	51.82245	76.35543	103.7073	133.1406	163.6085	193.2459	221.5757
600	B	1.731743	14.54691	30.68393	51.46815	75.92710	103.2086	132.5585	162.8971	192.3454	220.5522
	F	1.843132	14.75947	31.00707	51.89355	76.44128	103.8072	133.2573	163.7513	193.4274	221.7810
800	B	1.715420	14.51196	30.63047	51.39756	75.84163	103.1091	132.4423	162.7554	192.1666	220.3479
	F	1.864109	14.79537	31.06131	51.96474	76.52718	103.9071	133.3741	163.8942	193.6092	221.9866
1000	B	1.699701	14.47715	30.57713	51.32706	75.75624	103.0096	132.3263	162.6139	191.9882	220.1438
	F	1.885814	14.83139	31.11565	52.03599	76.61314	104.0071	133.4909	164.0373	193.7915	222.1925

Table 4.22 Frequency parameter f of tapered solid Timoshenko shaft
(taper ratio = 0.5; Flexible bearing at widest end)

spin speed Ω		Frequency parameter f									
		f_1	f_2	f_3	f_4	f_5	f_6	f_7	f_8	f_9	f_{10}
200	B	1.515667	15.70827	37.77474	65.14049	95.46413	127.5492	159.5810	187.6219	209.6254	230.8050
	F	1.543711	15.82066	37.95332	65.36162	95.71871	127.8420	159.9526	188.1493	210.3050	231.4830
400	B	1.502211	15.65231	37.68558	65.02996	95.33683	127.4029	159.3951	187.3582	209.2854	230.4696
	F	1.558311	15.87710	38.04274	65.47223	95.84598	127.9883	160.1384	188.4129	210.6444	231.8257
600	B	1.489123	15.59653	37.59653	64.91947	95.20953	127.2565	159.2093	187.0943	208.9450	230.1366
	F	1.573057	15.93370	38.13227	65.58285	95.97322	128.1347	160.3241	188.6764	210.9836	232.1708
800	B	1.476396	15.54091	37.50758	64.80901	95.08223	127.1101	159.0233	186.8304	208.6045	229.8061
	F	1.588699	15.99045	38.22185	65.69350	96.10044	128.2810	160.5098	188.9400	211.3224	232.8183
1000	B	1.464022	15.48547	37.41873	64.69859	94.95494	126.9638	158.8375	186.5665	208.2639	229.4778
	F	1.604497	16.04735	38.31153	65.80414	96.22763	128.4273	160.6953	189.2034	211.6608	232.8681

Table 4.23 Frequency parameter f of tapered solid Timoshenko shaft
(taper ratio = 0.8; Flexible bearing at widest end)

spin speed Ω		Frequency parameter f									
		f_1	f_2	f_3	f_4	f_5	f_6	f_7	f_8	f_9	f_{10}
200	B	1.382940	17.97345	42.52567	71.91262	103.3280	135.5565	163.5063	183.9447	191.8788	223.4508
	F	1.416886	18.11972	42.74914	72.17562	103.6290	135.9111	164.1111	184.7542	192.6549	224.0820
400	B	1.366756	17.90058	42.41401	71.78106	103.1774	135.3791	163.2017	183.5422	191.4945	223.1344
	F	1.434664	18.19312	42.86094	72.30705	103.7793	136.0882	164.4113	185.1609	193.0467	224.3970
600	B	1.351083	17.82790	42.30240	71.64947	103.0267	135.2017	162.8956	183.1412	191.1127	222.8174
	F	1.452991	18.26669	42.97276	72.43843	103.9295	136.2652	164.7099	185.5688	193.4412	224.7929
800	B	1.335912	17.75540	42.19084	71.51784	102.8759	135.0241	162.5881	182.7419	190.7331	222.4997
	F	1.471874	18.34043	43.08467	72.56975	104.0796	136.4420	165.0072	185.9779	193.8383	225.0260
1000	B	1.321231	17.68309	42.07934	71.38619	102.7250	134.8465	162.2790	182.3442	190.3558	222.1814
	F	1.491317	18.41433	43.19649	72.70100	104.2295	136.6188	165.3030	186.3880	194.2382	225.3402

Table 4.24 Frequency parameter f of tapered hollow Timoshenko shaft
(taper ratio = 0.1; Rigid bearing at widest end)

Whirl ratio	Frequency parameter f									
λ	f_1	f_2	f_3	f_4	f_5	f_6	f_7	f_8	f_9	f_{10}
0.0	12.59834	26.65363	44.48032	65.12438	87.97638	112.7107	121.8355	139.1649	168.0549	191.8916
1.0	13.01484	27.97541	47.16593	69.37091	93.85802	114.9486	120.3494	148.6893	178.5768	183.2649
-1.0	12.21611	25.44011	41.91775	60.77764	73.87334	82.25389	104.8112	116.7683	129.4342	152.9088

Table 4.25 Frequency parameter f of tapered hollow Timoshenko shaft
(taper ratio = 0.5; Rigid bearing at widest end)

Whirl ratio	Frequency parameter f									
λ	f_1	f_2	f_3	f_4	f_5	f_6	f_7	f_8	f_9	f_{10}
0.0	12.04211	30.44217	52.83319	77.33863	103.4477	115.5541	131.0919	157.3537	160.9976	186.9619
1.0	12.68250	33.03234	57.74094	84.35904	111.9303	112.4489	142.1175	151.9715	173.3295	177.2579
-1.0	11.47595	28.14455	48.11012	68.01823	70.54707	92.14985	96.36345	114.7082	121.6868	139.5228

Table 4.26 Frequency parameter f of tapered hollow Timoshenko shaft
(taper ratio = 0.8; Rigid bearing at widest end)

Whirl ratio	Frequency parameter f									
λ	f_1	f_2	f_3	f_4	f_5	f_6	f_7	f_8	f_9	f_{10}
0.0	12.80116	33.12709	56.73339	81.69458	106.8725	109.8055	128.9866	139.7605	156.5595	172.9496
1.0	13.77975	36.77098	62.92359	90.09821	107.3234	114.8013	139.8469	148.0421	176.6055	220.7203
-1.0	11.96965	29.90881	50.42149	63.94603	71.66524	82.30637	119.8849	132.7272	147.6418	162.1049

Table 4.27 Frequency parameter f of tapered hollow Timoshenko shaft
(taper ratio = 0.1; Rigid bearing at widest end)

spin speed Ω		Frequency parameter f									
		f_1	f_2	f_3	f_4	f_5	f_6	f_7	f_8	f_9	f_{10}
200	B	12.58047	26.62672	44.44676	65.08693	87.93657	112.6617	121.3159	139.5745	168.0166	191.3577
	F	12.61624	26.68053	44.51385	65.16179	88.01613	112.7588	122.3589	139.6555	168.0931	192.4271
400	B	12.56262	26.59981	44.41317	65.04942	87.89667	112.6115	120.8003	139.5341	167.9782	190.8257
	F	12.63415	26.70743	44.54736	65.19914	88.05579	112.8059	122.8859	139.6960	168.1314	192.9644
600	B	12.54478	26.57389	44.37954	65.01186	87.85671	112.5600	120.2887	139.4936	167.9398	190.2953
	F	12.65207	26.73432	44.58083	65.23645	88.09539	112.8525	123.4166	139.7366	168.1696	193.5034
800	B	12.52696	26.54597	44.34588	64.97426	87.81666	112.5070	119.7815	139.4532	167.9014	189.7668
	F	12.67002	26.76121	44.61427	65.27371	88.13491	112.8983	123.9506	139.7773	168.2077	194.0439
1000	B	12.50916	26.51904	44.31221	64.93660	87.77653	112.4523	119.2789	139.4128	167.8629	189.2401
	F	12.68798	26.78809	44.64767	65.31091	88.17436	112.9435	124.4879	139.8180	168.2458	194.5859

Table 4.28 Frequency parameter f of tapered hollow Timoshenko shaft
(taper ratio = 0.5; Rigid bearing at widest end)

spin speed Ω		Frequency parameter f									
		f_1	f_2	f_3	f_4	f_5	f_6	f_7	f_8	f_9	f_{10}
200	B	12.01391	30.39660	52.78057	77.28338	103.3901	115.0101	131.0305	156.9411	160.8036	186.7393
	F	12.07034	30.48769	52.88574	77.39375	103.5051	116.1011	131.1531	157.7430	161.2166	187.1764
400	B	11.98575	30.35101	52.72786	77.22803	103.3323	114.4690	130.9691	156.5096	160.6305	186.5085
	F	12.09859	30.53319	52.93821	77.44877	103.5623	116.6510	131.2142	158.1049	161.4649	187.3830
600	B	11.95761	30.30538	52.67507	77.17257	103.2743	113.9309	130.9075	156.0630	160.4742	186.2691
	F	12.12688	30.57865	52.99059	77.50367	103.6193	117.2038	131.2752	158.4360	161.7459	187.5882
800	B	11.92951	30.25973	52.62221	77.11700	103.2160	113.3958	130.8457	155.6047	160.3316	186.0211
	F	12.15520	30.62408	53.04290	77.55847	103.6762	117.7596	131.3361	158.7342	162.0617	187.7741
1000	B	11.90144	30.21404	52.56926	77.06131	103.1576	112.8637	130.7838	155.1373	160.1998	185.7644
	F	12.18355	30.66948	53.09512	77.61315	103.7329	118.3182	131.3969	158.9995	162.4122	187.9592

Table 4.29 Frequency parameter f of tapered hollow Timoshenko shaft
(taper ratio = 0.8; Rigid bearing at widest end)

spin speed Ω		Frequency parameter f									
		f_1	f_2	f_3	f_4	f_5	f_6	f_7	f_8	f_9	f_{10}
200	B	12.76142	33.06749	56.66724	81.62096	106.7062	109.3226	128.6889	139.4773	156.2749	172.7387
	F	12.84095	33.18661	56.79939	81.76791	107.0226	110.3070	129.2805	140.0489	156.8450	173.1614
400	B	12.72171	33.00781	56.60092	81.54704	106.5177	108.8640	128.3875	139.1989	155.9916	172.5285
	F	12.88077	33.24604	56.86523	81.84094	107.1606	110.8226	129.5704	140.3428	157.1315	173.3742
600	B	12.68205	32.94806	56.53445	81.47283	106.2992	108.4376	128.0826	138.9254	155.7095	172.3191
	F	12.92063	33.30541	56.93090	81.91368	107.2895	111.3493	129.8560	140.6414	157.4190	173.5881
800	B	12.64243	32.88823	56.46783	81.39831	106.0425	108.0516	127.7744	138.6564	155.4286	172.1102
	F	12.96053	33.36468	56.99641	81.98613	107.4119	111.8851	130.1373	140.9459	157.7073	173.8033
1000	B	12.60286	32.82834	56.40105	81.32350	105.7409	107.7125	127.4633	138.3917	155.1491	171.9019
	F	13.00046	33.42387	57.06176	82.05828	107.5288	112.4285	130.4141	141.2559	157.9964	174.0199

Table 4.30 Frequency parameter f of tapered hollow Timoshenko shaft
(taper ratio = 0.1; Flexible bearing at widest end)

Whirl ratio	Frequency parameter f									
λ	f_1	f_2	f_3	f_4	f_5	f_6	f_7	f_8	f_9	f_{10}
0.0	1.834316	14.31478	29.46997	48.13602	69.16799	91.54032	113.7122	133.9908	155.4133	178.9156
1.0	1.907609	15.37382	32.56295	54.06278	78.30945	93.16148	132.5527	162.1441	181.1860	193.0005
-1.0	1.774202	13.46974	27.06177	43.35764	61.29998	79.58564	95.59653	108.9803	123.9824	139.6006

Table 4.31 Frequency parameter f of tapered hollow Timoshenko shaft
(taper ratio = 0.5; Flexible bearing at widest end)

Whirl ratio	Frequency parameter f									
λ	f_1	f_2	f_3	f_4	f_5	f_6	f_7	f_8	f_9	f_{10}
0.0	1.573473	15.22852	34.97715	58.05821	82.21355	105.8391	125.0208	144.7559	157.3654	177.4279
1.0	1.619716	16.97006	40.50574	67.50604	95.73027	125.1629	155.9646	187.8684	219.3200	248.3207
-1.0	1.533089	13.87719	30.65935	49.89059	68.73602	83.66941	92.19329	108.4488	114.4889	134.8579

Table 4.32 Frequency parameter f of tapered hollow Timoshenko shaft
(taper ratio = 0.8; Flexible bearing at widest end)

Whirl ratio	Frequency parameter f									
λ	f_1	f_2	f_3	f_4	f_5	f_6	f_7	f_8	f_9	f_{10}
0.0	1.439135	17.27665	38.62416	62.71067	86.49244	108.7277	118.6796	139.4799	142.3051	169.9660
1.0	1.489988	19.71069	45.43999	73.11818	101.2758	130.616	161.3571	192.9605	224.0049	252.0106
-1.0	1.394449	15.36045	32.77387	52.23028	66.99864	79.20534	84.69400	104.32131	107.3148	131.7987

Table 4.33 Frequency parameter f of tapered hollow Timoshenko shaft
(taper ratio = 0.1; Flexible bearing at widest end)

spin speed Ω		Frequency parameter f									
		f_1	f_2	f_3	f_4	f_5	f_6	f_7	f_8	f_9	f_{10}
200	B	1.814369	14.27760	29.41694	48.06999	69.08909	91.44069	113.5721	133.8296	155.2864	178.7218
	F	1.855049	14.35209	29.52308	48.20206	69.24686	91.63986	113.8526	134.1535	155.5407	179.1063
400	B	1.795185	14.24057	29.36399	48.00399	69.01016	91.34100	113.4322	133.6697	155.1599	178.5248
	F	1.876589	14.38955	29.57626	48.26811	69.32569	91.73931	113.9930	134.3176	155.6688	179.2939
600	B	1.776743	14.20368	29.31113	47.93802	68.93121	91.24125	113.2925	133.5112	155.0340	178.3247
	F	1.898957	14.42714	29.62952	48.33418	69.40447	91.83866	114.1336	134.4830	155.7975	179.4786
800	B	1.759018	14.16693	29.25835	47.87207	68.85223	91.14144	113.1531	133.3540	154.9084	178.1462
	F	1.922167	14.46487	29.68285	48.40026	69.48319	91.93789	114.2744	134.6499	155.9268	179.6604
1000	B	1.741987	14.13034	29.20567	47.80617	68.77324	91.04160	113.0140	133.1982	154.7833	177.9149
	F	1.946239	14.50274	29.73625	48.46634	69.56187	92.03701	114.4152	134.8182	156.0569	179.8393

Table 4.34 Frequency parameter f of tapered hollow Timoshenko shaft
(taper ratio = 0.5; Flexible bearing at widest end)

spin speed Ω		Frequency parameter f									
		f_1	f_2	f_3	f_4	f_5	f_6	f_7	f_8	f_9	f_{10}
200	B	1.558231	15.17200	34.89612	57.96431	82.09925	105.6756	124.7911	144.5483	156.9903	177.2612
	F	1.589165	15.28516	35.05818	58.15198	82.32759	106.0023	125.2516	144.9626	157.7431	177.5961
400	B	1.543434	15.11562	34.81508	57.87302	81.98472	105.5118	124.5626	144.3396	156.6179	177.0959
	F	1.605318	15.34193	35.13918	58.24565	82.44138	106.1652	125.4837	145.1684	158.1233	177.7661
600	B	1.529072	15.05937	34.73404	57.77623	81.86996	105.3478	124.3354	144.1298	156.2484	176.9320
	F	1.621939	15.39882	35.22017	58.33919	82.55490	106.3278	125.7170	145.3735	158.5057	177.9378
800	B	1.515136	15.00326	34.65300	57.68204	81.75498	105.1836	124.1093	143.9187	155.8819	176.7693
	F	1.639033	15.45583	35.30114	58.43261	82.66816	106.4900	125.9515	145.5779	158.8902	178.1114
1000	B	1.501617	14.94730	34.57197	57.58773	81.63979	105.0192	123.8844	143.7063	155.5186	176.6077
	F	1.656607	15.51296	35.38208	58.52590	82.78112	106.6518	126.1872	145.7818	159.2767	178.2871

Table 4.35 Frequency parameter f of tapered hollow Timoshenko shaft
(taper ratio = 0.8; Flexible bearing at widest end)

spin speed Ω		Frequency parameter f									
		f_1	f_2	f_3	f_4	f_5	f_6	f_7	f_8	f_9	f_{10}
200	B	1.42073	17.20565	38.52631	62.60196	86.34334	108.5067	118.3144	139.1617	142.0513	169.7176
	F	1.45817	17.34774	38.72188	62.81914	86.64085	108.9482	119.0463	139.8018	142.5589	170.2169
400	B	1.40294	17.13475	38.42834	62.49304	86.19357	108.2854	117.9508	138.8468	141.7977	169.4719
	F	1.47784	17.41893	38.81949	62.92737	86.78856	109.1682	119.4147	140.1270	142.8128	170.4707
600	B	1.38576	17.06396	38.33027	62.38390	86.04312	108.0636	117.5888	138.5353	141.5441	169.2286
	F	1.49817	17.49027	38.91695	63.03536	86.93555	109.3876	119.7846	140.4558	143.0668	170.7270
800	B	1.36917	16.99329	38.23209	62.27455	85.89201	107.8416	117.2284	138.2272	141.2907	168.9879
	F	1.51916	17.56158	39.01427	63.14309	87.08182	109.6064	120.1560	140.7881	143.3209	170.9861
1000	B	1.35315	16.92273	38.13381	62.16499	85.74026	107.6192	116.8696	137.9225	141.0274	168.7497
	F	1.54082	17.63302	39.11145	63.25057	87.22737	109.8246	120.5291	141.0373	143.5751	171.2479

Table 4.36 Frequency parameter f of tapered solid Timoshenko shaft
(taper ratio = 0.1; Rigid bearings at both ends)

Whirl ratio	Frequency parameter f									
λ	f_1	f_2	f_3	f_4	f_5	f_6	f_7	f_8	f_9	f_{10}
0.0	3.05145	18.20567	37.35398	60.79711	87.70405	117.7985	150.9507	181.2012	187.9422	228.0795
1.0	3.12187	18.89624	39.53417	65.33004	95.24804	128.7136	165.6755	206.382	250.8422	297.6557
-1.0	2.98543	17.57865	35.40607	56.69969	80.72609	106.4611	111.0979	136.6093	165.7631	168.6855

Table 4.37 Frequency parameter f of tapered solid Timoshenko shaft
(taper ratio = 0.5; Rigid bearings at both ends)

Whirl ratio	Frequency parameter f									
λ	f_1	f_2	f_3	f_4	f_5	f_6	f_7	f_8	f_9	f_{10}
0.0	6.67861	25.48109	50.86571	80.40063	112.9353	148.1722	172.5151	186.227	226.4814	227.12
1.0	6.83383	26.20642	55.15706	88.07804	123.9303	162.2847	203.1053	245.991	289.4692	329.6476
-1.0	6.53262	24.1703	47.01804	73.05463	100.8719	103.1504	132.2753	137.2529	163.2671	165.8918

Table 4.38 Frequency parameter f of tapered solid Timoshenko shaft
(taper ratio = 0.8; Rigid bearings at both ends)

Whirl ratio	Frequency parameter f									
λ	f_1	f_2	f_3	f_4	f_5	f_6	f_7	f_8	f_9	f_{10}
0.0	8.337945	29.45520	57.19339	88.53482	122.4771	158.8931	163.8426	188.2552	197.9257	282.1947
1.0	8.564907	31.51967	62.44456	96.91191	133.4626	172.079	212.9165	255.5304	298.3755	337.3501
-1.0	8.126332	27.62825	25.28013	79.76065	95.66214	109.4931	111.0628	130.8329	141.4835	159.1549

Table 4.39 Frequency parameter f of tapered solid Timoshenko shaft
(taper ratio = 0.1; Rigid bearings at both ends)

spin speed Ω		Frequency parameter f									
		f_1	f_2	f_3	f_4	f_5	f_6	f_7	f_8	f_9	f_{10}
200	B	3.037367	18.18286	37.31908	60.75193	87.68758	117.7390	150.8873	180.6280	187.8563	228.0122
	F	3.065588	18.22851	37.38894	60.84216	87.79345	117.8567	151.0159	181.7713	188.0319	228.1473
400	B	3.023344	18.16006	37.28416	60.70767	87.63459	117.6801	150.8222	180.0556	187.7730	227.9446
	F	3.079788	18.25137	37.42387	60.88725	87.84632	117.9155	151.0822	182.3406	188.1256	228.2148
600	B	3.009382	18.13728	37.24923	60.66162	87.58156	117.6211	150.7583	179.4834	187.6918	227.8769
	F	3.094046	18.27425	37.45580	60.93232	87.89916	117.9742	151.1440	182.9068	188.2249	228.2822
800	B	2.995478	18.11452	37.21431	60.61644	87.52849	117.5621	150.6936	178.9118	187.6125	227.8091
	F	3.108363	18.29714	37.49373	60.97737	87.95197	118.0329	151.2079	183.4684	188.3312	228.3496
1000	B	2.981635	18.09178	37.17939	60.57124	87.47539	117.5030	150.6288	178.3412	187.5346	227.7413
	F	3.122738	18.32006	37.52867	61.02240	88.00473	118.0915	151.2717	184.0229	188.4470	228.4169

Table 4.40 Frequency parameter f of tapered solid Timoshenko shaft
(taper ratio = 0.5; Rigid bearings at both ends)

spin speed Ω		Frequency parameter f									
		f_1	f_2	f_3	f_4	f_5	f_6	f_7	f_8	f_9	f_{10}
200	B	6.664405	25.44656	50.81479	80.34028	112.8703	148.1039	171.9075	186.1592	226.0378	226.8999
	F	6.692878	25.51562	50.91657	80.46077	113.0000	148.2383	173.1267	186.2944	226.7291	227.5369
400	B	6.650201	25.41206	50.76386	80.27992	112.8053	148.0365	171.3015	186.0915	225.4973	226.8592
	F	6.707146	25.55016	50.96741	80.52091	113.0647	148.3052	173.7398	186.3621	226.7791	228.0736
600	B	6.636019	25.37756	50.71290	80.21951	112.7402	147.9690	170.6978	186.0239	224.9275	226.6893
	F	6.721437	25.58471	51.01822	80.58099	113.1294	148.3721	174.3552	186.4299	226.9518	228.6498
800	B	6.621859	25.34307	50.66190	80.15902	112.6750	147.9013	170.0966	185.9562	224.3483	226.6108
	F	6.735749	25.61927	51.06900	80.64101	113.1939	148.4389	174.9730	186.4976	227.0309	229.2412
1000	B	6.607721	25.30859	50.61087	80.09847	112.6098	147.8335	169.4977	185.8886	223.7657	226.5374
	F	6.750082	25.65383	51.11975	80.70095	113.2583	148.5055	175.5930	186.5656	227.1040	229.8404

Table 4.41 Frequency parameter f of tapered solid Timoshenko shaft
(taper ratio = 0.8; Rigid bearings at both ends)

spin speed Ω		Frequency parameter f									
		f_1	f_2	f_3	f_4	f_5	f_6	f_7	f_8	f_9	f_{10}
200	B	8.321359	29.41344	57.13632	88.47153	122.4125	158.8278	163.2222	187.6389	197.8643	212.6681
	F	8.354561	29.49696	57.25039	88.59799	122.5416	158.9579	164.4658	188.8737	197.9869	213.8534
400	B	8.304792	29.37168	57.07918	88.40812	122.3478	158.7619	162.6048	187.0248	197.8029	212.0786
	F	8.371195	29.53870	57.30732	88.66107	122.6059	159.0223	165.0917	189.4945	198.0479	214.4492
600	B	8.288246	29.32990	57.02197	88.34461	122.2830	158.6951	161.9906	186.4129	197.7412	211.4913
	F	8.387850	29.58044	57.36418	88.72403	122.6701	159.0864	165.7204	190.1174	198.1089	215.0472
800	B	8.271723	29.28812	56.96469	88.28098	122.2180	158.6271	161.3800	185.8032	197.6795	210.9060
	F	8.404527	29.62216	57.42097	88.78688	122.7341	159.1502	166.3517	190.7426	198.1697	215.6472
1000	B	8.255222	29.24633	56.90735	88.21725	122.1529	158.5569	160.7740	185.1957	197.6176	210.3229
	F	8.421226	29.66388	57.47769	88.84962	122.7981	159.2138	166.9855	191.3699	198.2303	216.2493

Table 4.42 Frequency parameter f of tapered solid Timoshenko shaft
(taper ratio = 0.1; Flexible bearings at both ends)

Whirl ratio	Frequency parameter f									
λ	f_1	f_2	f_3	f_4	f_5	f_6	f_7	f_8	f_9	f_{10}
0.0	1.33611	3.01036	17.20752	33.50578	53.77496	77.72138	104.6364	133.7342	163.8989	193.2468
1.0	1.33629	3.18684	18.3424	36.68924	60.4333	89.04811	121.4761	157.0106	195.3709	236.7318
-1.0	1.33591	2.85944	16.28223	31.04569	48.78582	69.2413	91.87616	115.8414	137.0826	151.2713

Table 4.43 Frequency parameter f of tapered solid Timoshenko shaft
(taper ratio = 0.5; Flexible bearings at both ends)

Whirl ratio	Frequency parameter f									
λ	f_1	f_2	f_3	f_4	f_5	f_6	f_7	f_8	f_9	f_{10}
0.0	1.198827	2.303935	16.00177	37.95383	65.29798	95.62044	127.7152	159.7799	187.8936	209.9703
1.0	1.199539	2.385729	17.60740	44.24499	78.17120	115.58119	155.2701	197.0803	240.6485	284.2581
-1.0	1.198079	2.230039	14.75047	33.43016	55.95591	80.41256	105.6947	121.9919	137.2663	150.9312

Table 4.44 Frequency parameter f of tapered solid Timoshenko shaft
(taper ratio = 0.8; Flexible bearings at both ends)

Whirl ratio	Frequency parameter f									
λ	f_1	f_2	f_3	f_4	f_5	f_6	f_7	f_8	f_9	f_{10}
0.0	1.048681	1.816676	18.11829	42.66280	72.05700	103.4860	135.7382	163.8107	184.3503	192.2657
1.0	1.048823	1.888985	20.57121	51.52928	88.23435	126.8564	166.9841	208.8629	252.2823	295.4777
-1.0	1.048529	1.752076	16.30084	36.42418	59.99903	84.35258	106.6629	110.4473	132.6641	138.0774

Table 4.45 Frequency parameter f of tapered solid Timoshenko shaft
(taper ratio = 0.1; Flexible bearings at both ends)

spin speed Ω		Frequency parameter f									
		f_1	f_2	f_3	f_4	f_5	f_6	f_7	f_8	f_9	f_{10}
200	B	1.336194	2.976391	17.17002	33.45278	53.70563	77.63689	104.5375	133.6182	163.7568	193.0670
	F	1.336017	3.044674	17.24514	33.55889	53.84438	77.80593	104.7355	133.8504	164.0411	193.4270
400	B	1.335925	2.942768	17.13264	33.39988	53.63638	77.55245	104.4385	133.5023	163.6149	192.8877
	F	1.336279	3.079329	17.28288	33.61209	53.91387	77.89055	104.8335	133.9666	164.1839	193.6077
600	B	1.335831	2.909496	17.09538	33.34708	53.56721	77.46809	104.3396	133.3864	163.4732	192.7088
	F	1.336364	3.114320	17.32074	33.66539	53.98344	77.97522	104.9338	134.0828	164.3262	193.7888
800	B	1.335736	2.876576	17.05825	33.29438	53.49813	77.38381	104.2408	133.2707	163.3317	192.5303
	F	1.336446	3.149645	17.35871	33.71878	54.05309	78.05995	105.0330	134.1992	164.4689	193.9703
1000	B	1.335638	2.844011	17.02124	33.24179	53.42914	77.29959	104.1421	133.1550	163.1904	192.3522
	F	1.336527	3.185299	17.39680	33.77226	54.12280	78.14473	105.1323	134.3156	164.6119	192.3522

Table 4.46 Frequency parameter f of tapered solid Timoshenko shaft
(taper ratio = 0.5; Flexible bearings at both ends)

spin speed Ω		Frequency parameter f									
		f_1	f_2	f_3	f_4	f_5	f_6	f_7	f_8	f_9	f_{10}
200	B	1.198437	2.282740	15.94620	37.86467	65.18742	95.49313	127.5688	159.5940	187.6298	209.6307
	F	1.199064	2.325328	16.05750	38.04308	65.40855	95.74775	127.8616	159.9658	188.1573	210.3100
400	B	1.198037	2.261745	15.89080	37.77560	65.07690	95.36581	127.4224	159.4081	187.3661	209.2901
	F	1.199577	2.346919	16.11339	38.13242	65.51915	95.87503	128.0089	160.1516	188.4209	210.6494
600	B	1.197627	2.240953	15.83556	37.68663	64.96641	95.23849	127.2760	159.2222	187.1022	208.9498
	F	1.199938	2.368706	16.16943	38.22185	65.62977	96.00230	128.1544	160.3373	188.6845	210.9886
800	B	1.197204	2.220363	15.78049	37.59777	64.85596	95.11116	127.1296	159.0362	186.8382	208.6093
	F	1.200289	2.390688	16.22564	38.31135	65.74040	96.12955	128.3007	160.5230	188.9480	211.3274
1000	B	1.196771	2.199975	15.72558	37.50900	64.74555	94.98385	126.9832	158.8503	186.5742	208.2687
	F	1.200633	2.412863	16.28199	38.40094	65.85105	96.25676	128.4470	160.7086	189.2117	211.6659

Table 4.47 Frequency parameter f of tapered solid Timoshenko shaft
(taper ratio = 0.8; Flexible bearings at both ends)

spin speed Ω		Frequency parameter f									
		f_1	f_2	f_3	f_4	f_5	f_6	f_7	f_8	f_9	f_{10}
200	B	1.048591	1.793101	18.04536	42.55108	71.92546	103.3355	135.5609	163.5076	183.9463	191.8790
	F	1.048767	1.840559	18.19141	42.77457	72.18851	103.6365	135.9155	164.1124	184.7557	192.6550
400	B	1.048496	1.769835	17.97261	42.43940	71.79387	103.1848	135.3835	163.2029	183.5437	191.4947
	F	1.048850	1.864753	18.26469	42.88637	72.31996	103.7898	136.0926	164.4126	185.1624	193.0468
600	B	1.048397	1.746881	17.90004	42.32777	71.66225	103.0341	135.2059	162.8968	183.1428	191.1128
	F	1.048929	1.889252	18.33815	42.99820	72.45136	103.9371	136.2697	164.7114	185.5703	193.4413
800	B	1.048293	1.724238	17.82765	42.21619	71.53060	102.8832	135.0284	162.5892	182.7434	190.7333
	F	1.049006	1.914058	18.41177	43.11007	72.58270	104.0872	136.4466	165.0087	185.9794	193.8384
1000	B	1.048185	1.701905	17.75545	42.10468	71.39893	102.7323	134.8507	162.2801	182.3458	190.3560
	F	1.049079	1.939169	18.48556	43.22195	72.71398	104.2371	136.6233	165.3045	186.3895	194.2383

Table 4.48 Frequency parameter f of tapered hollow Timoshenko shaft
(taper ratio = 0.1; Rigid bearings at both ends)

Whirl ratio	Frequency parameter f									
λ	f_1	f_2	f_3	f_4	f_5	f_6	f_7	f_8	f_9	f_{10}
0.0	3.01988	17.60018	35.10309	55.64314	78.52319	103.499	121.6679	130.9246	160.4314	191.8116
1.0	3.10663	18.33047	37.03	59.02714	83.43574	110.0074	138.8281	170.0221	203.2881	237.2508
-1.0	2.93974	16.93284	33.28803	52.23949	72.09041	75.38627	96.62104	116.7098	121.7382	149.0266

Table 4.49 Frequency parameter f of tapered hollow Timoshenko shaft
(taper ratio = 0.5; Rigid bearings at both ends)

Whirl ratio	Frequency parameter f									
λ	f_1	f_2	f_3	f_4	f_5	f_6	f_7	f_8	f_9	f_{10}
0.0	6.507358	23.75217	45.47384	69.62405	95.53322	115.5311	123.2801	152.7874	158.093	183.9957
1.0	6.684212	25.04759	48.40618	73.97517	101.0136	129.2601	159.9199	191.6055	223.5243	252.6867
-1.0	6.341894	22.55412	42.52364	64.59482	68.77510	88.80452	94.69451	113.7044	114.8109	134.4979

Table 4.50 Frequency parameter f of tapered hollow Timoshenko shaft
(taper ratio = 0.8; Rigid bearings at both ends)

Whirl ratio	Frequency parameter f									
λ	f_1	f_2	f_3	f_4	f_5	f_6	f_7	f_8	f_9	f_{10}
0.0	8.059561	26.90753	49.92311	74.85326	101.2585	109.1945	127.9814	129.3829	153.6302	159.1375
1.0	8.302427	28.51694	53.05456	79.01696	106.1013	134.6336	164.8089	196.2637	227.8018	256.3425
-1.0	7.833035	25.37999	46.53192	63.64663	69.60898	75.68787	93.63989	94.59559	117.9810	120.9180

Table 4.51 Frequency parameter f of tapered hollow Timoshenko shaft
(taper ratio = 0.1; Rigid bearings at both ends)

spin speed Ω		Frequency parameter f									
		f_1	f_2	f_3	f_4	f_5	f_6	f_7	f_8	f_9	f_{10}
200	B	3.004332	17.57777	35.07282	55.60836	78.48599	103.4588	121.1456	130.8815	160.3939	191.3119
	F	3.035497	17.62260	35.13334	55.67787	78.56032	103.5390	122.1925	130.9683	160.4685	192.2360
400	B	2.988856	17.55536	35.04252	55.57354	78.44873	103.4184	120.6259	130.8389	160.3566	190.7945
	F	3.051184	17.64503	35.16356	55.71255	78.59739	103.5788	122.7195	131.0127	160.5057	193.0875
600	B	2.973450	17.53296	35.01221	55.53867	78.41140	103.3778	120.1087	130.7969	160.3193	190.2721
	F	3.066940	17.66746	35.19376	55.74718	78.63439	103.6185	123.2485	131.0580	160.5429	193.5737
800	B	2.958115	17.51058	34.98187	55.50376	78.37401	103.3369	119.5941	130.7552	160.2819	189.7484
	F	3.082766	17.68991	35.22394	55.78178	78.67133	103.6579	123.7794	131.1045	160.5801	194.0948
1000	B	2.942852	17.48819	34.95151	55.46880	78.33655	103.2959	119.0823	130.7138	160.2444	189.2249
	F	3.098669	17.71237	35.25409	55.81633	78.70820	103.6972	124.3119	131.1523	160.6172	194.6279

Table 4.52 Frequency parameter f of tapered hollow Timoshenko shaft
(taper ratio = 0.5; Rigid bearings at both ends)

spin speed Ω		Frequency parameter f									
		f_1	f_2	f_3	f_4	f_5	f_6	f_7	f_8	f_9	f_{10}
200	B	6.492524	23.72244	45.43683	69.58580	95.49566	114.9882	123.2430	152.7548	157.5513	183.9650
	F	6.522209	23.78188	45.51079	69.66220	95.57068	116.0765	123.3174	152.8198	158.6369	184.0261
400	B	6.477708	23.69269	45.39976	69.54747	95.45797	114.4480	123.2061	152.7222	157.0117	183.9341
	F	6.537079	23.81157	45.54767	69.70028	95.60801	116.6245	123.3551	152.8522	159.1830	184.0563
600	B	6.646291	23.66292	45.36263	69.50306	95.42016	113.9105	123.1694	152.6895	156.4743	183.9027
	F	6.551967	23.84125	45.58450	69.73828	95.64524	117.1749	123.3933	152.8845	159.7312	184.0863
800	B	6.448133	23.63314	45.32544	69.47058	95.38222	113.3759	123.1329	152.6568	155.9392	183.8708
	F	6.566872	23.87091	45.62126	69.77619	95.68236	117.7276	123.4321	152.9168	160.2817	184.1162
1000	B	6.433372	23.60334	45.28816	69.43200	95.34415	112.8440	123.0963	152.6239	155.4062	183.8380
	F	6.581794	23.90034	45.65975	69.81402	95.71936	118.2823	123.4716	152.9489	160.8342	184.1459

Table 4.53 Frequency parameter f of tapered hollow Timoshenko shaft
(taper ratio = 0.8; Rigid bearings at both ends)

spin speed Ω		Frequency parameter f									
		f_1	f_2	f_3	f_4	f_5	f_6	f_7	f_8	f_9	f_{10}
200	B	8.043133	26.87439	49.88555	74.81723	101.2248	108.6384	127.4495	129.3346	153.0990	159.1103
	F	8.076001	26.94063	49.96057	74.88919	101.2919	109.7537	128.4955	129.4514	154.1636	159.1647
400	B	8.026719	26.84120	49.84791	74.78110	101.1909	108.0854	126.9123	129.2942	152.5700	159.0832
	F	8.092455	26.97369	49.99794	74.92503	101.3253	110.3159	128.9458	129.5864	154.6990	159.1921
600	B	8.010319	26.80797	49.81018	74.74486	101.1567	107.5355	126.3738	129.2575	152.0432	159.0561
	F	8.108921	27.00669	50.03524	74.96076	101.3585	110.8813	129.2198	129.9001	155.2365	159.2197
800	B	7.993933	26.77469	49.77235	74.70853	101.1223	106.9888	125.8359	129.2229	151.5187	159.0290
	F	8.125400	27.03966	50.07242	74.99639	101.3915	111.4496	129.3356	130.3746	155.7759	159.2476
1000	B	7.977561	26.74138	49.73443	74.67209	101.0874	106.4454	125.2993	129.1895	150.9964	159.0019
	F	8.141892	27.07258	50.10952	75.03193	101.4244	112.0210	129.3983	130.9047	156.3170	159.2760

Table 4.54 Frequency parameter f of tapered hollow Timoshenko shaft
(taper ratio = 0.1; Flexible bearings at both ends)

Whirl ratio	Frequency parameter f									
λ	f_1	f_2	f_3	f_4	f_5	f_6	f_7	f_8	f_9	f_{10}
0.0	1.37226	3.0405	16.86576	32.1222	50.2575	70.75562	92.71358	114.5394	134.5945	155.9368
1.0	1.37242	3.26533	18.17785	35.38946	56.23266	79.91077	105.7648	133.4989	162.8481	193.4427
-1.0	1.37208	2.85501	15.81793	29.54269	45.38645	62.81976	80.65788	96.25744	109.5353	124.4763

Table 4.55 Frequency parameter f of tapered hollow Timoshenko shaft
(taper ratio = 0.5; Flexible bearings at both ends)

Whirl ratio	Frequency parameter f									
λ	f_1	f_2	f_3	f_4	f_5	f_6	f_7	f_8	f_9	f_{10}
0.0	1.235539	2.364493	15.48143	35.07400	58.11016	82.24589	105.8599	125.0329	144.7684	157.3678
1.0	1.236429	2.469926	17.23159	40.62486	67.61639	95.89602	125.3828	156.2818	188.3839	220.3635
-1.0	1.234593	2.271455	14.13063	30.76227	49.96305	68.83344	83.74332	92.42865	108.5575	114.7657

Table 4.56 Frequency parameter f of tapered hollow Timoshenko shaft
(taper ratio = 0.8; Flexible bearings at both ends)

Whirl ratio	Frequency parameter f									
λ	f_1	f_2	f_3	f_4	f_5	f_6	f_7	f_8	f_9	f_{10}
0.0	1.081411	1.865559	17.35349	38.65191	62.72525	86.50026	108.7319	118.6796	139.4848	142.3052
1.0	1.081591	1.958745	19.87621	45.77912	73.69083	102.1533	131.5942	162.3559	194.2772	225.9764
-1.0	1.081214	1.784467	15.46292	32.93877	52.57937	67.33683	79.60679	85.03018	104.9659	107.5847

Table 4.57 Frequency parameter f of tapered hollow Timoshenko shaft
(taper ratio = 0.1; Flexible bearings at both ends)

spin speed Ω		Frequency parameter f									
		f_1	f_2	f_3	f_4	f_5	f_6	f_7	f_8	f_9	f_{10}
200	B	1.372187	3.002956	16.82653	32.07018	50.19301	70.67759	92.61387	114.3987	134.4350	155.8110
	F	1.372325	3.078447	16.90509	32.17429	50.32198	70.83362	92.81321	114.3987	134.7556	156.0631
400	B	1.372116	2.965826	16.78743	32.01823	50.12856	70.59952	92.51410	114.2582	134.2768	155.6857
	F	1.372391	3.116799	16.94454	32.22644	50.12856	70.91157	92.91274	114.8214	134.9180	156.1899
600	B	1.372043	2.921120	16.74845	31.96634	50.06411	70.52143	92.41443	114.1181	134.1200	155.5608
	F	1.372456	3.155547	16.98412	32.27864	50.45100	70.98948	93.01217	114.9627	135.0818	156.3173
800	B	1.371968	2.892818	16.70960	31.91453	49.99970	70.44332	92.31438	113.9782	133.9645	155.4362
	F	1.372520	3.194687	17.02380	32.33090	50.51552	71.06733	93.11149	115.1041	135.2471	156.4453
1000	B	1.371893	2.856946	16.67086	31.86279	49.93532	70.36520	92.21445	113.8386	133.8104	155.3120
	F	1.372582	3.234218	17.06358	32.38322	50.58003	71.14513	93.21067	115.2456	135.4138	156.5740

Table 4.58 Frequency parameter f of tapered hollow Timoshenko shaft
(taper ratio = 0.5; Flexible bearings at both ends)

spin speed Ω		Frequency parameter f									
		f_1	f_2	f_3	f_4	f_5	f_6	f_7	f_8	f_9	f_{10}
200	B	1.235113	2.340999	15.42557	34.99305	58.01625	82.13154	105.6963	124.8031	144.5607	156.9926
	F	1.235921	2.388219	15.53740	35.15493	58.20394	82.36000	106.0232	125.2637	144.9751	157.7455
400	B	1.234675	2.317741	15.36986	34.91210	57.92225	82.01695	105.5324	124.5747	144.3520	156.6202
	F	1.236354	2.412175	15.59350	35.23585	58.29761	82.47385	106.1862	125.4959	145.1809	158.1257
600	B	1.234225	2.294719	15.31428	34.83115	57.82815	81.90213	105.3684	124.3474	144.1421	156.2507
	F	1.236745	2.436361	15.64973	35.31674	58.39116	82.58743	106.3489	125.7292	145.3860	158.5081
800	B	1.233761	2.271936	15.25884	34.75020	57.73395	81.78709	105.2041	124.1212	143.9309	155.8843
	F	1.237126	2.460773	15.70607	35.39762	58.48459	82.70074	106.5112	125.9637	145.5905	158.8927
1000	B	1.233284	2.249393	15.20354	34.66926	57.63966	81.67183	105.0396	123.8963	143.7185	155.5210
	F	1.237497	2.485408	15.76254	35.47846	58.57789	82.81376	106.6731	126.1995	145.7945	159.2791

Table 4.59 Frequency parameter f of tapered hollow Timoshenko shaft
(taper ratio = 0.8; Flexible bearings at both ends)

spin speed Ω		Frequency parameter f									
		f_1	f_2	f_3	f_4	f_5	f_6	f_7	f_8	f_9	f_{10}
200	B	1.081311	1.839496	17.28264	38.55403	62.61650	86.35108	108.6487	118.3145	139.1665	142.0514
	F	1.081507	1.891987	17.42445	38.74967	62.83376	86.64874	108.9525	119.0464	139.8066	142.5590
400	B	1.081205	1.813796	17.21187	38.45604	62.50753	86.20122	108.2895	117.9508	138.8517	141.7977
	F	1.081598	1.918777	17.49550	38.84729	62.94203	86.79652	109.1725	119.4148	140.1318	142.8129
600	B	1.081094	1.788464	17.14122	38.35794	62.39835	86.05070	108.0677	117.5888	138.5403	141.5441
	F	1.081686	1.945926	17.56664	38.94478	63.05006	86.94359	109.3919	119.7847	140.4605	143.0670
800	B	1.080977	1.763498	17.07068	38.25972	62.28895	85.89952	107.8456	117.2284	138.2322	141.2907
	F	1.081771	1.973434	17.63786	39.04212	63.15784	87.08993	109.6108	120.1562	140.7928	143.3211
1000	B	1.080854	1.738900	17.00025	38.16140	62.17935	85.74769	107.6232	116.8697	137.9276	141.1286
	F	1.081851	2.001298	17.70916	39.13932	63.26536	87.23555	109.8291	120.5292	141.0374	143.5753

Table 4.60 Frequency parameter f of tapered hollow Timoshenko shaft
(taper ratio = 0.8; Flexible damped bearings at both ends)

spin speed Ω		Frequency parameter f									
		f_1	f_2	f_3	f_4	f_5	f_6	f_7	f_8	f_9	f_{10}
200	B	1.096740	2.107610	15.92973	37.86249	65.18653	95.49252	127.5683	159.5937	187.6295	209.6302
	F	1.292593	2.486921	16.07447	38.04431	65.40839	95.74737	127.8612	159.9654	188.1569	210.3098
400	B	1.096727	2.104361	15.88181	37.77427	65.07619	95.36526	127.4219	159.4078	187.3657	209.2900
	F	1.292574	2.490771	16.12287	38.13281	65.51881	95.87460	128.0076	160.1512	188.4206	210.6492
600	B	1.096704	2.099085	15.82951	37.68559	64.96576	95.23795	127.2756	159.2218	187.1019	208.9497
	F	1.292542	2.497047	16.17598	38.22195	65.62937	96.00185	128.1539	160.3369	188.6842	210.9884
800	B	1.096673	2.091971	15.77597	37.59686	64.85534	95.11064	127.1291	159.0359	186.8379	208.6092
	F	1.292499	2.505561	16.23065	38.31132	65.73998	96.12908	128.3003	160.5227	188.9478	211.3272
1000	B	1.096632	2.083240	15.72201	37.50818	64.74495	94.98333	126.9827	158.8499	186.5739	208.2685
	F	1.292442	2.516092	16.28607	38.40083	65.85060	96.25629	128.4466	160.7083	189.2113	211.6657

A study is conducted with different number of elements in order to establish a measure of anyalitical accuracy for a particular number of finite elements used in the system model. Figures 4.3 - 4.5, shows good convergence of frequency parameter values with the increase in number of elements for nonrotating as well as rotating Timoshenko and Euler-Bernoulli shafts. It is also seen clearly from these figures that the secondary effects like shear and rotary inertia are more pronounced at higer modes.

In Figures 4.6 - 4.9, the behaviour of the frequency parameter f with the increase in the spin rate Ω is studied. It is demonstrated clearly that for a particular mode, as the spin rate increases, the backward frequency parameter decreases and the forward frequency parameter increases. This difference between the backward and forward frequency parameter values become larger at higher modes.

In Figures 4.10 - 4.17, the behaviour of the frequency parameter f for a varying taper ratio is studied for a solid tapered rotating Timinshenko shaft. In Figures 4.10 - 4.13, the forward bending frequencies of a rotating shaft for different boundary conditions are plotted against taper ratio. It is found that the frequency parameter values increase with increase in taper ratio. As expected the frequency parameter values of taper shafts supported on flexible bearings are less when compared to the corresponding frequency parameter values of taper shafts supported on rigid bearings.

In Figures 4.14 - 4.17, the backward bending frequencies of a rotating shaft for different boundary conditions are plotted against taper ratio. The behaviour is similar to that of forward frequency parameter values.

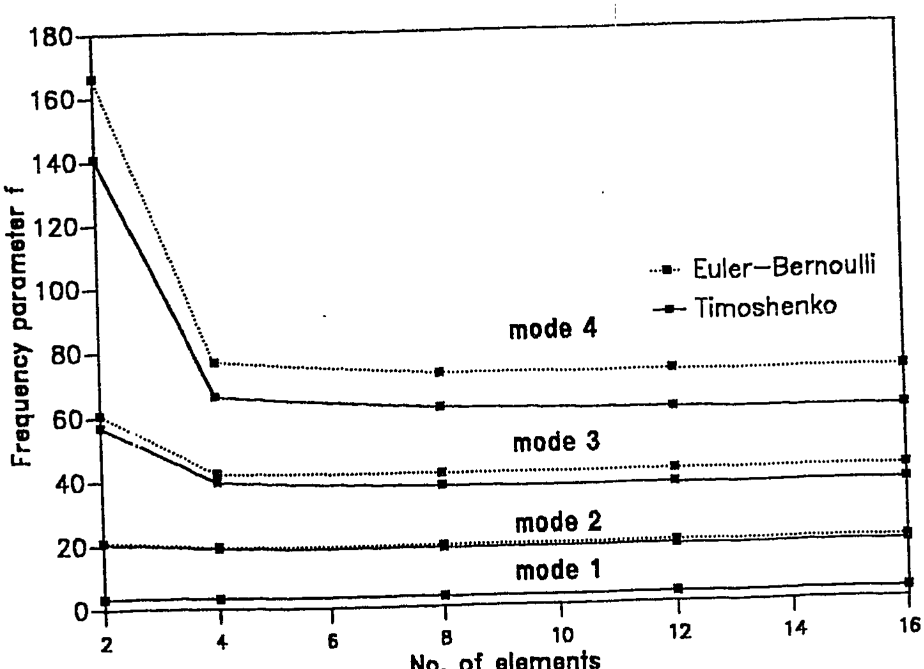

Figure 4.3: Convergence of frequency parameter f of tapered shaft
Rigid bearings at both ends;Taper ratio = 0.1

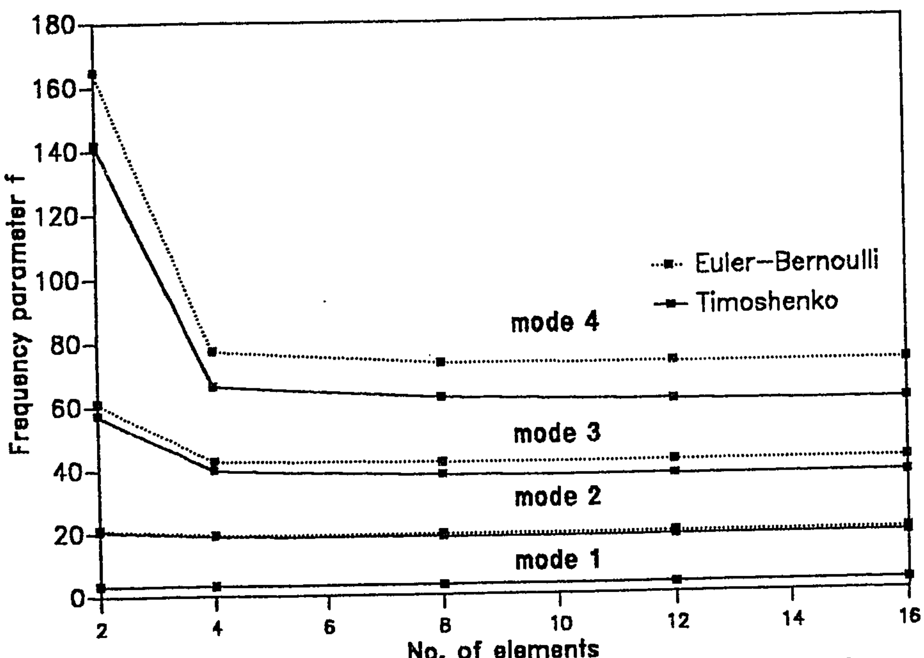

Figure 4.4: Convergence of forward bending frequencies of tapered shaft
Rigid bearings at both ends;Taper ratio = 0.1

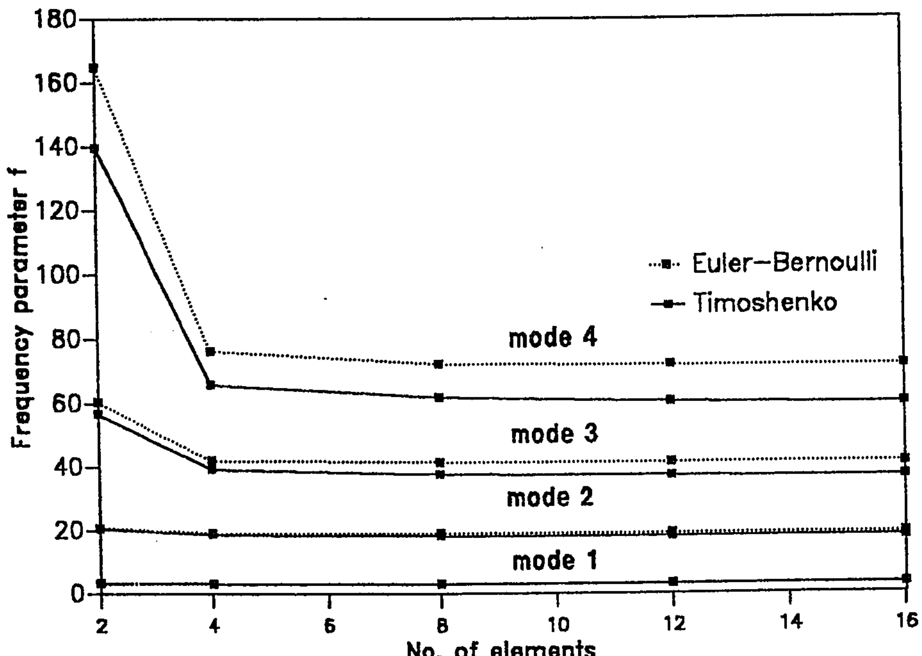

Figure 4.5: Convergence of backward bending frequencies of tapered shaft
Rigid bearings at both ends;Taper ratio = 0.1

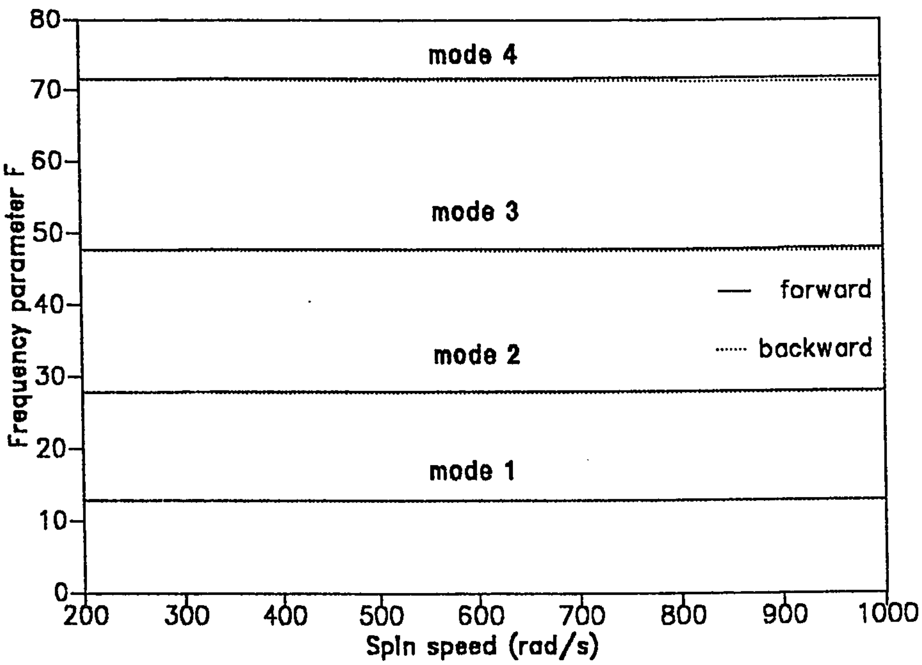

Figure 4.6: Frequency vs Speed (Rigid bearing at widest end);
Taper ratio = 0.1

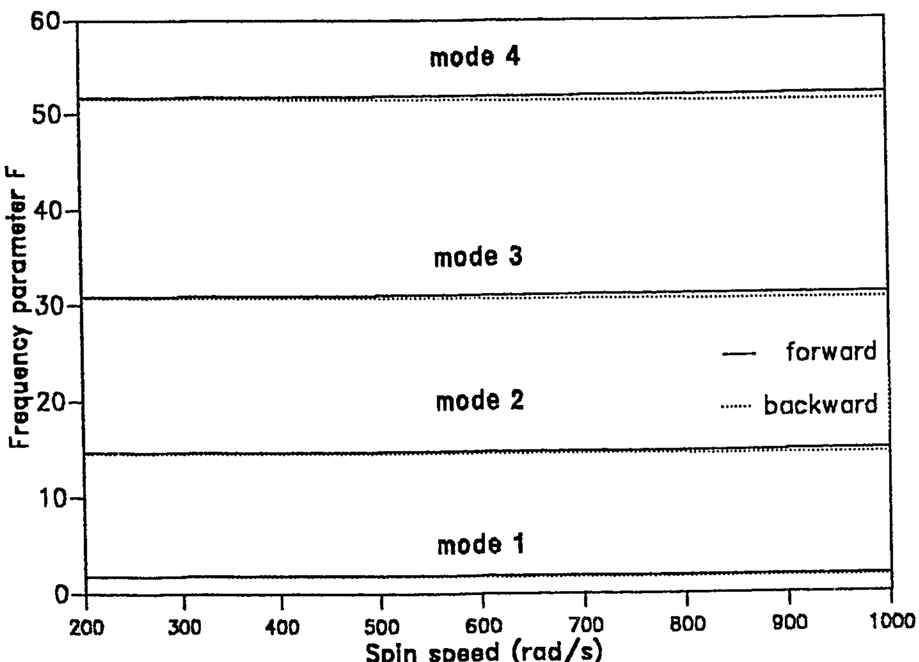

Figure 4.7: Frequency vs Spin speed (Flexible bearing at widest end); Taper ratio = 0.1

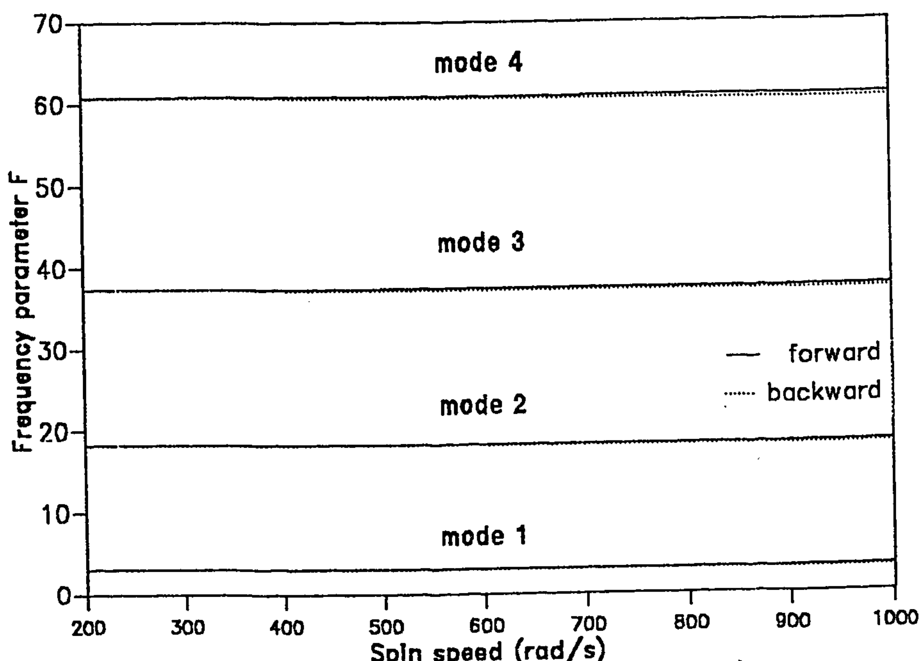

Figure 4.8: Frequency vs Spin speed (Rigid bearings at both ends);
Taper ratio = 0.1

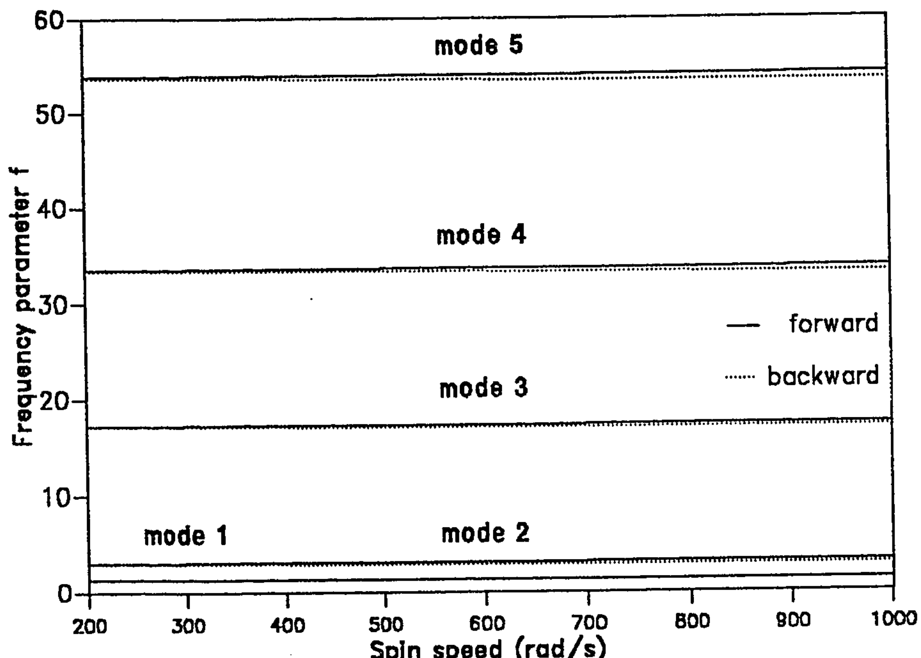

Figure 4.9: Frequency vs Spin speed (Flexible bearings at both ends);
Taper ratio = 0.1

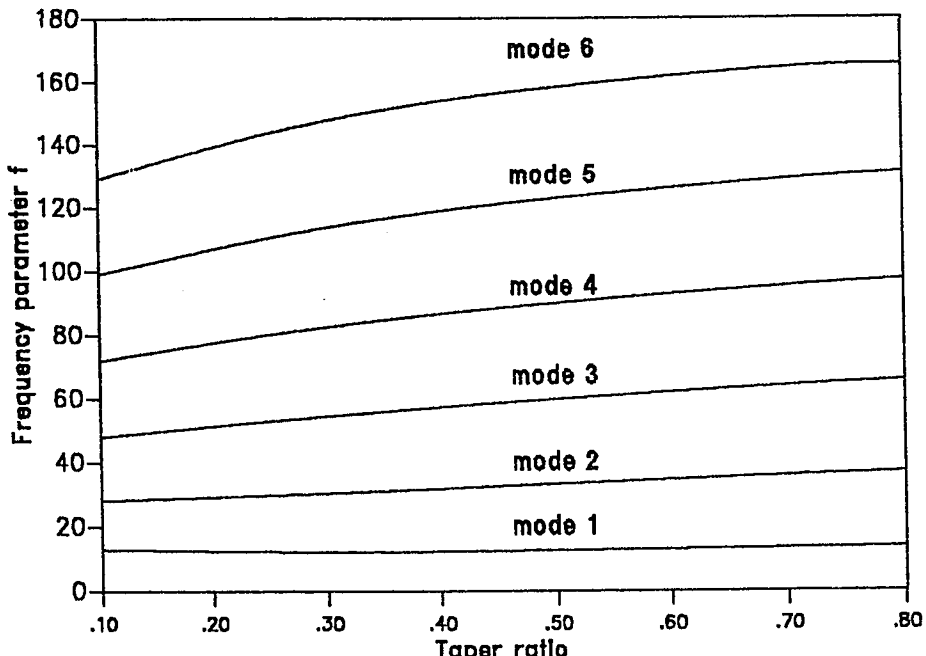

Figure 4.10: Frequency vs Taper ratio (Rigid bearing at widest end); Forward whirl

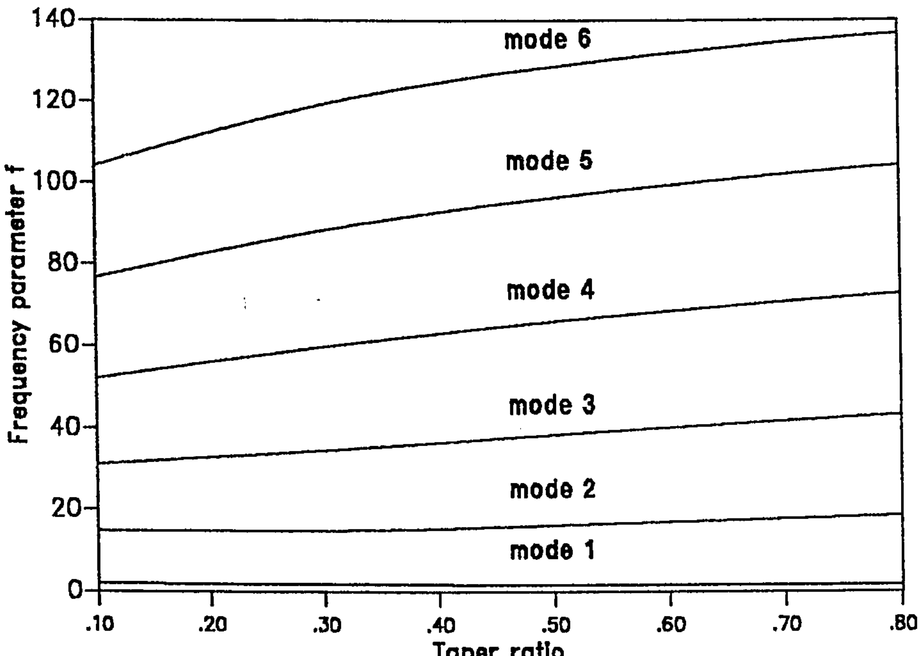

Figure 4.11: Frequency vs Taper ratio (Flexible bearing at widest end); Forward whirl

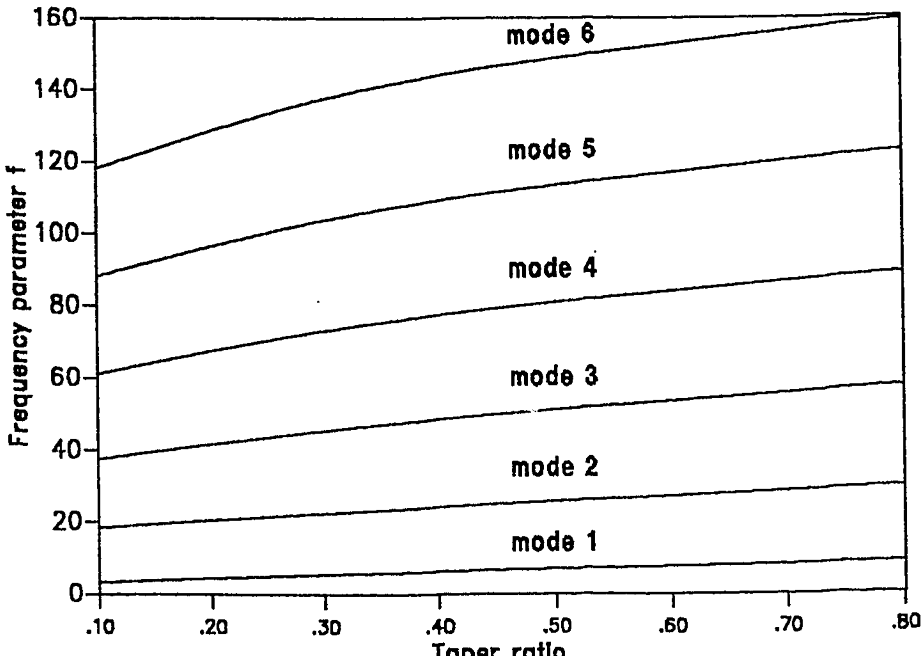

Figure 4.12: Frequency vs Taper ratio (Rigid bearings at both ends); Forward whirl

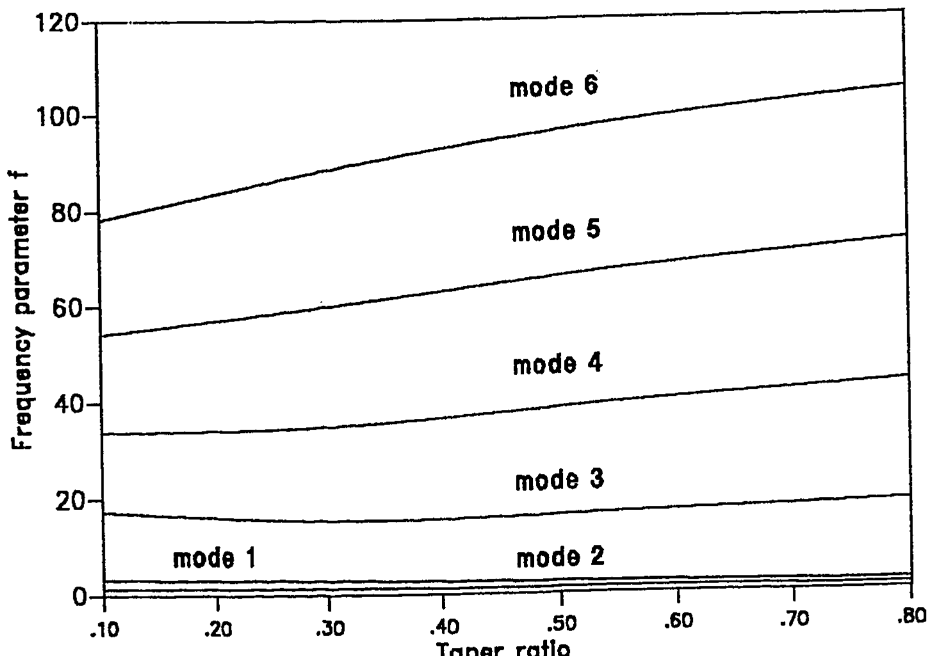

Figure 4.13: Frequency vs Taper ratio (Flexible bearings at both ends); Forward whirl

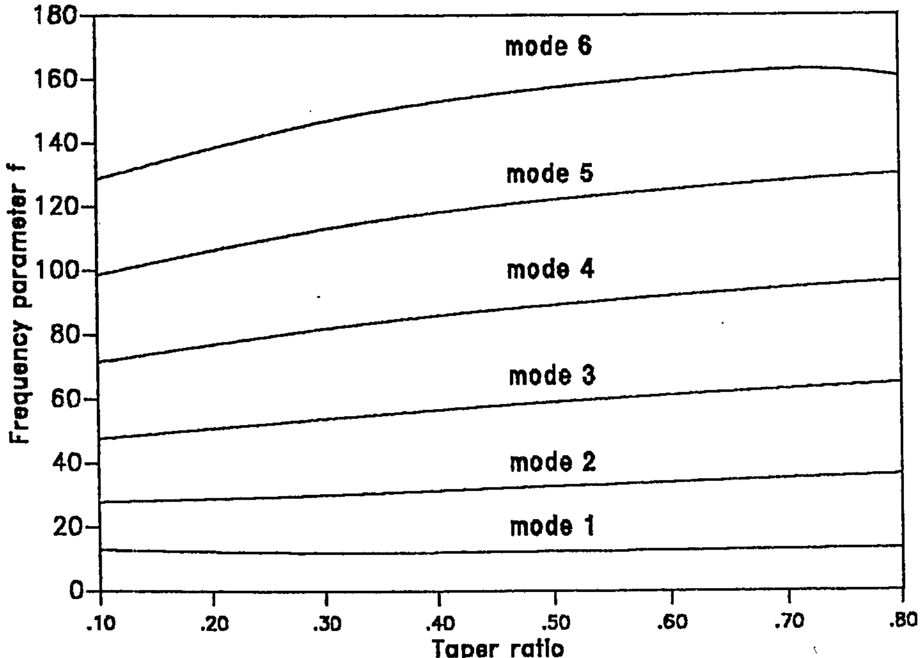

Figure 4.14: Frequency vs Taper ratio (Rigid bearing at the widest end); Backward whirl

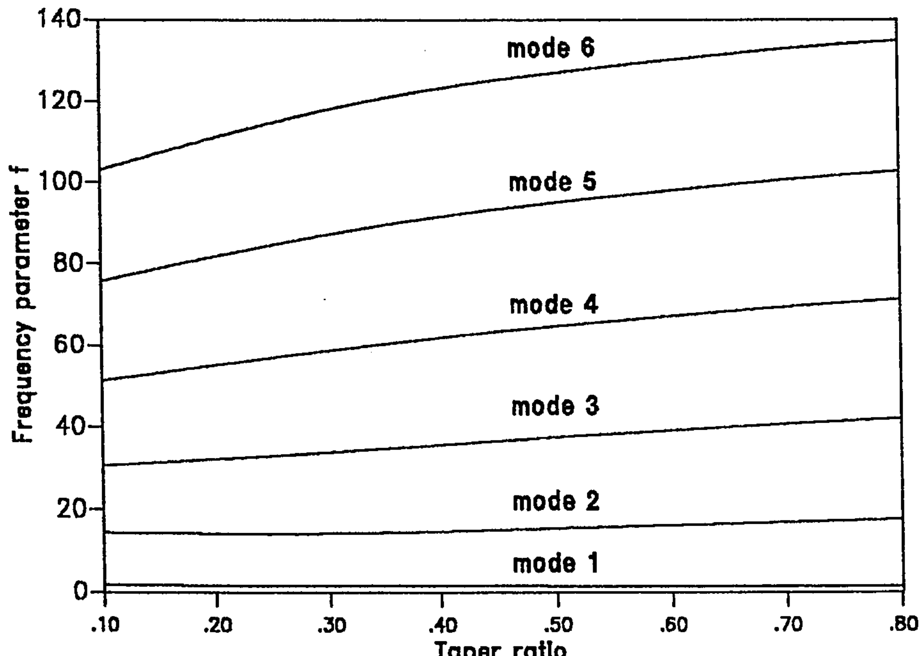

Figure 4.15: Frequency vs Taper ratio (Flexible bearing at widest end); Backward whirl

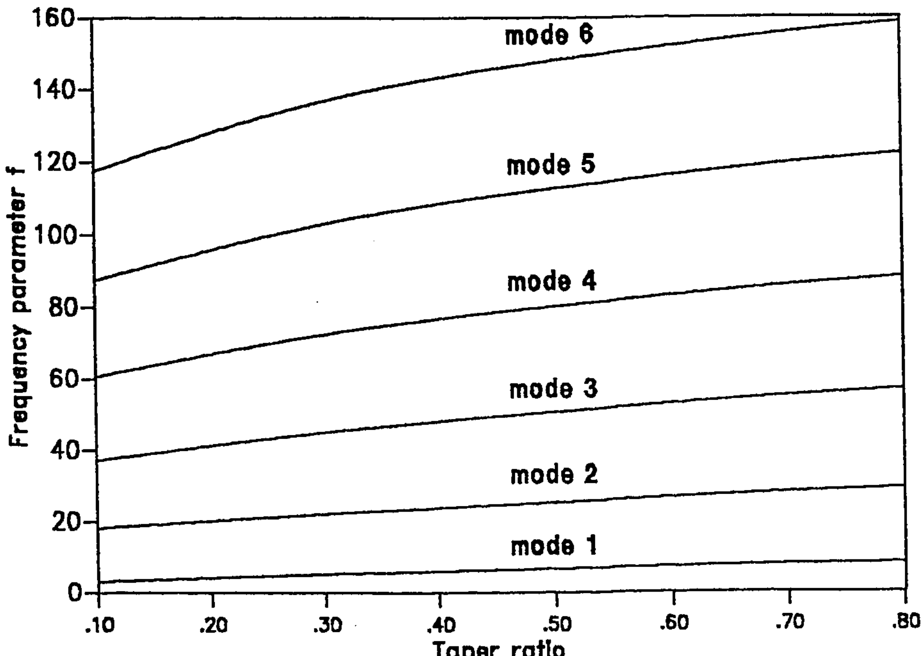

Figure 4.16: Frequency vs Taper ratio (Rigid bearings at bothends); Backward whirl

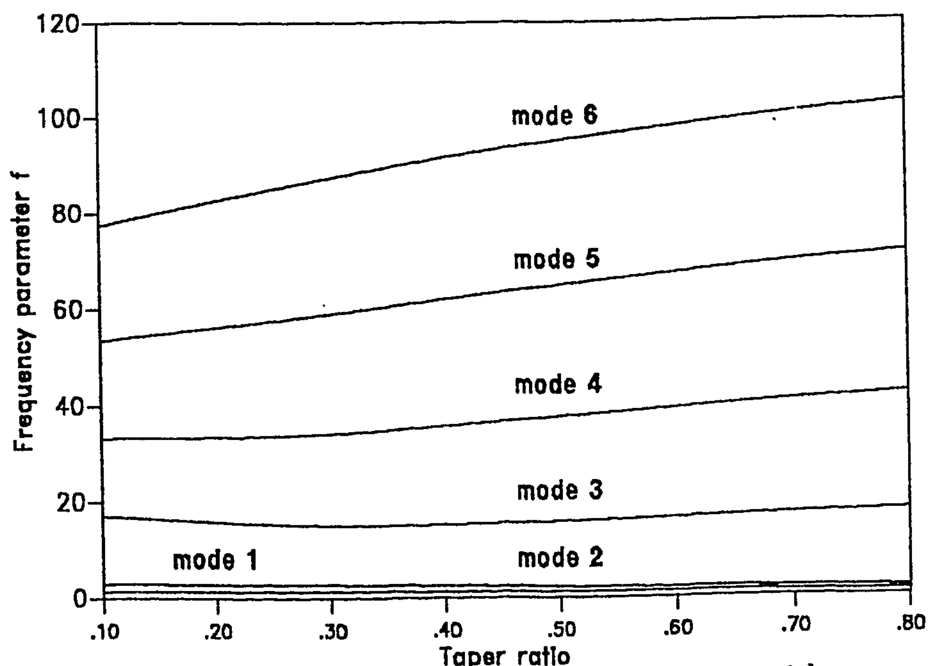

Figure 4.17: Frequency vs Taper ratio (Flexible bearings at both ends); Backward whirl

CONCLUSIONS

A Timoshenko beam finite element formulation is presented to study the free vibration characteristics of rotating and non-rotating tapered shafts with various end conditions. The explicit mass, stiffness and gyroscopic matrices of tapered rotating beam finite element have been developed using Timoshenko beam theory. These matrices are easily degenerated to those applicable to Euler-Bernoulli theory by equating the shear parameter to zero. The finite element is integrated into a procedure developed for calculating the natural frequencies of rotor-bearing systems. The procedure developed can take into account any hollow portions present in the shaft. The effects of taper ratio, spin rate, shear deformation, rotary inertia and gyroscopic moments of rotating shafts have been investigated. The results obtained give high accuracy when compared to the numerical results presented by other investigators.

Some of the capabitities of the finite element model developed to solve for the natural frequencies of the rotor-bearing systems are as follows:

1. It is applicable to circular, hollow or solid cross-sectional area of the shaft.
2. It can take into account the presence of bearings and disks.
3. It can handle all types of boundary conditions.
4. It is more efficient, accurate and of fast convergence.

The conclusions drawn from the present investigation are:

1. The effect of shear deformation and rotary inertia on the natural frequencies is more pronounced at higher modes.
2. The natural frequencies increase with increase in taper ratio.
3. The forward natural frequency increases and backward natural frequency decreases with the increase in spin rate.
4. The explicit mass and stiffness matrices eliminate the loss of computer time and round-off errors associated with extensive matrix operations which are necessary in the numerical evaluation of the expressions.
5. The tapered rotating beam finite element developed in this thesis can be easily integrated into any general purpose finite element code for the dynamic analysis of the rotor-bearing systems.

It is hoped that the tabulated results for such a wide range of parameter changes will serve as test data for future development of similar numerical schemes. It also furnishes an accurate set of data to be used directly in the dynamic analysis of rotors with similar configurations.

RECOMMENDATIONS FOR FUTURE WORK

1. The equation of motion of the rotor-bearing system and the element matrices are derived and tabulated. The free vibration study is done. To make the vibration analysis more complete, the unbalance response of the rotor-bearing system can be studied.

2. The dynamic analysis of the rotor-bearing system, under different loading conditions, using the conical beam finite element developed in this thesis, will be a direct extension to the free vibration analysis.

3. The disks are assumed as rigid in this thesis. Situations might arise where we have to consider the disks as flexible. To enhance the applicability and versatility of the model, the equation of motion of the system can be derived and eigenvalue problem formulated, taking the disks as flexible.

REFERENCES

1. Sankar, T.S., *Rotor Dynamics: A State-Of-The-Art*, Transactions of the Canadian Society of Mechanical Engineers, Vol. 15, No. 1, 1991, pp. 1-42.
2. Loewy, R. G. and Piarulli, V. J., ***Dynamics of Rotating Shafts***, The Shock and Vibration Information Center, United States Department of Defense, 1969.
3. Eshleman, R. L. and Eubanks, R. A., *On The Critical Speeds of a Continuous Rotor*, Journal of Engineering for Industry, Vol. 91, No. 4, 1969, pp. 1180-1188.
4. Bernasconi, O., *Bisynchronous Torsional Vibrations in Rotating Shafts*, Journal of Applied Mechanics, Vol. 54, December 1987, pp. 893-897.
5. Prohl, M. A., *A General Method for Calculating Critical Speeds of Flexible Rotors*, Journal of Applied Mechanics, Vol. 12, 1945, pp. A-142-A-148.
6. Lund, J. W., *Stability and Damped Critical Speeds of a Flexible Rotor in Fluid-Film bearings*, Journal of Engineering for Industry, Vol. 96, No. 2, 1974, pp. 509-517.
7. Jialiu Gu, *An Improved Transfer Matrix-Direct Integration Method for Rotor Dynamics*, Journal of Vibration and Acoustics, Vol. 108, April 1986, pp. 182-188.
8. Yim, K. B., Noah, S. T. and Vance, J. M., *Effect of Tangential Torque on The Dynamics of Flexible Rotors*, Journal of Applied Mechanics, Vol. 53, September 1986, pp. 711-718.

9. Diken, H. and Tadjbaksh, I. G., *Unbalance Response of Flexible Rotors Coupled With Torsion*, Journal of Vibration and Acoustics, Vol. 111, April 1989, pp. 179-186.

10. Adams, M. L., *Non-Linear Dynamics of Flexible Multi-Bearing Rotors*, Journal of Sound and Vibration, Vol. 71, No. 1, 1980, pp. 129-144.

11. Lee, C. -W. and Jei, Y. -G., *Modal Analysis of Continuous Rotor-Bearing Systems*, Journal of Sound and Vibration, Vol. 126, No. 2, 1988, pp.345-361.

12. Shiau, T. N. and Hwang, J. L., *Generalized Polynomial Expansion Method for the Dynamic Analysis of Rotor-Bearing Systems*, The 36th ASME International Gas Turbine and Aeroengine Congress and Exposition, Orlanda, Florida.

13. Ruhl, R. L. and Booker, J. F., *A Finite Element Model for Distributed Parameter Turborotor Systems*, Journal of Engineering for Industry, Vol. 94, No. 1, 1972, pp. 126-132.

14. Nelson, H. D. and McVaugh, J. M., *The Dynamics of Rotor-Bearing Systems Using Finite Elements*, Journal of Engineering for Industry, Vol. 98, No. 2, 1976, pp. 593-600.

15. Zorzi, E. S. and Nelson, H. D., *The Dynamics of Rotor-Bearing Systems With Axial Torque - A Finite Element Approach*, Journal of Mechanical Design, Vol. 102, January 1980, pp.158-161.

16. Childs, D. W. and Graviss, K., *A Note on Critical-Speed Solutions for Finite-Element-Based Rotor Models*, Journal of Mechanical Design, Vol. 104, April 1982, pp. 412-416.

17. Rajan, M., Nelson, H. D. and Chen, W. J., *Parameter Sensitivity in the Dynamics of Rotor-Bearing Systems*, Journal of Vibration and Acoustics, Vol. 108, April 1986, pp. 197-206.

18. Sakata, M., Kimura, K., Park, S. K. and Ohnabe, H., *Vibration of Bladed Flexible Rotor due to Gyroscopic Moment*, Journal of Sound and Vibration, Vol. 131, No. 3, 1989, pp. 417-430.

19. Sauer, G. and Wolf, M., *Finite Element Analysis of Gyroscopic Effects*, Finite Element in Analysis and Design, Vol. 5, 1989, pp. 131-140.

20. Nelson, H. D., *A Finite Rotating Shaft Element Using Timoshenko Beam Theory*, Journal of Mechanical Design, Vol. 102, October, 1980, pp.793-803.

21. Nevzat Ozguven, H. and Levent Ozkan, Z., *Whirl Speeds and Unbalance Response of Multibearing Rotors Using Finite Elements*, Journal of Vibration and Acoustics, Vol. 106, January 1984, pp. 72-79.

22. Chen, L. -W. and Ku, D. -M., *Finite Element Analysis of Natural Whirl Speeds of Rotating shafts*, Computer and Structures, Vol. 40, No. 3, 1991, pp. 741-747.

23. Suarez, L. E., Singh, M. P. and Rohanimanesh, M. S., *Seismic Response of Rotating Machines*, Earthquake Engineering And Structural Dynamics, Vol. 21, 1992, pp. 21-36.

24. Rouch, K. E. and Kao, J. S., *A Tapered Beam Finite Element For Rotor Dynamics Analysis*, Journal of Sound and Vibration, Vol. 66, No. 1, 1979, pp. 119-140.

25. Greenhill, L. M., Bickford, W. B. and Nelson, H. D., *A Conical Beam Finite Element for Rotor Dynamics Analysis*, Journal of Vibration and Acoustics, Vol. 107, October 1985, pp. 421-430.

26. Genta, G. and Gugliotta, A., *A Conical element for Finite Element Rotor Dynamics*, Journal of Sound and Vibration, Vol. 120, No. 1, 1988, pp.175-182.

27. Downs, B., *Reference Frequencies for the Validation of Numerical Solutions of Transverse Vibration of Non-Uniform Beams*, Journal of Sound and Vibration, Vol. 61, No. 1, 1978, pp.71-78.

28. Gmur, T. C. and Rodrigues, J. D., *Shaft Finite Elements for Rotor Dynamics Analysis*, Journal of Vibration and Acoustics, Vol. 113, October 1991, pp.482-493.

29. Genta, G., *Whirling of Unsymmetrical Rotors: A Finite Element Approach Based on Complex Co-ordinates*, Journal of Sound and Vibration, Vol. 124, No. 1, 1988, pp. 27-53.

30. Nikolajsen, J. L. and Holmes, R., *The Vibration of a Multi-Bearing Rotor*, Journal of Sound and Vibration, Vol. 72, No. 3, 1980, pp. 343-350.

31. Haddara, M. R., *On The Transverse Vibration of a Propeller-Tail Shaft System*, Ocean Engineering, Vol. 15, No. 2, 1988, pp. 119-126.

32. Shiau, T. N. and Hwang, J. L., *A New Approach to the Dynamic Characteristic of Undamped Rotor-Bearing Systems*, Journal of Vibration and Acoustics, Vol. 111, October 1989, pp. 379-385.

33. Hwang, J. L. and Shiau, T. N., *An Application of The Generalized Polynomial Expansion Method to Nonlinear Rotor Bearing Systems*, Journal of Vibration and Acoustics, Vol. 113, July 1991, pp. 299-308.

34. Cowper, G. R., *The Shear Coefficient in Timoshenko's Beam Theory*, Journal of Applied Mechanics, Vol. 33, June 1966, pp. 335-340.

35. Przemieniecki, J. S., ***Theory of Matrix Structural Analysis***, McGraw-Hill Co, NY, 1968.

36. Bazoune, A. and Khulief, Y. A., *A Finite Beam Element for Vibration Analysis of Rotating Tapered Timoshenko Beams*, Journal of Sound and Vibration, Vol. 156, No. 1, 1992, pp. 141-164.

37. Gupta, K. K., *Free Vibration Analysis of Spinning Structural Systems*, International Journal for Numerical Methods in Engineering, Vol. 5, 1973, pp. 395-418.

38. Gupta, K. K., *Eigenproblem Solution of Damped Structural Systems*, International Journal for Numerical Methods in Engineering, Vol. 8, 1974, pp. 877-911.

39. Meirovitch, L., *A New Method of Solution of the Eigenvalue Problem for Gyroscopic systems*, AIAA Journal, Vol. 12, No. 10, October 1974, pp.1337-1342.

40. Gupta, K. K., *Development of a Unified Numerical Procedure for Free Vibration Analysis of Structures*, International Journal for Numerical Methods in Engineering, Vol. 17, 1981, pp. 187-198.

41. Gupta, K. K., *Formulation of Numerical Procedures for Dynamic Analysis of Spinning Structures*, International Journal for Numerical Methods in Engineering, Vol. 23, 1986, pp. 2347-2357.

42. Gupta, K. K. and Lawson, C. L., *Development of a Block Lanczos Algorithm for Free Vibration Analysis of Spinning Structures*, International Journal for Numerical Methods in Engineering, Vol. 26, 1988, pp. 1029-1037.

43. Michel Lalanne and Guy Ferraris, ***Rotordynamics Prediction in Engineering***, John Wiley & Sons, 1990.

44. Archer, J. S., *Consistent Matrix Formulations for Structural Analysis Using Finite-Element Techniques*, AIAA Journal, Vol. 3, No. 10, 1965, pp. 1910-1918.